

**NUMERICAL EVALUATION OF THE DYNAMIC RESPONSE  
OF STRUCTURES USING AUXETIC-TYPE BASE  
ISOLATION**

By

Preyolin Naidoo

In fulfilment of the Master of Science in Civil Engineering, the College of Agriculture, Engineering  
and Science, University of Kwa-Zulu Natal

30 November 2018

Supervisor: Dr GA Drosopoulos

Examiner's Copy

## **DECLARATION 1 - PLAIGERISM**

I, ....., declare that

1. The research reported in this thesis, except where otherwise indicated, is my original research.
2. This thesis has not been submitted for any degree or examination at any other university.
3. This thesis does not contain other persons' data, pictures, graphs or other information, unless specifically acknowledged as being sourced from other persons.
4. This thesis does not contain other persons' writing, unless specifically acknowledged as being sourced from other researchers. Where other written sources have been quoted, then:
  - a. Their words have been re-written but the general information attributed to them has been referenced
  - b. Where their exact words have been used, then their writing has been placed in italics and inside quotation marks, and referenced.
5. This thesis does not contain text, graphics or tables copied and pasted from the Internet, unless specifically acknowledged, and the source being detailed in the thesis and in the References sections.

Signed:

.....

As the candidate's supervisor, I agree/do not agree to the submission of this thesis.

Signed:

.....

## **DECLARATION 2 – PUBLICATIONS**

This dissertation will be submitted for publication in an international journal.

## **ACKNOWLEDGEMENTS**

I would like to express my deepest appreciation and gratitude to the following people, to whom, made the completion of my research possible.

- Dr GA Drosopoulos for his constant inspiration, encouragement and supervision throughout the research period.
- My parents for their love and support during my studies.

## ABSTRACT

Base isolation is a widely-used method to minimise the harmful effects of earthquakes on buildings. Unlike a fixed base building, a building with a base isolation system essentially decouples the superstructure from the substructure resting on the ground. During earthquakes, the superstructure's relative displacement is significantly reduced, thereby minimising the structural damage incurred. Auxetics, which are materials or structures with a negative Poisson's ratio, are known for possessing properties such as high energy absorption. Based on the energy absorbing capabilities of auxetic materials, it is proposed that incorporating them into base isolation structures would positively impact on the performance of the system. Therefore, the research aims to investigate the response of structures under seismic loading incorporating re-entrant hexagon layers into their base isolation system. This is assessed by defining and numerically testing the system using finite element models. The models developed for this study represent multi-story structural steel frames combined with fixed base, conventional lead-rubber bearing and auxetic composite base isolation. Differences in the response obtained from the mentioned systems are highlighted. Results indicate that the auxetic base isolation may improve the dynamic response of structures, although a unique performance is not recorded.

## **EXECUTIVE SUMMARY**

Traditionally, seismic isolators utilise solid rubber layers as part of their damping mechanism. The research undertaken provides an analysis and evaluation of a base isolation system which incorporates re-entrant hexagon layers into its design. Based on the vibrational damping performance of auxetic materials in past literature, the capabilities of auxetic materials in a structural and seismic engineering context is explored. This was done through conducting a time history analysis using three earthquakes with varying characteristic. This analysis was performed on models representing multi-story structural steel frames combined with fixed base, conventional lead-rubber bearing and auxetic composite base isolation. Differences in the response obtained from these systems are highlighted and compared with the fixed base frame which serves as a baseline for evaluating the base isolated models. Results indicate that the auxetic base isolation does have the potential to improve critical seismic performance indicators. Response comparisons drawn between the lead-rubber bearing model show that the performance of the auxetic system, particularly relating to floor accelerations, has shown a notable improvement. While the study has noted this, a unique performance of the system is not recorded. Future research should investigate the response of similar systems which incorporate three-dimensional auxetic structures as it has been found to more readily attain the mechanical properties necessary for structural applications. Additionally, topology optimisation should be used to parametrically determine the most suitable geometric properties for the auxetic materials incorporated into the base isolation structures.

# TABLE OF CONTENTS

Declaration 1 - Plaiigerism .....	i
Declaration 2 – Publications .....	ii
Acknowledgements .....	iii
Abstract .....	iv
Executive Summary .....	v
List of Tables .....	ix
List of Figures .....	x
Chapter 1: Introduction .....	1
1.1 Background .....	1
1.2 Research Question .....	2
1.3 Aims and Objectives .....	2
1.3.1 Aims .....	2
1.3.2 Objectives .....	2
Chapter 2: Literature Review .....	3
2.1 Introduction .....	3
2.2 Auxetic Materials .....	3
2.2.1 Positive and Negative Poisson’s Ratio Materials .....	3
2.2.2 Auxetic Structures and Properties .....	4
2.2.3 Current Applications .....	6
2.3 Base Isolation .....	7
2.3.1 A Brief History .....	7
2.3.2 Base Isolation Theory .....	8
2.3.3 Application of Base Isolation Systems .....	12
2.3.4 Classification of Base Isolation Systems .....	13
2.3.5 Lead Rubber Bearing (LRB) Base Isolation .....	15
Chapter 3: Methodology .....	18
3.1 Introduction .....	18

3.2	Research Approach .....	18
3.2.1	Literature Review.....	18
3.2.2	Computational Analysis.....	19
3.3	Review of Past Literature and Planning of the Study .....	19
3.3.1	Designing Models .....	19
3.3.2	Performing the Computational Analysis of the Models.....	20
3.3.3	Analysing and Comparing the Performance of the Models .....	20
3.4	Computational Analysis and Model Data .....	20
3.4.1	Superstructure .....	20
3.4.2	Lead-Rubber Bearing Base Isolator .....	22
3.4.3	Auxetic-Type Base Isolator .....	23
3.4.4	Material Properties.....	25
3.4.5	Earthquake Data.....	27
3.4.6	Meshing and Elements .....	29
3.4.7	Computational Analysis.....	33
3.5	Limitations and Uncertainties .....	35
Chapter 4:	Results and Discussion.....	36
4.1	Introduction.....	36
4.2	Eigenvalue Analysis.....	36
4.3	Time History Analysis .....	42
4.4	Northridge, California 1994.....	43
4.4.1	Total Deformation.....	44
4.4.2	Total Relative Displacement .....	48
4.4.3	Relative Displacement: X-Axis .....	51
4.4.4	Relative Displacement: Y-Axis .....	53
4.4.5	Relative Displacement: Z-Axis .....	55
4.4.6	Acceleration .....	57
4.4.7	Reaction Forces.....	59
4.5	Irpinia, Italy 1980.....	60

4.5.1	Total Relative Displacement .....	62
4.5.2	Acceleration .....	65
4.6	Düzce, Turkey 1999.....	67
4.6.1	Total Relative Displacement .....	69
4.6.2	Relative Displacement: X-Axis .....	72
4.6.3	Relative Displacement: Y-Axis .....	74
4.6.4	Relative Displacement: Z-Axis .....	76
4.7	Discussion and Recommendations.....	78
Chapter 5:	Conclusion .....	81
References.....		84
Appendix A – Irpinia, Italy .....		87
A.1	Three-Dimensional Model Deformation.....	87
A.2	Relative Displacement: X-Axis .....	90
A.3	Relative Displacement: Y-Axis .....	92
Appendix B - Düzce, Turkey .....		94
B.1	Three-Dimensional Model Deformation.....	94
B.2	Acceleration .....	97
B.3	Reaction Forces.....	99

## LIST OF TABLES

Table 3 - 1: Material Properties .....	26
Table 3 - 2: Stress-Strain Properties of Structural Steel .....	26
Table 3 - 3: Earthquake Data .....	27
Table 3 - 4: Nodes and Element Details per Model.....	30
Table 4 - 1: Eigenvalue Analysis Results .....	38
Table 4 - 2: Reaction Forces .....	59
Table B - 1: Reaction Forces.....	99

## LIST OF FIGURES

Figure 2 - 1: Deformation of positive and negative Poisson’s Ratio materials (Mir, et al., 2014) .....	4
Figure 2 - 2: Deformation of Conventional Hexagon and Re-Entrant Hexagon Structures (Mir, et al., 2014).....	5
Figure 2 - 3: Elastic Design Spectrum Graph (Chopra, 2015).....	9
Figure 2 - 4: Displacement of Fixed-Base vs Base Isolated Structures under Earthquake Loading (Mayes & Naeim, 2001) .....	10
Figure 2 - 5: Idealised Force-Displacement Hysteresis Loop (Kelly, 2001) .....	12
Figure 2 - 6: The General Classification of Base Isolation Systems.....	13
Figure 2 - 7: Cross Section through Lead Rubber Bearing (LRB) Base Isolator (Doshin Rubber Products, 2018).....	16
Figure 2 - 8: Lead Rubber Bearing (LRB) Undergoing Shear Testing (TechStar Inc., 2018).....	16
Figure 3 - 1: H203x203x46 Section Dimensions (mm).....	21
Figure 3 - 2: Ten-Story Structural Steel Superstructure.....	21
Figure 3 - 3: Typical Lead-Rubber Bearing Base Isolator Details (mm).....	22
Figure 3 - 4: Three-Dimensional Lead-Rubber Bearing Base Isolator Model.....	23
Figure 3 - 5: Typical Auxetic-Type Base Isolator Details (mm) .....	24
Figure 3 - 6: Typical Re-Entrant Hexagon Cell Details (mm).....	24
Figure 3 - 7: Three-Dimensional Auxetic-Type Base Isolator Model .....	25
Figure 3 - 8: Stress-Strain Curve of Structural Steel.....	26
Figure 3 - 9: Northridge Earthquake – California, USA 1994.....	28
Figure 3 - 10: Irpinia Earthquake – Italy 1980.....	28
Figure 3 - 11: Düzce Earthquake – Turkey 1999.....	29
Figure 3 - 12: Mesh Generated on the Superstructure .....	30
Figure 3 - 13: Mesh Generated on the LRB Base Isolator.....	31
Figure 3 - 14: Mesh Generated within the LRB Base Isolator.....	31
Figure 3 - 15: Mesh Generated on the Auxetic-Type Base Isolator.....	32
Figure 3 - 16: Mesh Generated within the Auxetic-Type Base Isolator .....	32
Figure 3 - 17: Mesh Generated on the Auxetic Layers .....	33
Figure 3 - 18: Time History Analysis Setting for Fixed Base and LRB Models vs Settings for Auxetic-Type Base Isolator .....	34
Figure 4 - 1: Mode Shapes 1, 2 and 5 of the Fixed Frame.....	39

Figure 4 - 2: Mode Shapes 10, 15 and 20 of the Fixed Frame .....	40
Figure 4 - 3 : Mode Shapes 1, 2 and 5 of the LRB System.....	40
Figure 4 - 4: Mode Shapes 10, 15 and 20 of the LRB System.....	41
Figure 4 - 5: Mode Shapes 1, 2 and 5 of the Auxetic System.....	41
Figure 4 - 6: Mode Shapes 10, 15 and 20 of the Auxetic System.....	42
Figure 4 - 7: Northridge Earthquake Data .....	43
Figure 4 - 8: Total Deformation under the Northridge Earthquake .....	44
Figure 4 - 9: Deformation of the Fixed Base System at Approximately $t = 2, 4$ and $7s$ .....	45
Figure 4 - 10: Deformation of the Fixed Base System at Approximately $t = 10, 13$ and $15s$ .....	45
Figure 4 - 11: Deformation of the LRB System at Approximately $t = 2, 4$ and $7s$ .....	46
Figure 4 - 12: Deformation of the LRB System at Approximately $t = 10, 13$ and $15s$ .....	46
Figure 4 - 13: Deformation of the Auxetic-Type System at Approximately $t = 2, 4$ and $7s$ .....	47
Figure 4 - 14: Deformation of the Auxetic-Type System at Approximately $t = 10, 13$ and $15s$ .....	47
Figure 4 - 15: Relative Displacement of Floors 1 and 2 .....	48
Figure 4 - 16: Relative Displacement of Floors 5 and 6 .....	49
Figure 4 - 17: Relative Displacement of Floors 9 and 10 .....	49
Figure 4 - 18: Average Inter-Story Drift.....	50
Figure 4 - 19: Maximum Relative Displacement.....	50
Figure 4 - 20: Orientation of the X-Y-Z Axes .....	51
Figure 4 - 21: Relative Displacement of Floors 1 and 2 about the X-Axis.....	51
Figure 4 - 22: Relative Displacement of Floors 5 and 6 about the X-Axis.....	52
Figure 4 - 23: Relative Displacement of Floors 9 and 10 about the X-Axis.....	52
Figure 4 - 24: Relative Displacement of Floors 1 and 2 about the Y-Axis.....	53
Figure 4 - 25: Relative Displacement of Floors 5 and 6 about the Y-Axis.....	54
Figure 4 - 26: Relative Displacement of Floors 9 and 10 about the Y-Axis.....	54
Figure 4 - 27: Relative Displacement of Floors 1 and 2 about the Z-Axis .....	55
Figure 4 - 28: Relative Displacement of Floors 5 and 6 about the Z-Axis .....	56
Figure 4 - 29: Relative Displacement of Floors 9 and 10 about the Z-Axis .....	56
Figure 4 - 30: Acceleration on Floor 1.....	57
Figure 4 - 31: Acceleration on Floor 5.....	58
Figure 4 - 32: Acceleration on Floor 10.....	58
Figure 4 - 33: Average Floor Acceleration with Respect to Time .....	59
Figure 4 - 34: Irpinia Earthquake Data .....	60
Figure 4 - 35: Total Deformation of the Irpinia Earthquake .....	61
Figure 4 - 36: Relative Displacement of Floors 1 and 2 .....	62
Figure 4 - 37: Relative Displacement of Floors 5 and 6 .....	62
Figure 4 - 38: Relative Displacement of Floors 9 and 10 .....	63

Figure 4 - 39: Average Inter-Story Drift.....	63
Figure 4 - 40: Maximum Relative Displacement.....	64
Figure 4 - 41: Acceleration on Floor 1.....	65
Figure 4 - 42: Acceleration on Floor 5.....	66
Figure 4 - 43: Acceleration on Floor 10.....	66
Figure 4 - 44: Düzce Earthquake Data.....	67
Figure 4 - 45: Total Deformation under the Düzce Earthquake.....	68
Figure 4 - 46: Relative Displacement of Floors 1 and 2 .....	69
Figure 4 - 47: Relative Displacement of Floors 5 and 6 .....	69
Figure 4 - 48: Relative Displacement of Floors 9 and 10 .....	70
Figure 4 - 49: Average Inter-Story Drift.....	70
Figure 4 - 50: Maximum Relative Displacement.....	71
Figure 4 - 51: Relative Displacement of Floors 1 and 2 about the X-Axis.....	72
Figure 4 - 52: Relative Displacement of Floors 5 and 6 about the X-Axis.....	73
Figure 4 - 53: Relative Displacement of Floors 9 and 10 about the X-Axis.....	73
Figure 4 - 54: Relative Displacement of Floors 1 and 2 about the Y-Axis.....	74
Figure 4 - 55: Relative Displacement of Floors 5 and 6 about the Y-Axis.....	75
Figure 4 - 56: Relative Displacement of Floors 9 and 10 about the Y-Axis.....	75
Figure 4 - 57: Relative Displacement of Floors 1 and 2 about the Z-Axis .....	76
Figure 4 - 58: Relative Displacement of Floors 5 and 6 about the Z-Axis .....	77
Figure 4 - 59: Relative Displacement of Floors 9 and 10 about the Z-Axis .....	77
Figure A - 1: Deformation of the Fixed Base System at Approximately $t = 2, 4$ and $7s$ .....	87
Figure A - 2: Deformation of the Fixed Base System at Approximately $t = 10, 13$ and $15s$ .....	87
Figure A - 3: Deformation of the LRB System at Approximately $t = 2, 4$ and $7s$ .....	88
Figure A - 4: Deformation of the LRB System at Approximately $t = 10, 13$ and $15s$ .....	88
Figure A - 5: Deformation of the Auxetic-Type System at Approximately $t = 2, 4$ and $7s$ .....	89
Figure A - 6: Deformation of the Auxetic-Type System at Approximately $t = 10, 13$ and $15s$ .....	89
Figure A - 7: Relative Displacement of Floors 1 and 2 about the X-Axis.....	90
Figure A - 8: Relative Displacement of Floors 5 and 6 about the X-Axis.....	90
Figure A - 9: Relative Displacement of Floors 9 and 10 about the X-Axis.....	91
Figure A - 10: Relative Displacement of Floors 1 and 2 about the Y-Axis.....	92
Figure A - 11: Relative Displacement of Floors 5 and 6 about the Y-Axis.....	93
Figure A - 12: Relative Displacement of Floors 9 and 10 about the Y-Axis.....	93
Figure B - 1: Deformation of the Fixed Base System at Approximately $t = 2, 4$ and $7s$ .....	94

Figure B - 2: Deformation of the Fixed Base System at Approximately $t = 10, 13$ and $15s$ .....	94
Figure B - 3: Deformation of the LRB System at Approximately $t = 2, 4$ and $7s$ .....	95
Figure B - 4: Deformation of the LRB System at Approximately $t = 10, 13$ and $15s$ .....	95
Figure B - 5: Deformation of the Auxetic-Type System at Approximately $t = 2, 4$ and $7s$ .....	96
Figure B - 6: Deformation of the Auxetic-Type System at Approximately $t = 10, 13$ and $15s$ .....	96
Figure B - 7: Acceleration on Floor 1 .....	97
Figure B - 8: Acceleration on Floor 5 .....	98
Figure B - 9: Acceleration on Floor 10 .....	98

# CHAPTER 1: INTRODUCTION

## 1.1 Background

The impacts of earthquakes on structures and services has historically resulted in large scale damage, leading to great financial implications. This has led to multiple alterations the seismic design philosophy of structures in earthquake prone areas. Some of these improvements to the design criteria include increasing the lateral strength of a structure and considering ductility in the design. However, due to high construction costs, among other factors, it is not a practical measure to increase a building's strength indefinitely. The concept of decoupling a structure from its substructure was introduced as a means of isolating it from the harmful effects of the earthquake. Base isolation systems aim to reduce the physical demand placed on a building as opposed to improving the ability of the building to resist the seismic vibrations. By incorporating base isolation into a buildings design, this relieves a building's structural components from the role of dissipating seismic energy and significantly reduces the structure's relative displacements induced by the seismic waves.

Past literature shows that auxetic or negative Poisson's Ratio materials are capable of vibration damping and high energy absorption. This property is derived from its unusual deformation characteristics resulting from its internal microstructure. When a tensile force is applied on an auxetic structure along one direction, it expands in the direction perpendicular to the force as opposed to most structures which shrink in that direction. Based on the energy absorbing capabilities of auxetic materials, it is proposed that incorporating auxetic materials into base isolation structures would positively impact on the performance of the system.

Traditionally, seismic isolators utilise solid rubber layers as part of their damping mechanism. This study explores replacing the rubber layers with layers of re-entrant hexagon auxetic layers in order to evaluate the vibration damping capabilities of auxetics in a structural and seismic engineering context. The performance of the proposed auxetic-type system will be analysed and evaluated by numerically testing a finite element model. The response of the model, composed of the isolation system and a ten-story structural steel frame, is evaluated with respect to performance indicators as defined by Kelly (2001) and Chopra (2015). Comparisons are drawn between the auxetic systems response and the response of similar sized fixed base and a lead-rubber bearing isolation system models which serve as a baseline against which the holistic performance is measured.

## **1.2 Research Question**

How would a structure incorporating re-entrant hexagon layers into its base isolation system, respond to seismic loading?

## **1.3 Aims and Objectives**

### **1.3.1 Aims**

- To incorporate auxetic materials into base isolation.
- To carry out numerical analyses on fixed base, lead-rubber bearing and the auxetic-type base isolation systems.

### **1.3.2 Objectives**

- Determine the seismic performance of the fixed base, lead-rubber bearing and the auxetic-type base isolation systems.
- Evaluate the performance of the auxetic-type system relative to the fixed base and lead-rubber bearing systems.

## CHAPTER 2: LITERATURE REVIEW

### 2.1 Introduction

This chapter details information and explores concepts, applications and technology pertaining to auxetic materials, earthquakes and base isolation systems. Whilst exhibiting this information, it serves as a theoretical framework to support and justify the methodological approach and outcomes resulting from the research.

### 2.2 Auxetic Materials

#### 2.2.1 Positive and Negative Poisson's Ratio Materials

Poisson's ratio serves as a numerical indication of a material's performance under deformation and is considered to be one of the most fundamental mechanical properties of a material (Mir, et al., 2014). When a material under a compressive force, it has a tendency to expand in the direction perpendicular to the force. Likewise, should a tensile force be applied to the material, it will contract in the direction perpendicular to the force. The ratio is defined as the negative of the ratio of lateral strain to axial strain, i.e.  $\nu = -\frac{\epsilon_{lateral}}{\epsilon_{axial}}$ . Poisson's Ratio has provided greater insight into the way in which a material is expected to deform (Liu, 2006; Ungureanu, et al., 2015). A greater understanding of a property such as this is essential when optimising performance in situations whereby deformation should be minimised. The theory behind Poisson's Ratio has also resulted in the relationship between the Bulk and Shear Moduli of a material being defined (Lakes, 1993).

These parameters hold true for most conventional materials, however there exists a group of materials which possesses a negative Poisson's Ratio. These materials are known as auxetic materials. The term 'auxetic' is derived from the Greek word *auxetos* which means 'that which may be increased' (Stavroulakis, 2005; Liu, 2006). Unlike conventional materials, these auxetic or negative Poisson's Ratio (NPR) materials experience a contraction in the transverse direction while under a compressive force and expand while under a tensile force (Ungureanu, et al., 2015). Figure 2-1 provides a graphical representation of the deformation of both positive and negative Poisson's Ratio materials.

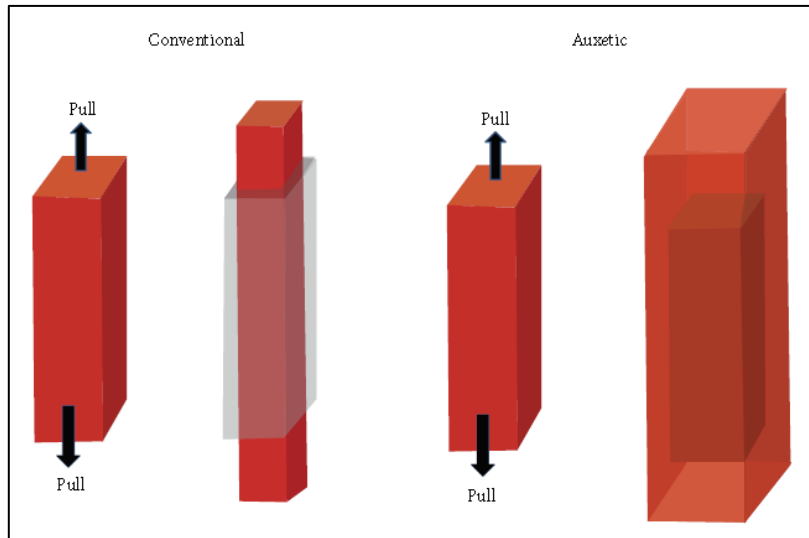


Figure 2 - 1: Deformation of positive and negative Poisson's Ratio materials (Mir, et al., 2014)

## 2.2.2 Auxetic Structures and Properties

Mir, et al. (2014) has found that all auxetic materials possess a microstructure which is conducive to creating a negative Poisson's Ratio. This microstructure generally involves a deformation method such as hinging, rotating, stretching or bending. While most auxetic materials are man-made porous foams or hinged metamaterials with re-entrant type microstructures, natural auxetic materials do exist (Dagdelen, et al., 2017). For example, living bone tissue is a natural, anisotropic auxetic material. (Ungureanu, et al., 2015).

Majority of designed auxetic materials are based on a few simple motifs. The simplest auxetic structure is based on the general shape of a bow tie (Ungureanu, et al., 2015). The 'bow tie' auxetic structure is more commonly known as the re-entrant hexagon structure. This structure is a modified, non-convex or inverted form of a simple hexagon structure. As displayed in figure 2-2, a conventional hexagonal or honeycomb structure presents a typical positive Poisson's Ratio behaviour when it is exposed to a lateral load. By slightly reorienting the hexagonal geometry to adopt a re-entrant structure, the modified honeycomb is seen to exhibit an auxetic behaviour. The re-entrant hexagon structure is anisotropic in nature, displaying different Poisson's Ratio values when loaded about the x and y axes respectively (Stavroulakis, 2005; Mir, et al., 2014).

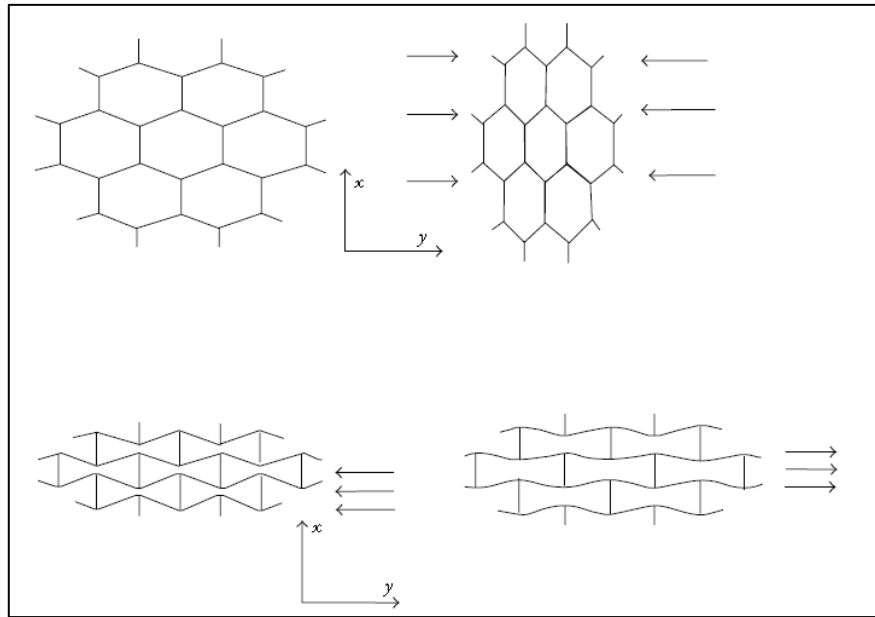


Figure 2 - 2: Deformation of Conventional Hexagon and Re-Entrant Hexagon Structures (Mir, et al., 2014)

The field of auxetic materials has developed substantially with numerous auxetic structures having been discovered. In addition to the re-entrant hexagon, other extensively researched auxetic structures include rotating rectangles and triangles, arrowhead and star shaped arrangements (Ma, et al., 2013). These auxetic structures have been manufactured into foams, polymers, composites and metals (Zhang & Yang, 2016).

Mir, et al. (2014) noted that the unique deformable nature of auxetics is also independent of the scale of the structure. Therefore, mechanical properties exhibited in auxetic structures will be applicable at a micro and macro scale. Additionally, it has been shown that auxetic materials may be designed based on the principal that the global stiffening effects of the structure may be determined by a unit cell of the auxetic material (Zhang & Yang, 2016).

The Poisson's ratio of isotropic elastic materials is typically a positive value, ranging between 0 and 0.5. This limit is based on the constraint that no material instabilities are allowed for and that no energy is produced during any possible deformation of the material. The upper limit of the Poisson's Ratio of isotropic materials is 0.5, which is defined by the functions of thermodynamics. Particularly this refers to incompressible materials as well as rubber-like materials and polymers. Certain unique internal structures and materials may fall within the negative range of the Poisson's Ratio limit. Typically, this occurs in materials with a low bulk modulus and a high shear modulus.

While isotropic materials are bound by this limit, the theory of anisotropic elasticity does not preclude the existence of negative Poisson's Ratio materials. Anisotropic materials may pass this limit due to the nature of their structure resulting in the material to perform in an irregular manner. The Poisson's Ratio limits for anisotropic materials is related to the material's elasticity constraints. Therefore, it is theoretically possible for the Poisson's Ratio to reach significantly large and small values (Theocaris, et al., 1997; Stavroulakis, 2005; Mir, et al., 2014).

According to Hu, et al. (2018), when cellular structures such as auxetic materials are used in a practical engineering setting, the plasticity of the material plays an essential role in the overall performance. This is especially important in systems used for energy absorption. A study carried out by (Scarpa, et al., 2005) analysed the static and dynamic properties of polyurethane foams with an auxetic microstructure. The tests carried out aimed to evaluate the vibration reduction properties of foams for use in gloves in order to protect workers from the harmful effects of mechanical vibrations. In comparison to a non-auxetic polyurethane foam, the auxetic foam exhibited a notable increase in stiffness while under compression. This result correlates with studies undertaken by Yang, et al. (2015) who, along with Zhang & Yang (2016), noted the significant effects that the Poisson's Ratio of an auxetic cell has on its mechanical properties. In practical testing conducted in these studies, larger Poisson's Ratios largely corresponded with larger strength values. In their research on two-dimensional re-entrant hexagon structures, Zhang & Yang (2016) found that the vibration isolation performance of these structures is dependent on various geometric properties of the auxetic cells. Numerical modelling results has shown that optimisation of the cell thickness and cell angle of an auxetic cell results in significant increases in the vibration level difference, when compared to preliminary models.

### **2.2.3 Current Applications**

In terms of their practical applications, auxetics have been found to exhibit heightened hardness and bending stiffness as well as shear and buckling resistance. Auxetic materials are notable proficiency in decreasing the propagation of imposed vibrations (Dagdelen, et al., 2017; Hu, et al., 2018). Due to these properties, the development of auxetic materials has facilitated the advancement and improvement of a technology in various fields such as the automobile and aerospace industries, the medical field, the defence industry (particularly in high-performance body armour) and in sports equipment (Jiang & Hu, 2017). Auxetics are

effective in designing components with a double curvature such as aircraft wings and car doors (Zhang & Yang, 2016).

## **2.3 Base Isolation**

Kelly (2001) likens the relationship between earthquakes and the need for base isolation as one of demand and supply. Due to the unpredictable nature of earthquakes, buildings which require base isolation must have a system in place which possesses the capacity to perform well under unexpected ground accelerations. Base isolation systems aim to reduce the physical demand placed on a building as opposed to improving the capacity or ability of the building to resist the seismic vibrations. By incorporating base isolation into a buildings design, this relieves a building's structural components from the role of dissipating seismic energy. This in turn significantly reduces damage to the structure and the architectural façade during an earthquake (Mayes & Naeim, 2001).

### **2.3.1 A Brief History**

The concept of base isolation is believed to have originated in the late 1800s in Japan. Upon the turn of the century, similar ideas began to develop around the world with the earliest recorded patent being filed by a British medical doctor. Dr J.A. Calentarients theorised that if a building were to be constructed on a layer of fine sand, mica or talc, this may enable the building to slide when exposed to seismic loading. The idea was that this induced sliding motion would reduce the seismic energy transmitted to the building, thereby reducing the damaged ensued as a result of the earthquake. Over time the flexible nature of rubber was viewed as a potential means of increasing the flexibility of the base isolation system. This prompted the development of laminated rubber bearings (LRB). These bearings provide high stiffness in the vertical direction which is suitable to support the mass of the superstructure, while in the horizontal direction LRBs are flexible enough to move when subjected to seismic loading. Developments in the study of base isolation combined with an improvement in isolation material as well as more sophisticated methods of modelling and analysing the performance of base isolation has led to base isolation becoming a practical means of earthquake protection (Bhuiyan & Okui, 2012; Ismail, 2018).

### **2.3.2 Base Isolation Theory**

In seismic theory, frequency is the number of vibrational cycles made by a seismic wave per second. As a whole, an earthquake is comprised of vibrations of different frequencies which are complexly superimposed. This complexity of the vibrations is determined by the site, soil conditions and the path of the seismic waves. Each structure possesses its own set of frequencies which determine the response of the system to ground motion events. The lowest of these frequencies is known as the fundamental frequency. As the frequency of the seismic loading on a structure reaches the fundamental frequency of the structure, resonance will start to occur. Historically, resonance can be described as highly unfavourable in any structure. The effect of resonance intensifies the response of a structure to the applied seismic loading, which can lead to widespread structural damage or as a worst case, structural failure (Nelson, 1999; Chopra, 2015).

Base or seismic isolation is a vastly used means of minimising the harmful effect of seismic vibrations on buildings and various other structures. It assists by reducing damage to these relatively stiff buildings by decoupling the structure from the horizontal components of the earthquake i.e. the x and y components of the seismic loading. The decoupling of the structure is achieved by the addition of a flexible component, to the otherwise rigid structure, at the isolation level. This enables resonance to be avoided as the fundamental frequency of the building is now out of direct contact with the major range of frequencies associated with earthquakes (Varnava & Komodromos, 2012; Cancellara & De Angelis, 2016).

The fundamental principle of seismic isolation is to incorporate an element of lateral flexibility at the base of a structure, while simultaneously including a damping element to the structure (Mayes & Naeim, 2001). This is achieved by the addition of an isolation system between the structure and the foundation. With the addition of this system, the new natural period of the base isolated structure is considerably longer when compared to the natural period of the rigid fixed-base structure. By elongating the natural period of a structure using base isolation, it is possible to reduce the base acceleration experienced by the structure. Thereby, the resultant damage on the structure is reduced (Chopra, 2015). The elastic design spectrum displayed in figure 2-3 graphically presents this concept.

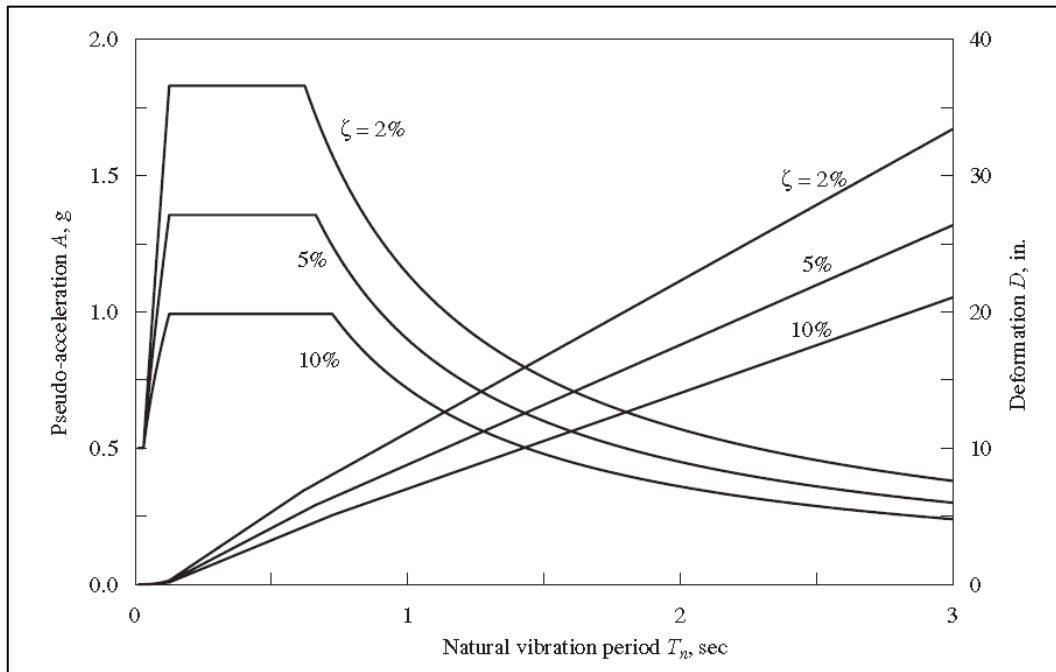


Figure 2 - 3: Elastic Design Spectrum Graph (Chopra, 2015)

An increase in the natural period implies that there is an increase in displacement, however the displacement is focused primarily on the isolation system. Deformation in the superstructure will still occur, although the deformation is notably reduced when compared to a fixed-base structure. The two primary mechanisms related to ground motion that leads to structural and non-structural damage is the inter-story drift between floors in a building as well as floor accelerations. The inter-story drift in a building refers to the relative displacement between two floors, divided by the height of that story. While floor acceleration describes the absolute acceleration that occurs on a floor as a result of seismic vibrations. In most buildings, the floor acceleration increases in higher floors in a structure (Mayes & Naeim, 2001; Chopra, 2015). Figure 2-4 illustrates the behaviour of fixed-base structures and base isolated structures when exposed to seismic loading. When comparing fixed base and base isolated structures, the prominence of inter-story drifts in fixed base structures is highlighted. Significant inter-story drifts lead to notable damage in the fixed base structure, as compared to a base isolated structure.

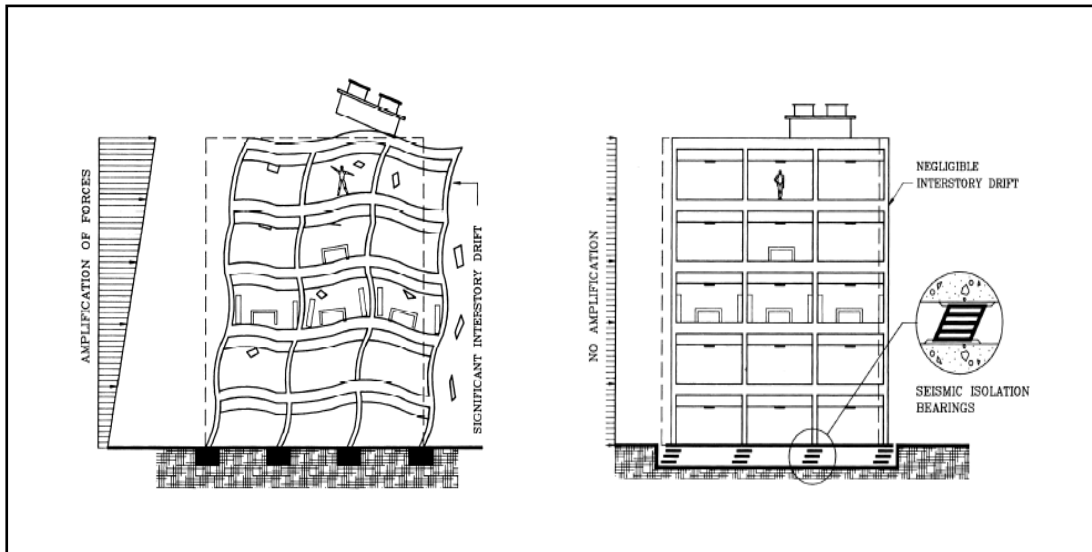


Figure 2 - 4: Displacement of Fixed-Base vs Base Isolated Structures under Earthquake Loading (Mayes & Naeim, 2001)

Earthquakes are able to generate inertial forces that are proportionate to the product of the mass of a building and the seismic vibrations. In order to avoid structural damage from larger ground accelerations, a building's structural characteristics will need to be improved in order to resist the earthquake. However, this is only feasible to a certain extent. Due to high construction costs, among other factors, it is not a practical measure to increase a building's strength indefinitely (Kelly, 2001).

By providing a structure with a base isolation system, the seismic performance of the structure improves and allows for the seismic design loading on the structure itself to be reduced, thereby ensuring that its construction remains feasible. The primary design objective of base isolated structures is achieved by ensuring that the system is proficient in dissipating seismic vibrations as well as controlling the displacement and structural damage associated with the maximum design earthquake. However, the base isolation system must be capable of resisting lateral service loads, such as wind loading, without yielding. Should the system be unable to counteract these service loads, unacceptable displacements will occur (Mayes & Naeim, 2001). Kircher (2012) states that the system must allow the superstructure to remain in an essentially elastic state during an earthquake. It is critical for the ductility demand of the base isolation to remain limited in order for the optimal functioning of the system. Should the superstructure respond to the seismic vibrations in a notable inelastic manner, this may result in excessively large inter-story drifts resulting from long period of vibration. According to Kelly (2001), excessive ductility in a structure may result in its natural period degrading to a

new natural period similar to that of the base isolation system. This may lead to the structure and base isolation system essentially becoming ‘coupled’ and introducing the possibility of resonance in the system.

Base isolation systems have been found to work optimally when incorporated into relatively heavy structures. This is due to the relationship between the period and the mass of the isolated structure. The period (T) is proportional to the square root of the mass of the isolated structure (M) and inversely proportional to the stiffness (K). This relationship is represented by the

formula:  $T = 2\pi \sqrt{\frac{M}{K}}$ . In buildings with a low mass, a base isolation system with a relatively low stiffness should be incorporated (Kelly, 2001).

Chopra (2015) describes damping as the process in which free vibration progressively diminishes in amplitude. In simple experimental models, it is reasonably assumed that energy from the continuous elastic straining of the models and its internal friction is converted to thermal energy which is subsequently released. However, in buildings, energy dissipation occurs through mechanisms such as friction at steel connections and the opening and closing of micro cracks in concrete. In base isolation systems, damping is usually considered as either viscous, dependent on velocity, or hysteretic, dependent on displacement (Kelly, 2001). When an object is subjected to cyclic loading or deformations, this suggests that a force-displacement hysteresis loop is applicable. Hysteresis loops serve as an accurate means of representing the energy dissipation in base isolation systems considering that earthquakes can induce a type cyclic deformation in buildings (Chopra, 2015). Mayes & Naeim (2001) consider hysteretic energy dissipation to be an efficient and effective method of providing a considerable level of damping to a system. The term hysteric describes the offset in the loading and unloading curves under the cyclic loading that the system is subjected to. During the unloading phase, most of the work done is recovered, however a portion is converted to and lost as thermal energy. Figure 2-5 illustrates the idealised force-displacement hysteresis loop. Kelly (2001) states that lengthening a system’s period, brought about by the addition of base isolation, generally reduces the acceleration, but increases the total displacement of the system. Conversely, in most instances, damping will lead to the reduction of both acceleration and displacement in a structure subjected to ground motion. However, this reduction in acceleration is brought about with respect to base shear, which is controlled by the first mode response. Notably high damping may result in higher accelerations in higher modes of the system. Therefore, high damping may not always be the optimal solution.

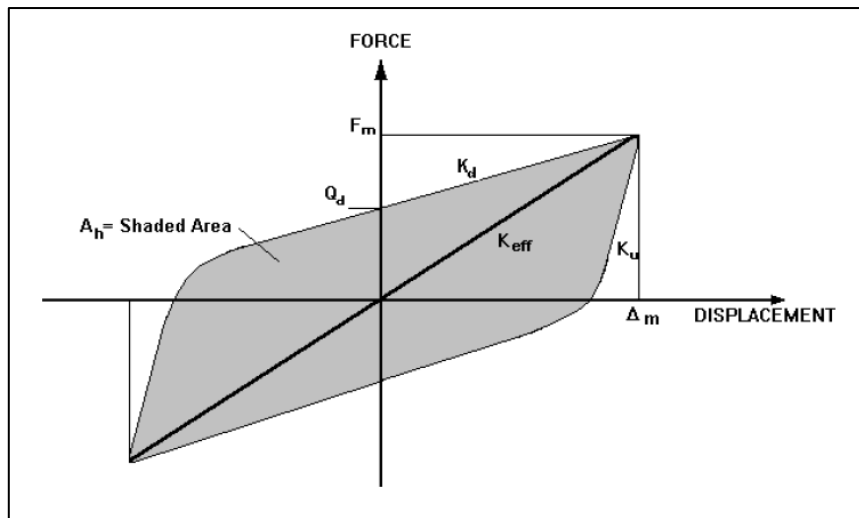


Figure 2 - 5: Idealised Force-Displacement Hysteresis Loop (Kelly, 2001)

According to Kelly (2001), flexibility and damping properties of a base isolation system are two of the core mechanical properties responsible for the improvement of a structure's response to ground motion. Flexibility in particular has the more notable effect if the isolation system's period is fairly short, with an approximate limit of 0.7 seconds. A reduction in acceleration brought about by flexibility is dependent on the overall stiffness of the building, while damping is capable of accomplishing the same outcome, it does so independent of the structure's stiffness property.

### 2.3.3 Application of Base Isolation Systems

A base isolation system can be a highly costly element of a building. It is necessary to perform a cost benefit analysis to determine if base isolation would be suitable as opposed to alternate measure of earthquake resistance (Kelly, 2001). Owing to their considerable financial implications, base isolation is more frequently used in medium to moderately high-rise buildings and important buildings, such as hospitals, as opposed to low-rise residential buildings (Varnava & Komodromos, 2012). The potential seismic dissipation benefits of base isolation are most pronounced in stiff structures which are rigidly fixed to the ground and structures which have a short fundamental period. The fundamental period of a building increases with an increase in height. There is a limit at which the natural period of a building is long enough to resist low earthquake forces without the necessity for base isolation. Hence, base isolation is most effective in low to medium rise buildings as opposed to high-rise buildings. It has also been found to be effective in structures such as bridges, nuclear power

plants and various types of equipment. Tectonic conditions and the nature of the soil that a structure has been founded on may not be conducive to base isolation. Particularly soft soils have been known to result in poor performance in base isolation systems (Mayes & Naeim, 2001). Kelly (2001) notes that soft soils result in the long period motion being lengthened. This is a common occurrence in alluvial basins and may lead to resonance in the isolated period range. In such cases, base isolation may prove to negatively impact on the seismic performance of the building. Structures which are founded on rock or stiff soil conditions result in the optimum performance of base isolation systems.

### 2.3.4 Classification of Base Isolation Systems

The most frequently used forms of base isolation can be divided into two categories, sliding bearings and laminated rubber bearings (Varnava & Komodromos, 2012). In figure 2-6, the different types of base isolation systems are categorised into their respective groups.

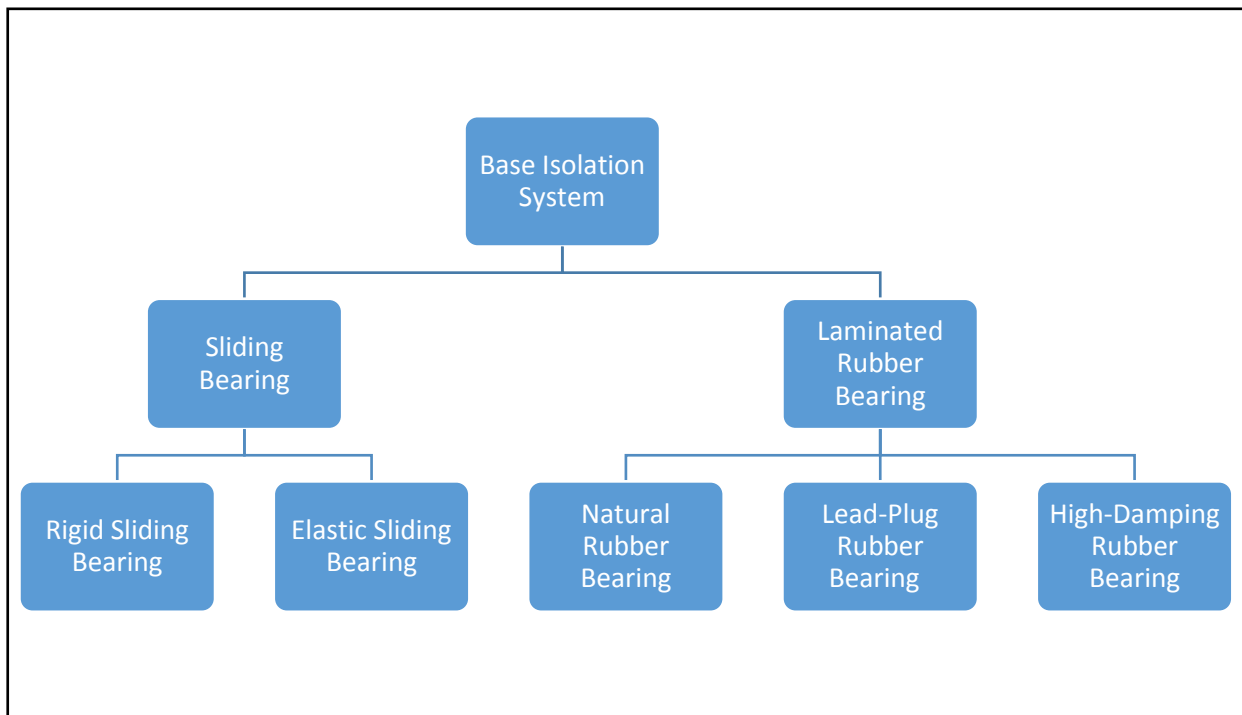


Figure 2 - 6: The General Classification of Base Isolation Systems

All base isolation systems essentially carry out the same task of decoupling a structure from the ground, however sliding and laminated rubber bearings achieve this through a slightly different means.

#### **2.3.4.1 Sliding Bearing Systems**

The broad class of sliding base isolation systems operate on the fundamental mechanism of frictional sliding, whereby a frictional force within the system resists motion induced by seismic vibrations and dissipates its energy (Fallah & Zamiri, 2012). The sliding system allows for the shear force transferred to the across the structure-isolator interface to be limited. This is achieved by ensuring that the coefficient of friction is as low enough to allow the system to remain practical. A frictional coefficient which is too low will be unable to sustain significantly strong wind loading as well as minor earthquakes and tremors without sliding (Chopra, 2015). By employing a coefficient of friction that is significantly high, the performance of the sliding system will be compromised especially when it is subjected to minor to moderate seismic vibrations (Chakraborty, et al., 2016).

Most variations of this type of base isolation includes three shared attributes, namely a friction slider, a sliding surface and an enclosed cylinder for lateral displacement restraint (Tafheem, et al., 2015). Flat sliding bearings are able to reduce the inter-story drifts in a building by reducing the transfer of forces from the ground to the superstructure. This is regardless of the frequency composition of the seismic waves. These flat bearing do not have the capabilities to produce a restoring force, thereby they are unable to re-centre themselves. This may result in residual displacements (Chakraborty, et al., 2016).

Due to this issue, sliding base isolation systems are often accompanied by high-tension springs or laminated rubber bearings to induce a restoring force and control the sliding displacements. Another means of generating this restoring force is by introducing a curved surface into the sliding system. This has been implemented in a popular form of sliding base isolation, the friction pendulum system (FPS). Its isolation method combines the traditional system of sliding isolation with the response mechanism of a pendulum. This system supports the weight of the structure on a set of concave, spherical surfaces. The structure slides relative to the FPS system once the imposed seismic waves surpass the threshold of the concave surfaces' coefficient of friction. The concave, spherical nature of the FPS system's plates results in the structure being slightly raised during ground motion. This results a restoring force being induced by the pendulum mechanism of the system, thereby enabling the system to return to its equilibrium position (Chopra, 2015; Tafheem, et al., 2015).

#### **2.3.4.2 Laminated Rubber Bearings**

Laminated rubber bearings are highly dependent on the mechanical properties of the isolation system. Typically, this class of base isolation adopt an overall square or circular form. Each isolator consists of alternating layers of rubber and steel plates, connected by means of vulcanisation. This is a chemical process whereby rubber or other polymers are made to be more durable by altering the material's structure through creating crosslinks with other elements such as sulphur. The steel plate within the base isolators assist the system by increasing its vertical stiffness, thereby preventing the rubber layers from 'bulging' laterally under the substantial vertical loading of the structure. In general, the type of rubber used in laminated bearings is either characterised as soft, normal or hard. The mechanical properties of the type of rubber compound used in the system has an impact on the damping capacity of the system, with damping in the range of 2 to 3 per cent of critical damping. The natural rubber bearings used in these systems have been shown to exhibit linear behaviour while in shear up to shear strains above 100 per cent. Their shear moduli usually vary between 0.4 MPa to 1,4 MPa (Choun, et al., 2014; Rizzian, et al., 2017).

#### **2.3.5 Lead Rubber Bearing (LRB) Base Isolation**

The scope of this study focuses on a type of laminated rubber bearing, the lead-core or lead-plug rubber bearing. This type of laminated bearing is comprised of alternating cylindrical or square rubber bearings and steel plates. Additionally, at the centre of the base isolator is a short cylindrical core or plug made of lead. This system provides a great deal of stiffness under the considerable vertical load from the superstructure and is simultaneously flexible while under horizontal loading from an earthquake (Chopra, 2015). According to Kelly (2001), the damping ability of natural rubber is limited to 2-3% of the critical viscous damping. This is relatively low and therefore negatively impacts on the bearing's ability to dissipate seismic energy. Due to this property, the base isolation system may incorporate a lead core to provide additional damping to the system. Additionally, the lead core introduces an element of non-linearity into the system (Chopra, 2015). Figure 2-7 displays a cross section through the centre of a LRB base isolator, while figure 2-8 shows a LRB base isolator undergoing shear testing while being subjected to a cyclic load.

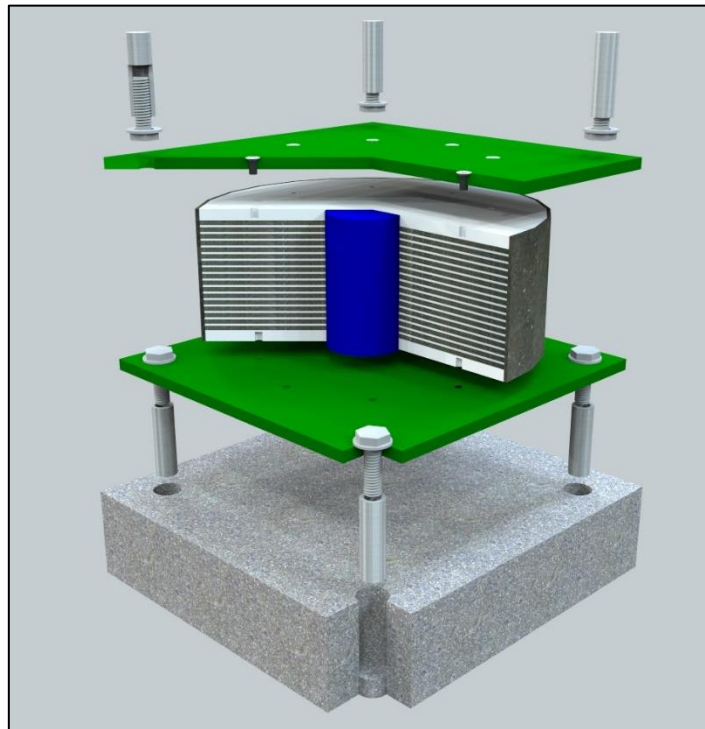


Figure 2 - 7: Cross Section through Lead Rubber Bearing (LRB) Base Isolator (Doshin Rubber Products, 2018)



Figure 2 - 8: Lead Rubber Bearing (LRB) Undergoing Shear Testing (TechStar Inc., 2018)

During typical static conditions, base isolated structures behave in a similar manner as conventional fixed base structure. It is necessary for a base isolator to provide low lateral stiffness under earthquake loading, but provide enough stiffness to remain un-deformed under

typical static conditions. During an earthquake, the lead core yields in almost pure shear which leads to the dissipation of seismic energy through hysteresis damping. Lead was identified as an ideal material for the core due to its low yield stress of approximately 10 MPa and its elastoplastic load deformation relationship. The lead core yields at a low level of stress and under normal temperature conditions which induces the hysteric behaviour. This remains stable over multiple cycles due to the lead core recrystallizing at these temperatures. Therefore, this allows for the core to yield numerous times without this occurrence resulting in fatigue failure. In this application, the fatigue and mechanical characteristic of lead is shown to be highly advantageous to its purpose in the LRB isolator. Furthermore, the lead core can also improve the damping characteristics of the system especially in cases where a soft rubber is used (Skinner, et al., 1993; Choun, et al., 2014).

## **CHAPTER 3:    METHODOLOGY**

### **3.1 Introduction**

This chapter presents the methodological approach undertaken to analyse and assess performance of auxetic-type base isolation compared to lead rubber bearing base isolation systems. The vibration damping capabilities of both base isolation systems is analysed and compared to a fixed base frame, in order to evaluate the performance of the systems relative to a neutral baseline. Furthermore, research undertaken, relevant data collected and analysed as well as the influence of limitations and uncertainties to the results attained is discussed.

The methodological approach includes the following:

1. Research Approaches
2. Review of past literature and planning of the study
3. Data analysis
4. Limitations and uncertainties

### **3.2 Research Approach**

In order to achieve the aims specified in Chapter 1, the most appropriate research approaches must be implemented to ensure that the most accurate outcome. Two research approaches were deemed to be the most suitable methods for a study of this nature. These approaches are the ‘theoretical’ and ‘computational’ based approaches. The integration of the two research approaches will ensure that data is most accurately collected, analysed and represented.

#### **3.2.1 Literature Review**

The literature review involves the investigation of past literature pertaining to the topic. It provides detailed background information into the topic to provide greater insight into each element involved in the study through research into theoretical concepts, theoretical models and past analyses that have been undertaken. The literature examined should be used to enhance the understanding and interpretation of any data collected as well as support findings.

### **3.2.2 Computational Analysis**

Undertaking a computation analysis involves creating models relating to the area of study and investigating properties and the mechanical performance of the models in order to achieve the desired aims of the study. This form of research generates empirical data which is unique to the models being investigated in the study. The knowledge gained from the theoretical approach will allow for the data to be more accurately analysed, interpreted and evaluated. Moreover, the models created and the parameters that are investigated are determined and reinforced by the theoretical part of the study. This research approach will aid in filling in gaps in research in the vibrational reduction potential of auxetic materials when incorporated into structures.

### **3.3 Review of Past Literature and Planning of the Study**

In the initial stages of the study, a literature review was performed in order to attain greater insight into the topic. This research enabled the structuring of the report as well as the preparation of a research proposal. The literature review drew upon research from journal articles, research reports and published theoretical books among other sources with information relevant to the study.

The knowledge gained from this portion of the research also aided in the formulation of a methodological approach for the computational analysis portion of the research approach. The following steps serves as an outline of the methodological approach:

1. Designing models
2. Performing the computational analysis of the models
3. Evaluating and comparing the performance of the models

#### **3.3.1 Designing Models**

Models should be designed and drawn based on the insight gained from the literature review. The dimensions of the super structure such as width, breadth and story height should be reasonable when compared to practical structures so as to ensure that results gained from the study are accurate and reliable. Properties of the superstructure such as mass, geometric properties and static loading should be considered when sizing the base isolation system. The

properties of the materials used should be extensively investigated and chosen based on the aim and nature of the study being undertaken.

### **3.3.2 Performing the Computational Analysis of the Models**

Earthquake data should be collected and analysed to ensure that it is suitable to be used in the study being undertaken. The properties and behaviour of the earthquake should be identified in order to predict the response of the models during the analysis phase. To determine the response of the systems to seismic loading, a non-linear time history analysis should be performed. Subsequently an eigenvalue analysis should be performed in order to determine properties such as the natural frequency and the natural period of the models.

### **3.3.3 Analysing and Comparing the Performance of the Models**

In order to evaluate the performance of the models, performance indicators should be identified from past literature. This allows for the evaluation criteria to be justified and the behaviour and performance of the models to be correctly interpreted and analysed. Properties such as total and axial relative displacement of floors, inter-story drifts and acceleration per floor should be considered in this assessment. Moreover, data should be graphically represented in appropriate formats in order to most effectively display the results.

## **3.4 Computational Analysis and Model Data**

### **3.4.1 Superstructure**

The superstructure of the models consists of beams and columns made from 203x203x46 H Sections as defined by the Red Book of Steel (South African Institute of Steel Construction, 2013). The dimensions of the H-Section are shown in figure 3-1. It is ten stories high with a story height of 3.5m and a floor dimension of 5m x 5m. The total height of the superstructure is 35m. In the case of the fixed frame model, fixed supports are considered on the base of the four steel columns. Figure 3-2 shows the steel superstructure.

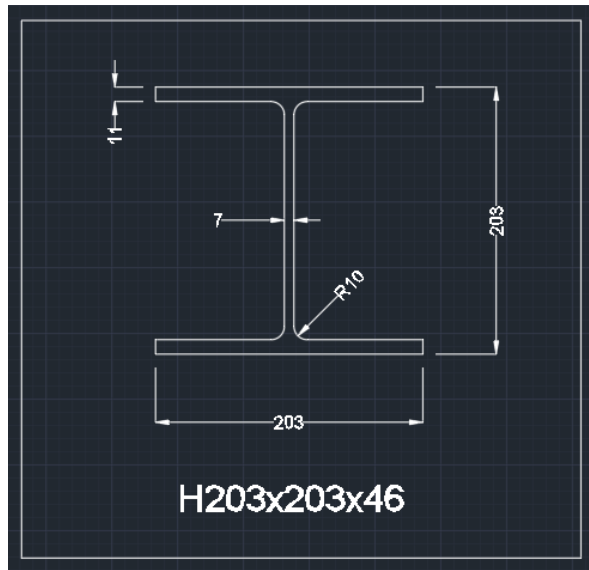


Figure 3 - 1: H203x203x46 Section Dimensions (mm)

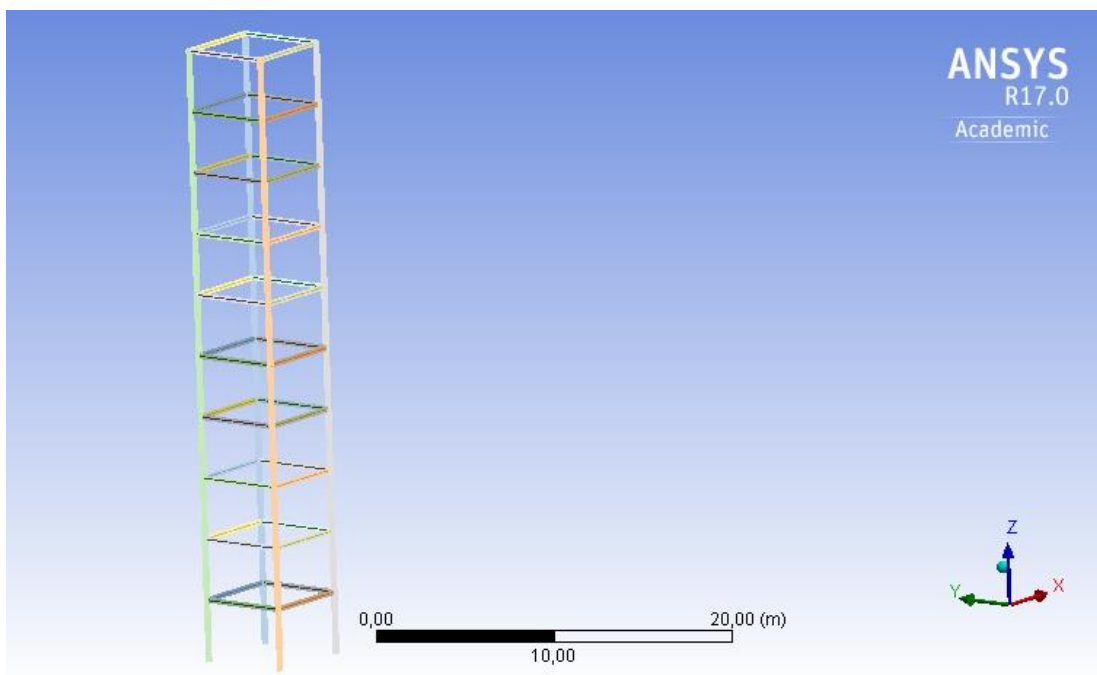


Figure 3 - 2: Ten-Story Structural Steel Superstructure

### 3.4.2 Lead-Rubber Bearing Base Isolator

The lead-rubber bearing base isolator consists of 0.14 m x 0.14 m x 0.01 m steel layers between rubber layers of the same dimensions. In the middle of these layers, lies the lead core with a height of 0.15 m and a radius of 0.02 m. At both the top and the bottom of the base isolator are two 0.3 m x 0.3 m x 0.01 m steel plates. The bottom steel plate is fixed to the surface and the top steel plate is bonded to the bottom faces of the superstructure. Figure 3-3 depicts a typical cross-section and top view of the LRB base isolator, while figure 3-4 shows a three-dimensional view of the base isolator.

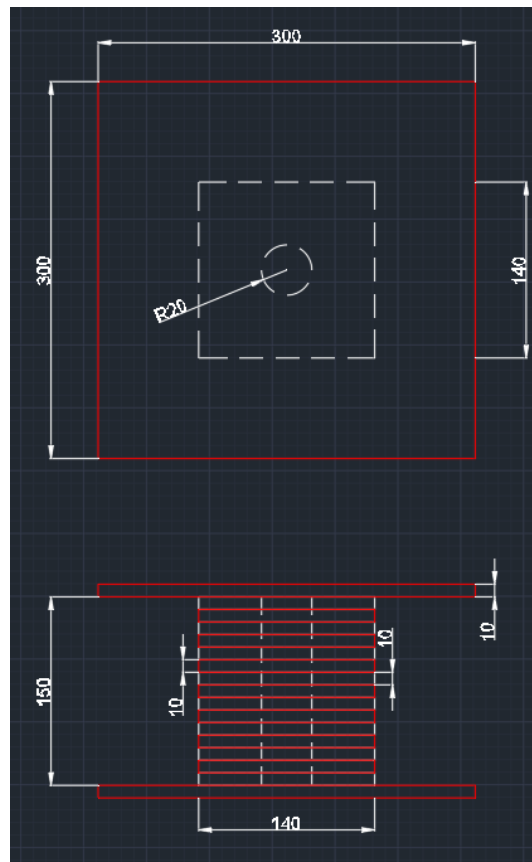


Figure 3 - 3: Typical Lead-Rubber Bearing Base Isolator Details (mm)

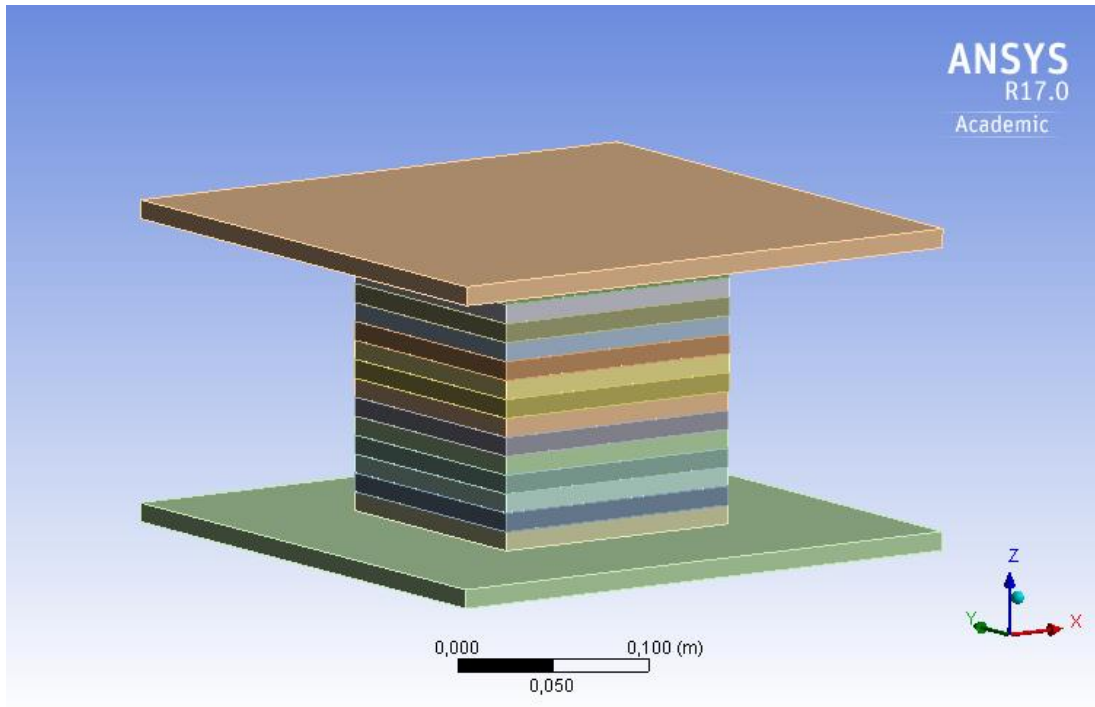


Figure 3 - 4: Three-Dimensional Lead-Rubber Bearing Base Isolator Model

### 3.4.3 Auxetic-Type Base Isolator

The dimensions and general configuration of the auxetic-type base isolator was chosen to be similar to that of the LRB base isolator in order to evaluate the two systems based on the same geometric criteria. The dimensions of the auxetic-type base isolator are shown in the typical cross-section and top view in figure 3-5. In this model, the rubber layers in the LRB base isolator have been replaced with auxetic layers. The auxetic cell chosen for this study is a re-entrant hexagon. As illustrated in figure 3-6, the cell height and width are 0.01 m and 0.02 m respectively, while the cell angle is  $13^\circ$ . Figure 3-7 shows a three-dimensional view of the auxetic-type base isolator.

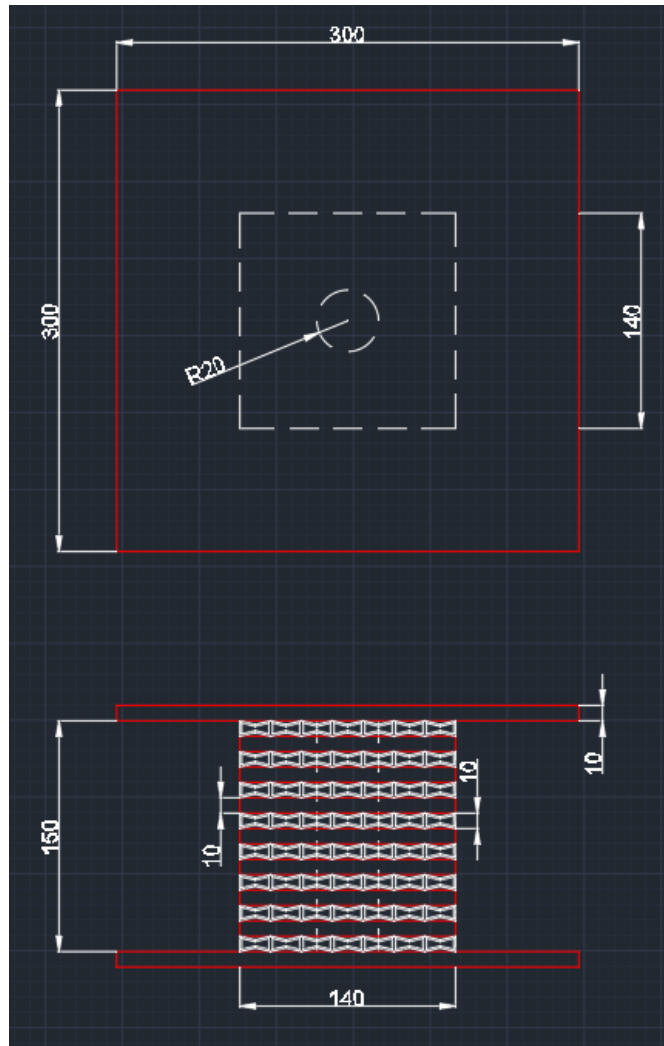


Figure 3 - 5: Typical Auxetic-Type Base Isolator Details (mm)

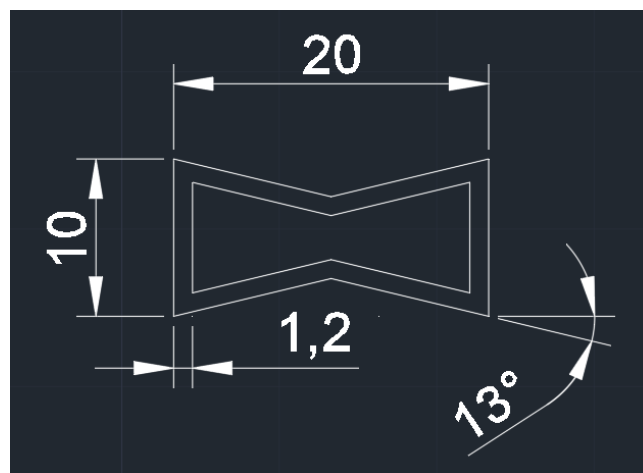


Figure 3 - 6: Typical Re-Entrant Hexagon Cell Details (mm)

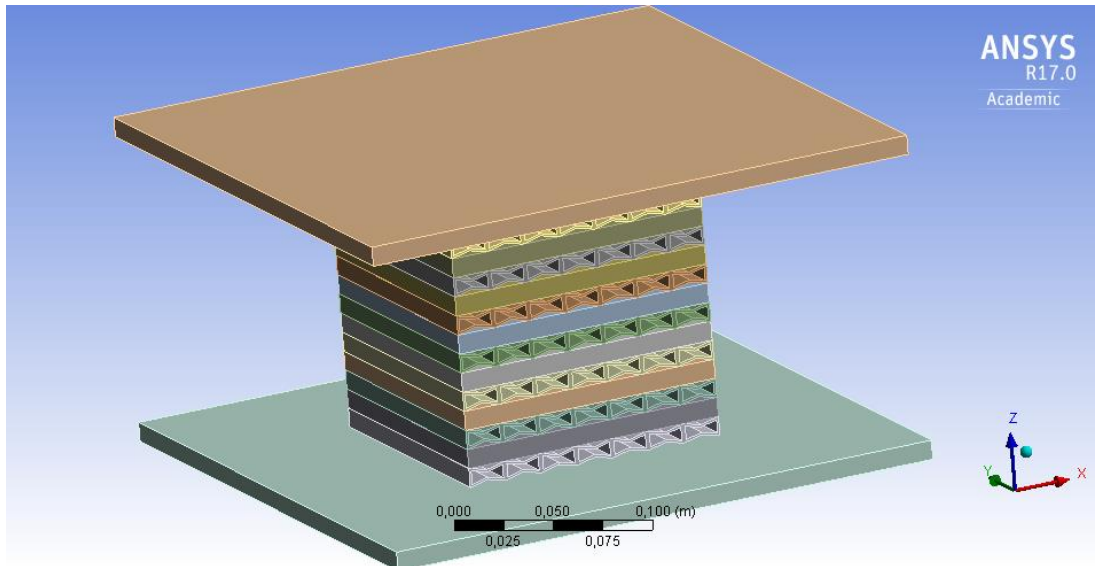


Figure 3 - 7: Three-Dimensional Auxetic-Type Base Isolator Model

### 3.4.4 Material Properties

The models analysed in the study consisted of three materials: lead, rubber and steel. Rubber was used as the material in the rubber bearings and the auxetic layers, while lead was used as the core in both isolation systems. S355 Steel was used in the superstructure and in the steel plates in both the LRB and auxetic-type isolators. Table 3-1 details relevant data pertaining to the linear properties of these three materials. In order to determine if plastic damage occurs and to account for large displacements in the models during the earthquake loading, steel with non-linear properties was used. Figure 3-8 illustrates the multilinear isotropic hardening properties used in the model and table 3-2 details the data used in the graph. For the purpose of this study, no non-linear properties in the lead used was considered.

Table 3 - 1: Material Properties

Property	Lead	Rubber	Steel
Density (Kg/m <sup>3</sup> )	11340	1200	7850
Young's Modulus (Mpa)	0.014	100	2E+05
Poisson's Ratio	0.43	0.48	0.3
Bulk Modulus (Mpa)	0.0328	833.300	16667
Shear Modulus (Mpa)	0.0048	33.780	76923

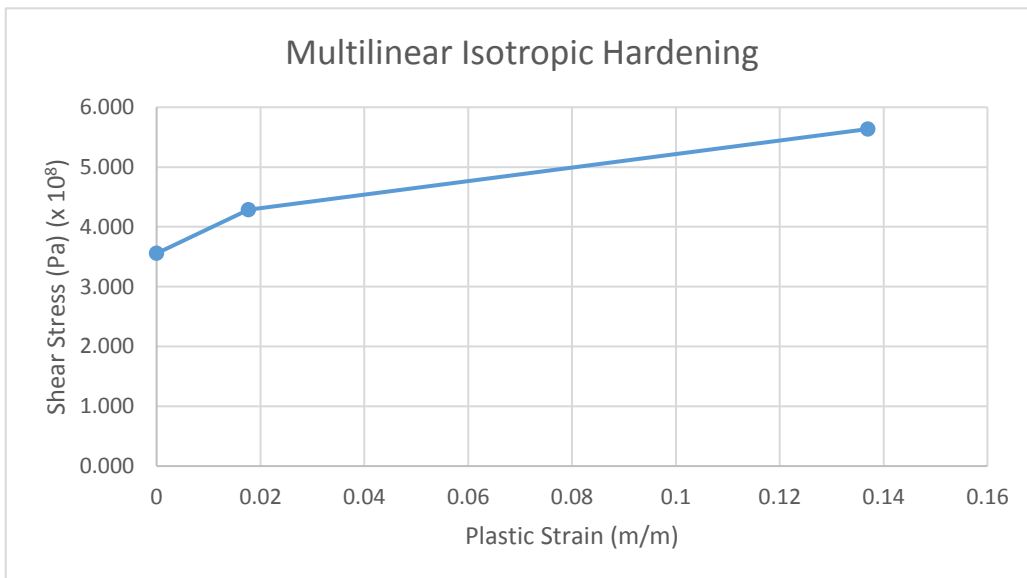


Figure 3 - 8: Stress-Strain Curve of Structural Steel

Table 3 - 2: Stress-Strain Properties of Structural Steel

Plastic Strain (m/m)	Shear Stress (Pa) (x 10 <sup>8</sup> )
0	3.556
0.017661	4.284
0.136944	5.635

### 3.4.5 Earthquake Data

The earthquakes used for the analysis occurred in Irpinia, Italy; Düzce, Turkey and Northridge, California. Table 3-3 details the characteristics and data available of the three earthquakes and figures 3-9 to 3-11 provide a visual representation of the x, y and z components of the seismic vibrations. Due to computational limitations by either the ANSYS program, the computer hardware or a combination of both and the computationally demanding nature of a non-linear time history analysis, this resulted in non-convergence for the full duration of the earthquakes. Despite numerous modifications made to the analysis parameters, the solution was unable to converge for the full duration of the loading on the auxetic-type analysis. Due to this issue, the most seismically intense portion of the earthquake was chosen for the analyses. Hence, a 15 second duration was chosen for each simulation.

Table 3 - 3: Earthquake Data

<b>Earthquake</b>	<b>Northridge 1</b>	<b>Irpinia</b>	<b>Düzce</b>
Location	California, USA	Italy	Turkey
Year	1994	1980	1999
Magnitude	6.69	6.9	7.15
Epicentral Distance (Km)	25.42	30.35	
Site class	B	B	
Peak Ground Acceleration (PGA) (g)	0.2458	0.29	
Total Duration (s)	46.935	39.340	43.150
Duration of Interval Used (s)	15.000	15.048	15.000
Time Interval Used (s)	0 - 15.0	0 - 15.048	15.0 - 30.0

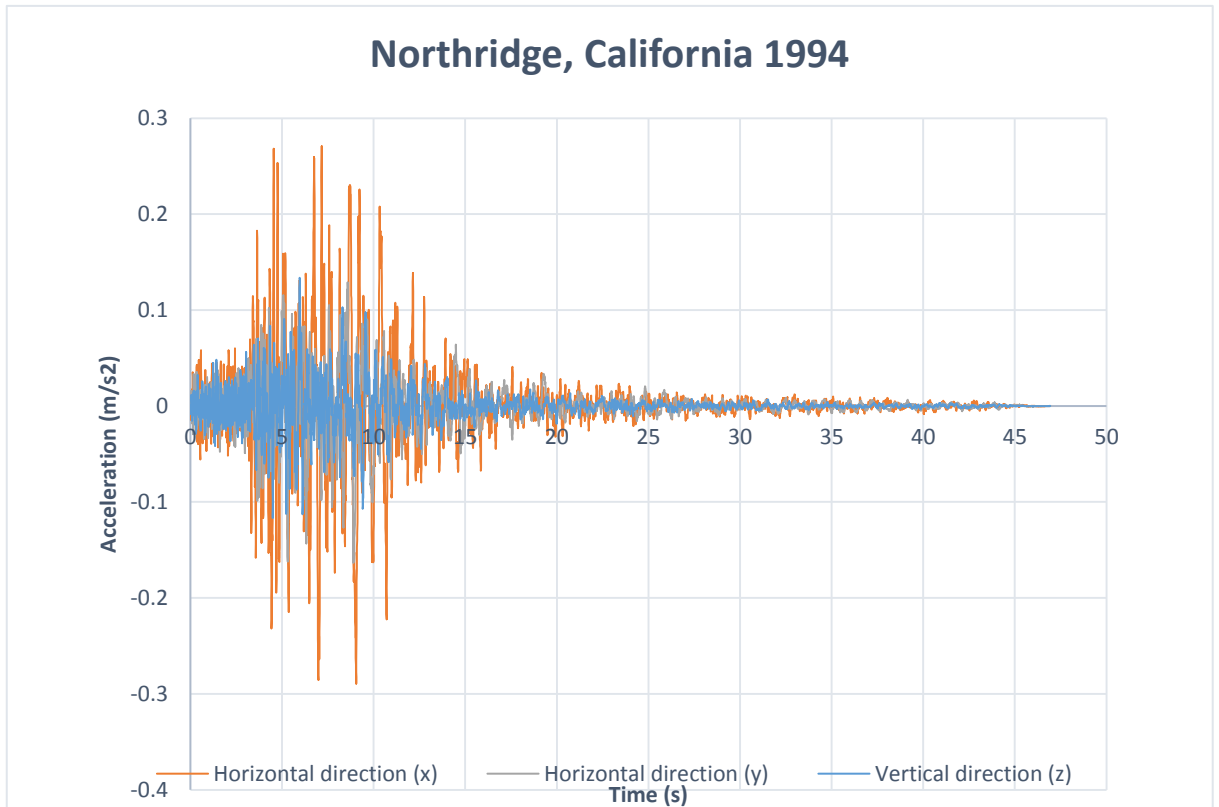


Figure 3 - 9: Northridge Earthquake – California, USA 1994

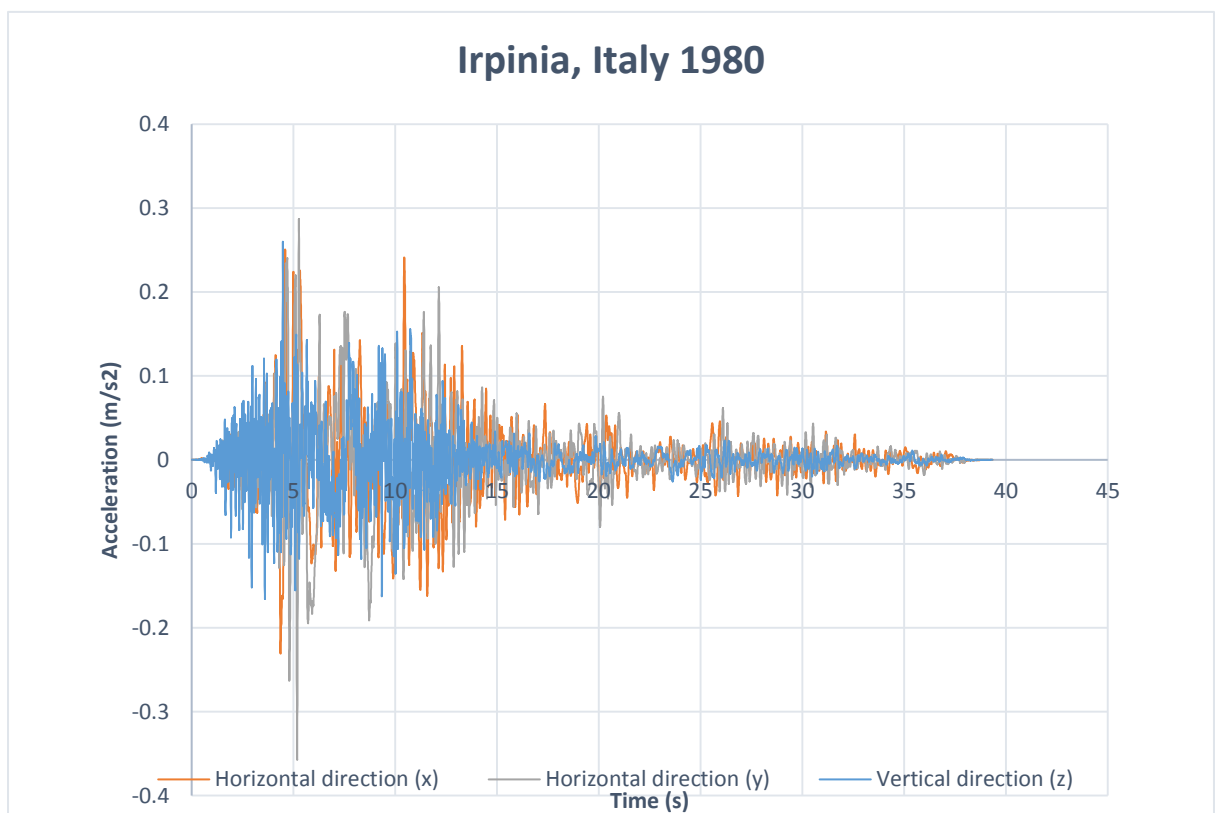


Figure 3 - 10: Irpinia Earthquake – Italy 1980

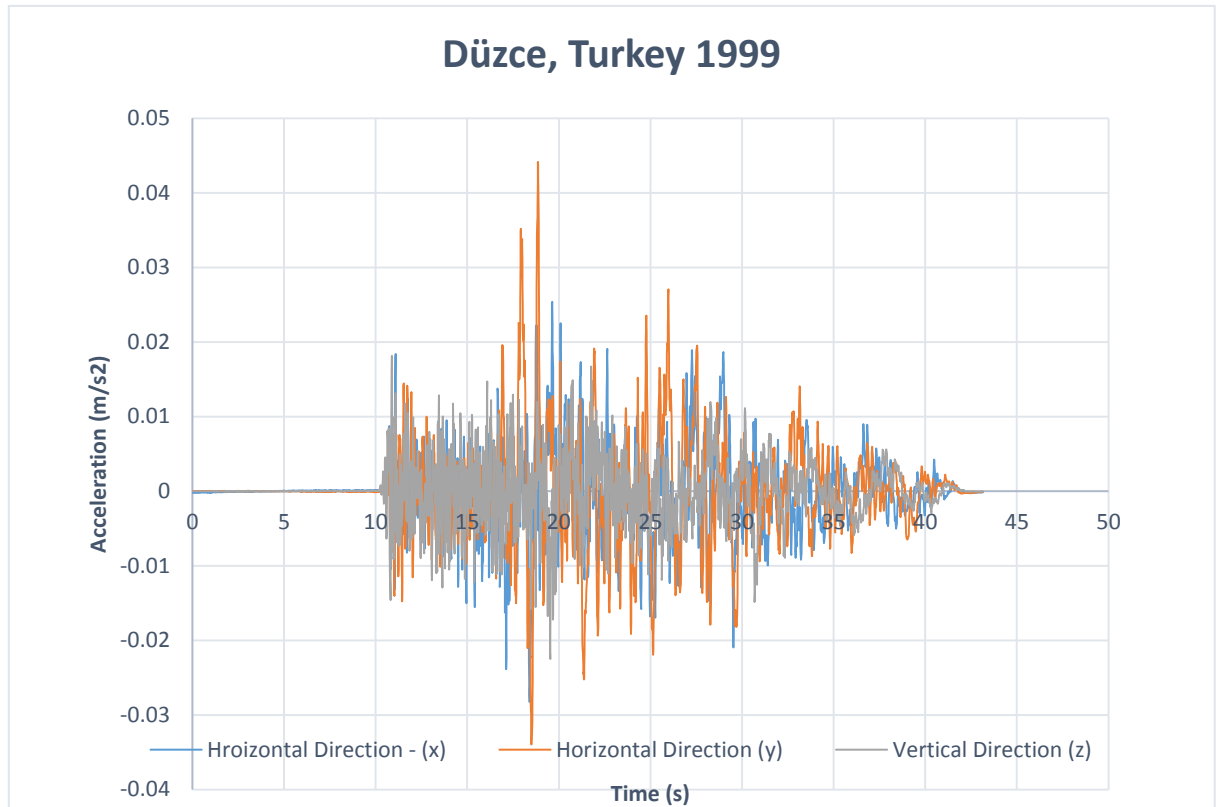


Figure 3 - 11: Düzce Earthquake – Turkey 1999

### 3.4.6 Meshing and Elements

The accuracy of results achieved from any finite element model is determined by the quality of the mesh used. The mesh is used as a means of subdividing the model into smaller elements. The computational model solves the required output for each of these smaller domains. The finer a mesh is, the more accurate the results achieved will be. Although, as the sizing of the mesh becomes smaller and more refined, the computational time increases. Due to this factor, the properties of the mesh used on the models have been altered accordingly to allow for reasonable computation times, while maintaining an appropriate level of accuracy. Additionally, regarding the generation of the mesh, no midside nodes were included. Altering the inclusion of midside nodes in a mesh determines if the mesh would be generated with quadratic elements or linear elements. By not considering midside nodes, the number of degrees of freedom are reduced, and hence the computational demands (ANSYS Inc., 2015).

Considering the large dimensions of the superstructure, an element size of 0.5m was used. A mesh with this characteristic enabled the simulation to run smoothly while computing results within a reasonable time frame. Figure 3-12 illustrates the superstructure's mesh. A program controlled mesh was used for the base isolators. The LRB system's mesh is shown in figures

3-13 and 3-14 while the auxetic system's mesh is displayed in figures 3-15 to 3-17. In figure 3-17, it can be seen that the mesh on the inner faces of the auxetic layers is much more fine than the planar faces on the Y-axis. This should provide a greater deal of accuracy relating to the vibrational response of the auxetic layers. The systems used in this study were all modelled using solid elements. The number of nodes and elements included in each model is displayed in table 3-4.

Table 3 - 4: Nodes and Element Details per Model

Model	No. of Nodes	No. of Elements
Fixed Frame	21484	15448
LRB	26934	16480
Auxetic-Type	54642	116976

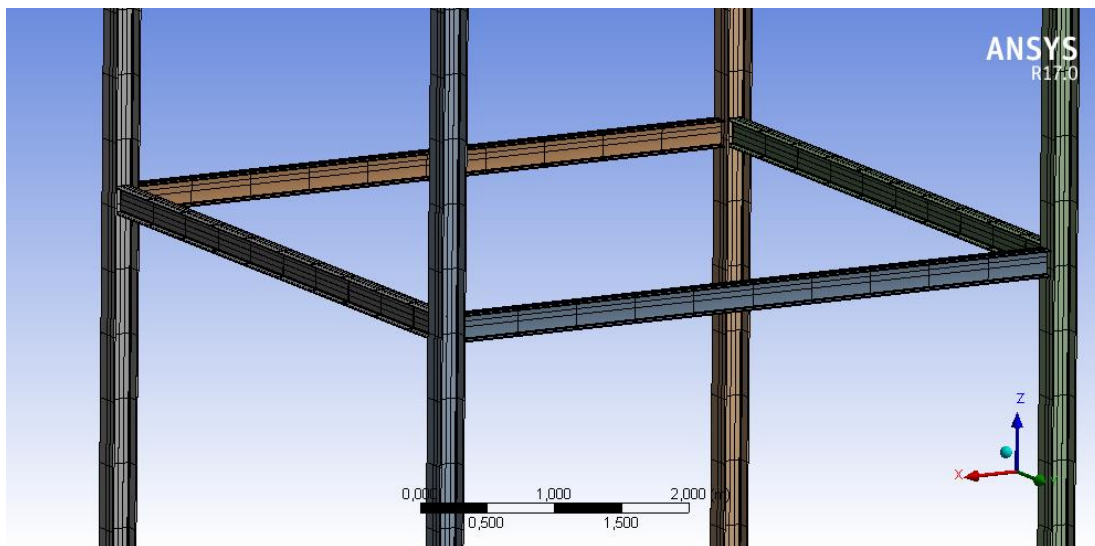


Figure 3 - 12: Mesh Generated on the Superstructure

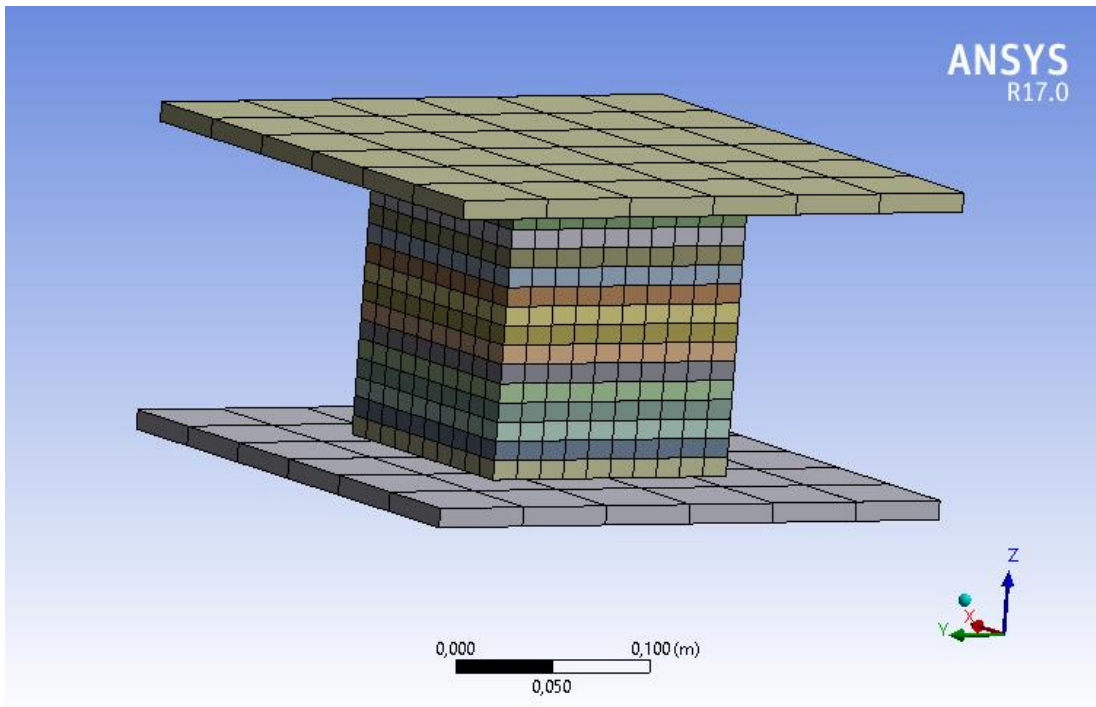


Figure 3 - 13: Mesh Generated on the LRB Base Isolator

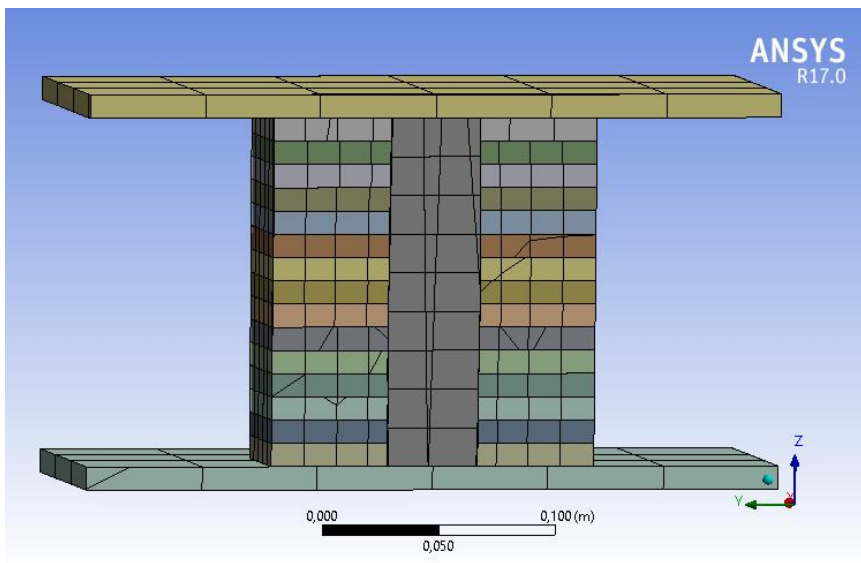


Figure 3 - 14: Mesh Generated within the LRB Base Isolator

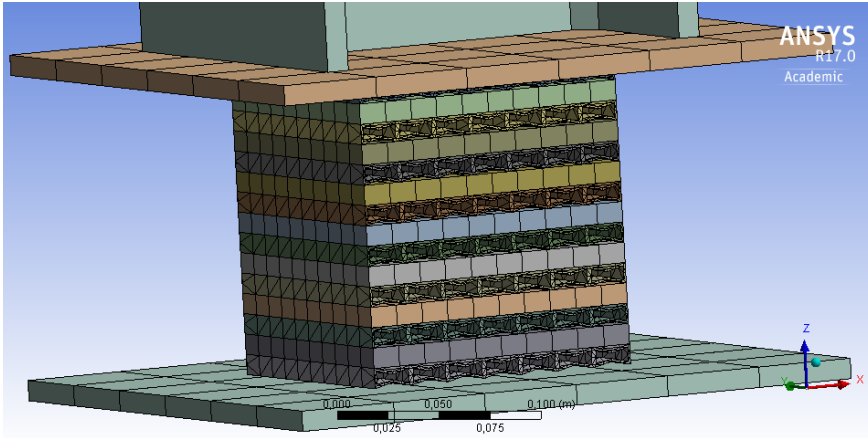


Figure 3 - 15: Mesh Generated on the Auxetic-Type Base Isolator

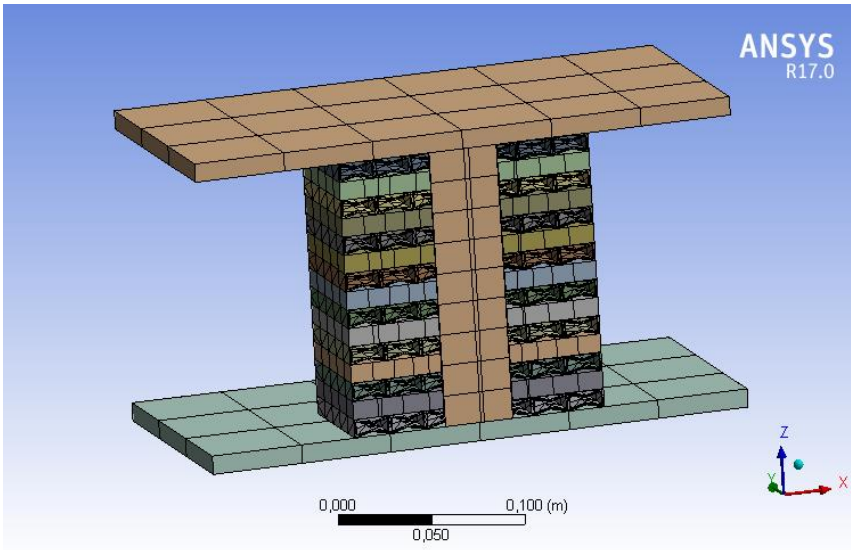


Figure 3 - 16: Mesh Generated within the Auxetic-Type Base Isolator

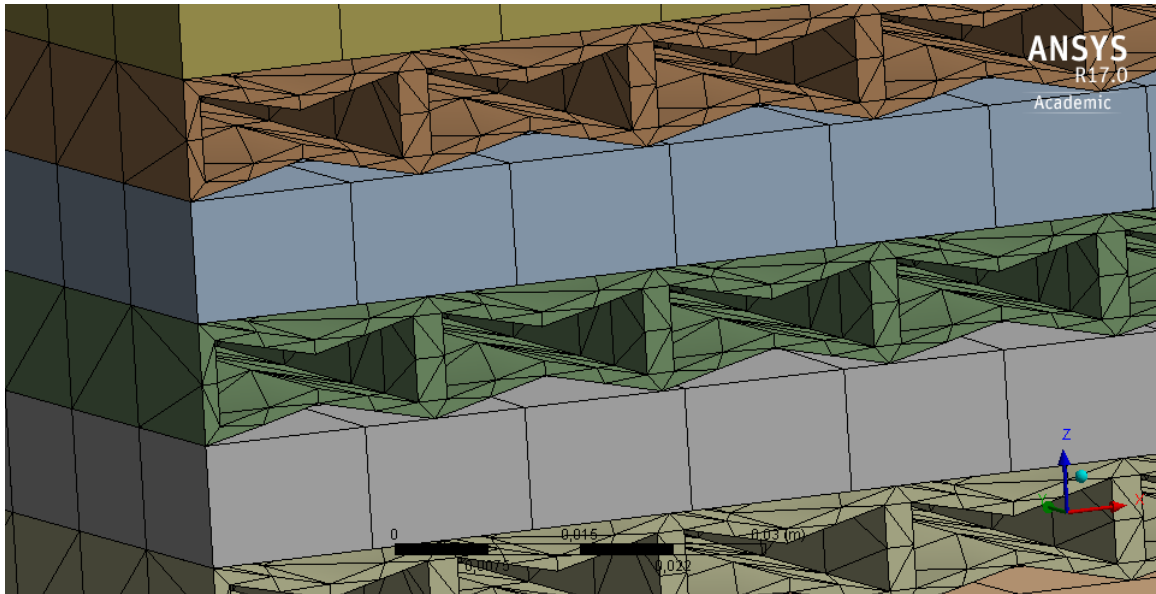


Figure 3 - 17: Mesh Generated on the Auxetic Layers

### 3.4.7 Computational Analysis

The finite element analysis (FEA) software used to analyse the performance of the three systems is ANSYS version 17.0. An eigenvalue analysis was performed as an initial dynamic analysis to determine the eigenfrequency associated with each mode. Subsequently, the eigenperiod was calculated for each mode by finding the inverse of the eigenfrequency. In a base isolation study, the base isolated systems should serve as a means of increasing the eigenperiod of the model due to the increase in lateral flexibility at the base. For the analyses performed, a total of 20 eigenvalues were found.

To determine the seismic performance of the systems, a non-linear time history analysis was performed. A time history analysis enables seismic loading to be applied to the model by means of applying an acceleration load. It requires for a number of time-steps to be chosen as well as a minimum, maximum and initial time-step. The number of time-steps chosen for the analysis was 300. The minimum time-step was chosen to be 0.01 seconds, while the maximum and initial were chosen to be 0.05 which is the same as the time interval between the seismic loading data. Due to the computationally demanding nature of a non-linear time history analysis, amendments to the time step data was made for the auxetic-type system. The time step input used for the previous two models ensure that the program computes an output every 0.05 seconds. When this was used in the auxetic-type system, solution convergence issues

arose due to the complex nature and geometry of the system, as well as computational limits. Therefore, the number of time-steps chosen was 1, however the full 15 second duration of the earthquake was still included in the step. The analysis settings were changed as well. The initial time-step was chosen to be 0.05 seconds while the minimum time-step was 0.01 seconds and a maximum of 1.0 seconds. By assigning this time-step analysis data to the time history analysis, it allows the solver to use larger time-steps of up to 1 second when the analysis converges. Figure 3-18 details the differences in time-steps chosen for the three systems. Should the full 300 steps be used as opposed to 1 and the initial and minimum time-steps remain as 0.05 and 0.01 seconds respectively, the maximum time-step could not exceed 0.05 seconds. This is due to the 0.05 second interval of the seismic loading data and an analysis parameter that does not allow a maximum time-step to exceed the interval of the steps. The number of steps require numerous iterations which under standard program controlled settings may either not converge or require excessively long computational times.

Details of "Analysis Settings"	
<b>Step Controls</b>	
Number Of Steps	300,
Current Step Number	1,
Step End Time	5,e-002 s
Auto Time Stepping	On
Define By	Time
Initial Time Step	5,e-002 s
Minimum Time Step	1,e-002 s
Maximum Time Step	5,e-002 s
Time Integration	On
<b>Solver Controls</b>	

Details of "Analysis Settings"	
<b>Step Controls</b>	
Number Of Steps	1,
Current Step Number	1,
Step End Time	15, s
Auto Time Stepping	On
Define By	Time
Initial Time Step	5,e-002 s
Minimum Time Step	1,e-002 s
Maximum Time Step	1, s
Time Integration	On
<b>Solver Controls</b>	

Figure 3 - 18: Time History Analysis Setting for Fixed Base and LRB Models vs Settings for Auxetic-Type Base Isolator

Further changes from the standard settings in ANSYS were made for the auxetic-type system. The base isolation systems consist of numerous contact interfaces between steel, rubber and lead components. The way in which the contacts are defined was modified. The standard contact formulation in ANSYS is the 'Pure Penalty' method. This penalty based system uses penalty terms to simulate unilateral contact, without additional unknowns. The contact elements have stiffness in the normal direction that defines property of non-penetration in that direction. When a model using this method of contact formulation is subjected to severe loading, it may result in non-convergence. Due to this, the contact method chosen for the auxetic-type base isolator was the Multi-Point Constraint (MPC) contact. The MPC contact does not use the penalty method. Instead, it develops and solves additional equations,

describing the tie conditions at the interface of the two materials. This method utilises a simpler means of bonding the contact interfaces in a model, thereby allowing for easier convergence in the analysis (ANSYS Inc., 2015). By using the MPC contact method, the computation time increases due to additional MPC equations that need to be solved. The amendments made to the time-step input also assisted the auxetic-type model to maintain a reasonable computation time.

Lastly, amendments were made to the number of integration points taken into account at each element. Considering the size of the models in the study, even with coarse meshes, the models consist of numerous elements. Integration points are set in predefined locations within each element. The standard method that the solver uses is 'Full', incorporating 8 integration points per element. This was changed to manual and then under 'Brick Integration Scheme', it was set to 'reduced', thus, 1 integration point per element, for all parts in the model. This lessens the number of integration points considered at each element, thereby reducing the computational demand when solving the system.

### **3.5 Limitations and Uncertainties**

Due to the computational issues and lack of sufficient computer hardware to support large numerical models, which have been encountered during the analysis for the auxetic-type base isolator, just the most severe duration of the earthquake was tested. The full duration of the earthquake's effects has not been evaluated and therefore a holistic performance overview which includes the dissipation of the earthquake has not been achieved.

## CHAPTER 4: RESULTS AND DISCUSSION

### 4.1 Introduction

This chapter aims to investigate the response and performance of auxetic type base isolation systems under seismic loading. Furthermore, its performance is evaluated with respect to that of a traditional lead-rubber bearing base isolation system and a fixed base system. Appropriate methods of analysis are used in order to holistically analyse the auxetic type system. Performance indicators identified in past literature as being critical to effective base isolation is used to assess the system's isolation capabilities. Additionally, this chapter serves as a means of contextually representing elements of auxetic materials and base isolation systems that have been explored in the Literature Review.

### 4.2 Eigenvalue Analysis

Owing to a dynamic analysis being performed, an eigenvalue analysis was performed in order to determine the natural frequency, natural period and mode shapes of each system. The eigenvalue analysis forms an important part of any dynamic analysis as the results of the analysis characterise the way in which the system will behave when subjected to dynamic loads. It is considered to be the most basic dynamic analysis. Table 4-1 details results from the eigenvalue analysis carried out on the three systems. Base isolation facilitates the reduction of the physical demand placed on a structure during a seismic event. With the addition of this system, the new natural period of the base isolated structure is significantly longer when compared to the natural period of the ridged fixed-base structure. By elongating the natural period of a structure using base isolation, it is possible to reduce the base acceleration experienced by the structure. This in turn significantly reduces damage to the structure and the architectural façade during an earthquake.

Figures 4-1 to 4-6 represent various mode shapes for each system. For certain modes, the mode shapes of the base isolated structures present distinct changes when compared to the fixed-base system. Modes 1 and 2 are similar to the fixed-base, however the 5<sup>th</sup> eigen shape of the LRB system exhibits a distinct positive displacement along the Y-axis, creating a curved appearance. Eigen shape 10 of the fixed-base shows an expansion in both directions along the Y-axis, from floors 0 to 7, while the LRB system experiences a torsional-like displacement throughout the frame. The auxetic system however, experiences a contraction towards the

upper floors. The 15<sup>th</sup> mode shape of the fixed-base and auxetic systems show displacements at each third of the frame. This however occurs in different directions in each system. The LRB system however, shows no significant visible changes. The 20<sup>th</sup> mode shapes of the fixed-base and auxetic systems follows a similar trend to the 15<sup>th</sup> mode shape, however the displacements at each third of the frame are significantly lower. Additionally, the displacement in the first third of the frame is in the opposite direction to that of the respective systems in their 15<sup>th</sup> mode shapes. The LRB system exhibits displacements in both directions along the Y-axis at the middle of the frame, creating the appearance of a central bulge. It can be seen in table 4-1 that the auxetic base isolation experiences higher eigenperiods than the other two systems. The LRB system however, experiences higher eigenperiods than the fixed frame for the first three modes, after which the eigen periods are slightly reduced.

Table 4 - 1: Eigenvalue Analysis Results

No.	Fixed Frame		LRB		Auxetic-Type	
	Frequency (Hz)	Period (s)	Frequency (Hz)	Period (s)	Frequency (Hz)	Period (s)
1	1.229	0.814	1.196	0.836	0.509	1.965
2	1.977	0.506	1.914	0.522	0.572	1.749
3	3.836	0.261	3.782	0.264	1.248	0.801
4	6.018	0.166	6.136	0.163	1.887	0.530
5	6.152	0.163	6.988	0.143	2.322	0.431
6	6.896	0.145	8.296	0.121	2.721	0.367
7	7.357	0.136	9.397	0.106	3.680	0.272
8	8.043	0.124	10.547	0.095	4.110	0.243
9	9.684	0.103	10.695	0.094	4.600	0.217
10	10.092	0.099	11.183	0.089	5.102	0.196
11	10.336	0.097	11.540	0.087	5.329	0.188
12	10.511	0.095	12.740	0.078	6.398	0.156
13	12.837	0.078	14.450	0.069	6.520	0.153
14	13.636	0.073	14.703	0.068	6.934	0.144
15	14.303	0.070	15.335	0.065	7.349	0.136
16	15.164	0.066	15.335	0.065	8.147	0.123
17	16.849	0.059	15.335	0.065	8.325	0.120
18	18.119	0.055	15.335	0.065	8.812	0.113
19	18.710	0.053	15.649	0.064	9.083	0.110
20	20.153	0.050	15.799	0.063	9.981	0.100

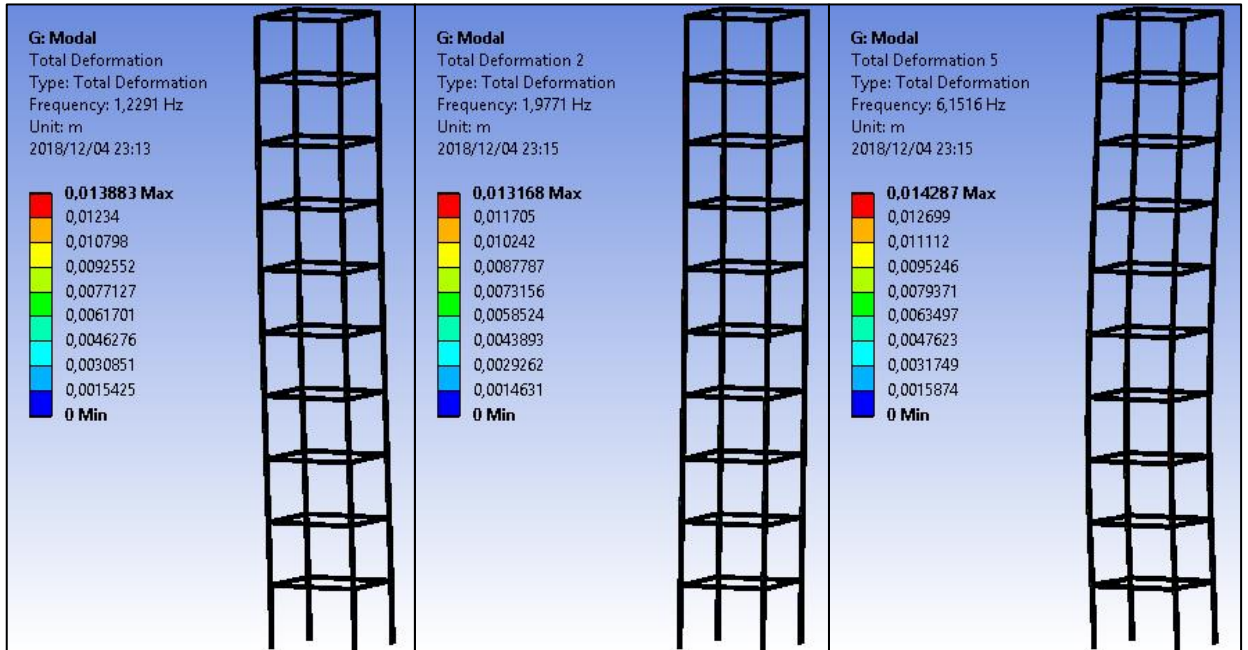


Figure 4 - 1: Mode Shapes 1, 2 and 5 of the Fixed Frame

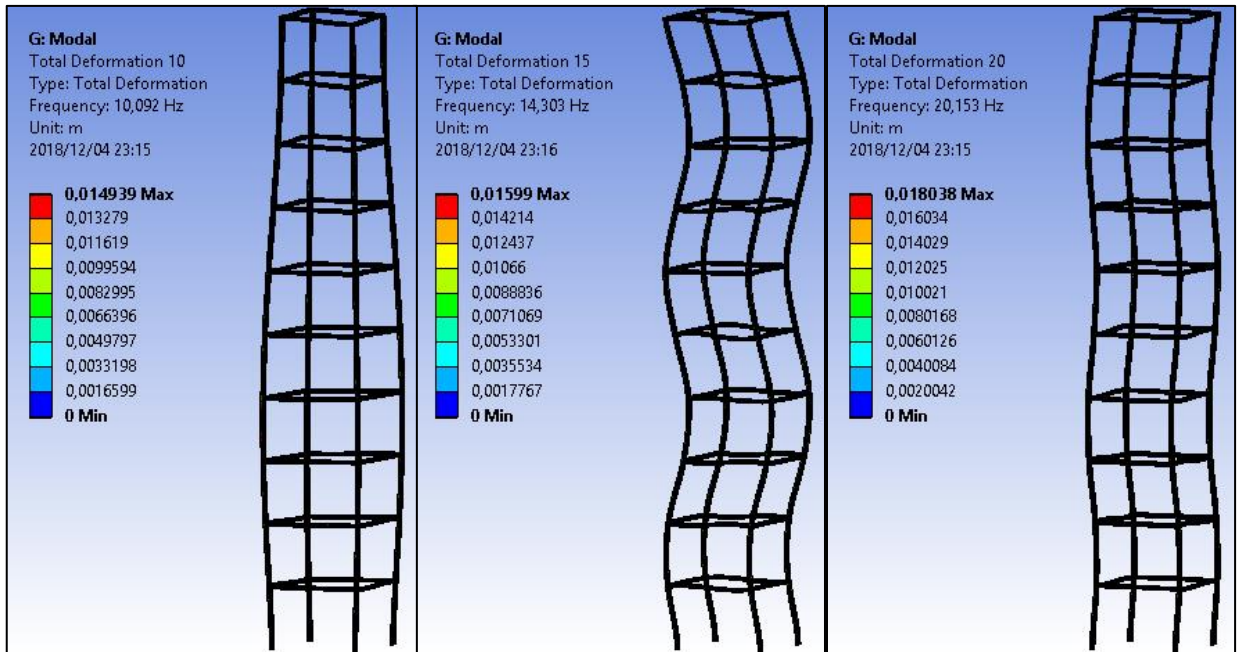


Figure 4 - 2: Mode Shapes 10, 15 and 20 of the Fixed Frame

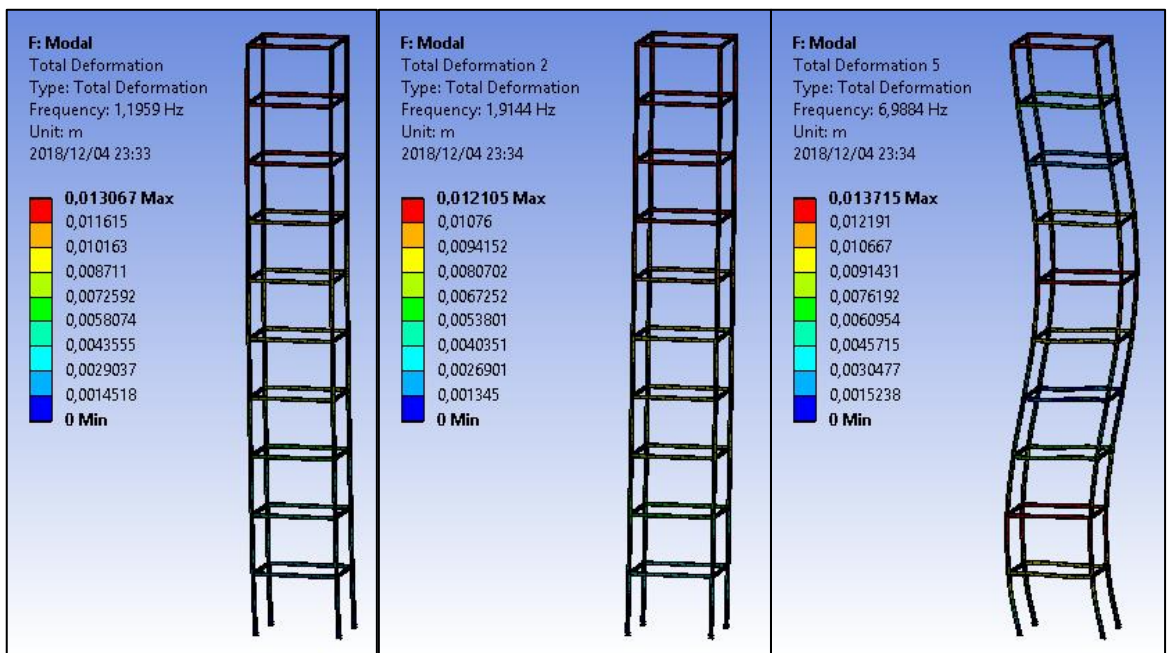


Figure 4 - 3 : Mode Shapes 1, 2 and 5 of the LRB System

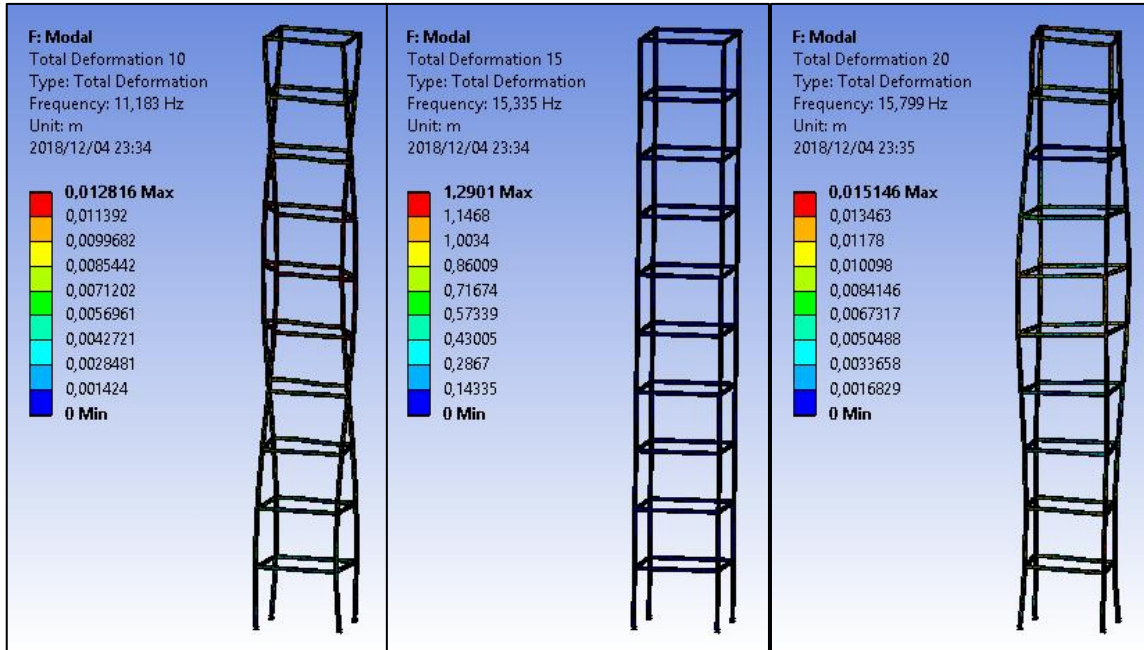


Figure 4 - 4: Mode Shapes 10, 15 and 20 of the LRB System

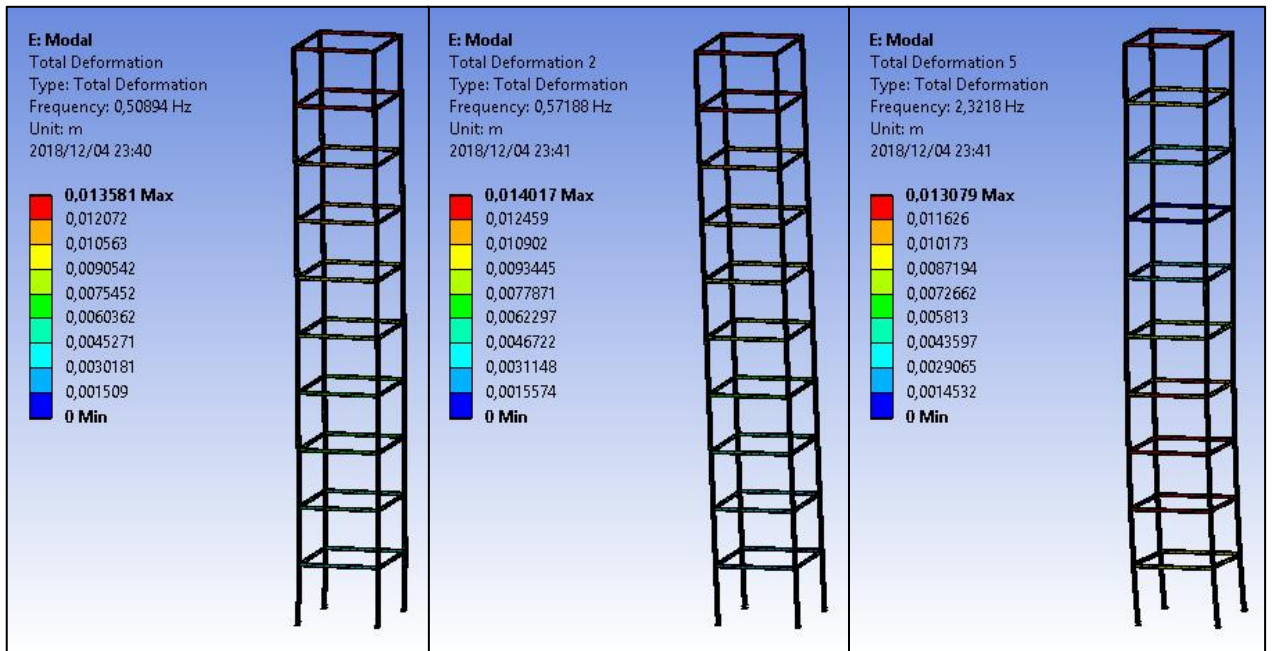


Figure 4 - 5: Mode Shapes 1, 2 and 5 of the Auxetic System

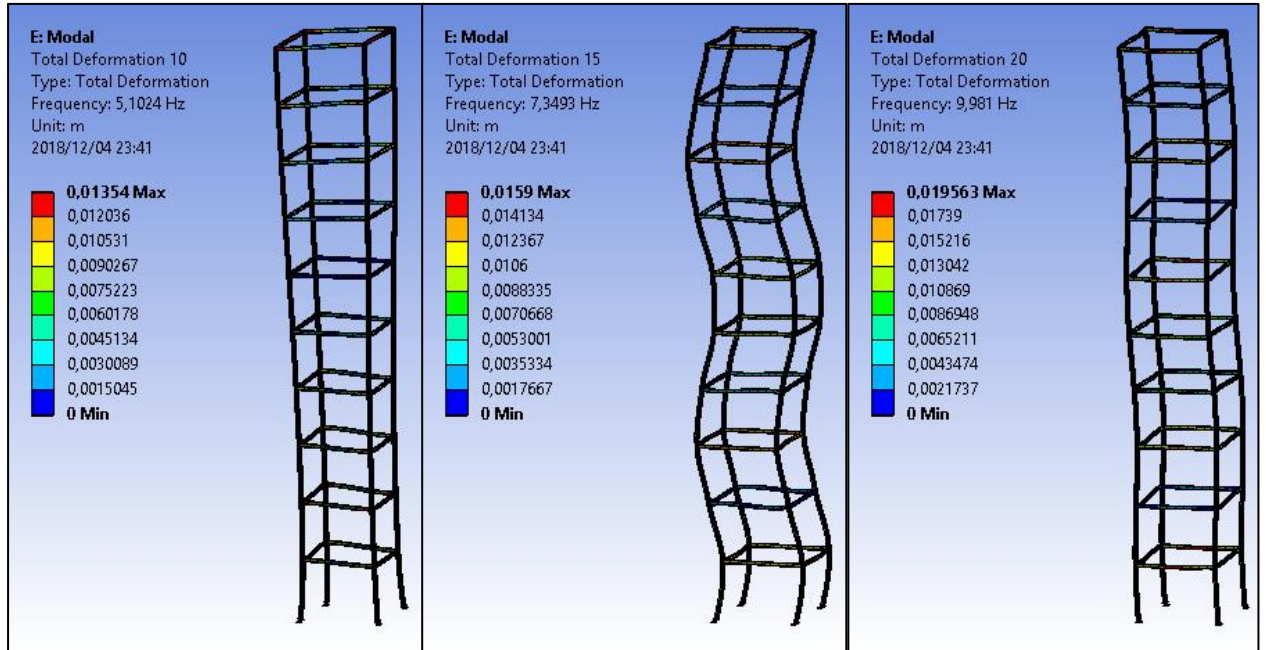


Figure 4 - 6: Mode Shapes 10, 15 and 20 of the Auxetic System

### 4.3 Time History Analysis

A non-linear time history analysis was performed on a ten-story steel frame with a fixed base and steel. The analysis used seismic data gathered from the Irpinia, Italy; Düzce, Turkey and Northridge, California earthquakes. The portion of the earthquakes that were used were considered to be the most intense portion was used for the analysis. Similar analyses were performed on ten-story frames with lead-rubber bearing and auxetic type base isolation systems. In all three investigations, all steel components in the models possessed non-linear properties. The performance of the systems has been evaluated at the bottom, middle and top of the superstructures i.e. floors 1 - 2, 5 - 6 and 9 - 10.

#### 4.4 Northridge, California 1994

The 6.69 magnitude Northridge earthquake occurred in California, USA in 1994. It can be described as being very intense early on with more minor vibrations occurring from 12 seconds onwards. This earthquake is most impulsive along the x-axis, with all of the most notable seismic waves occurring in this direction. The most seismically severe portion of the earthquake was used in the analysis i.e. 0 – 15 seconds. This earthquake data is shown in figure 4-7.

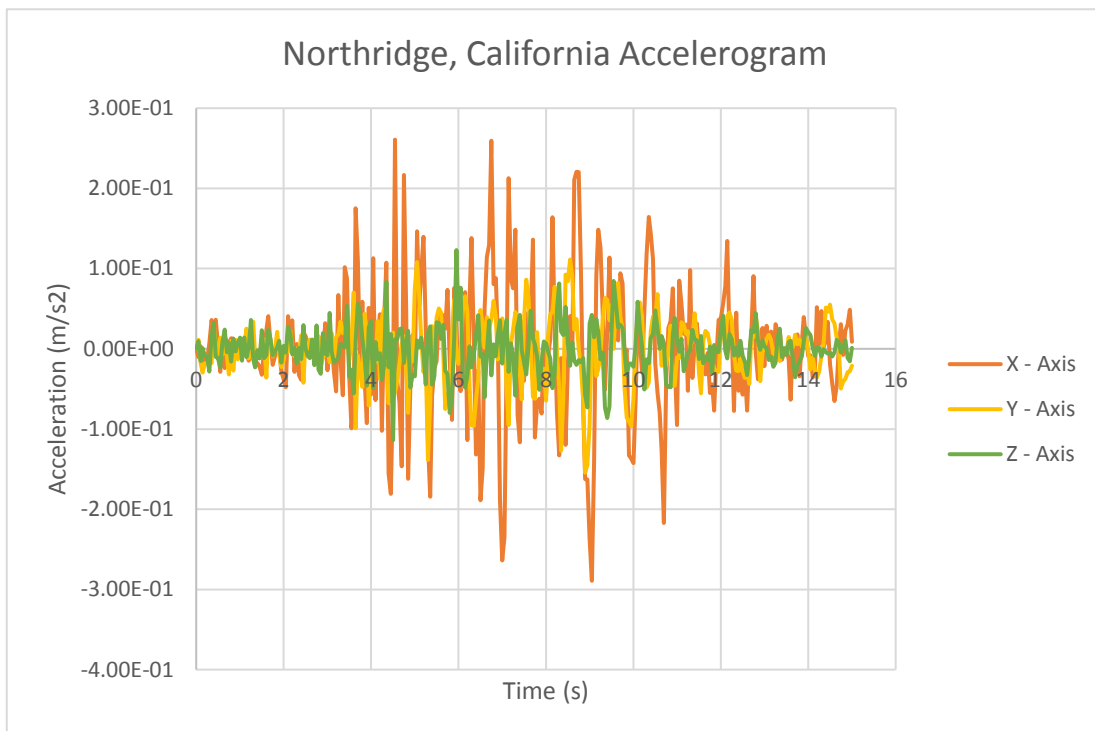


Figure 4 - 7: Northridge Earthquake Data

#### 4.4.1 Total Deformation

The total displacement refers to the average relative displacement along each axis i.e.  $u_x$ ,  $u_y$  and  $u_z$ . The total deformation of the system behaves in line with trends highlighted in past literature. The deformation of the LRB system exceeds that of the fixed frame due to the lateral flexibility introduced into the system by the base isolators. The auxetic-type system however displays a notably higher total deformation during the most severe portion of the earthquake, however as the seismic waves begin to weaken, the total deformation decreases to levels lower than that of the fixed frame. Figure 4-8 depicts the total deformation of the three systems analysed. This is measured as the maximum displacement that occurs in the system at each time-step in the analysis. Figures 4-9 to 4-14 depict three-dimensional models of the systems along with their total deformation.

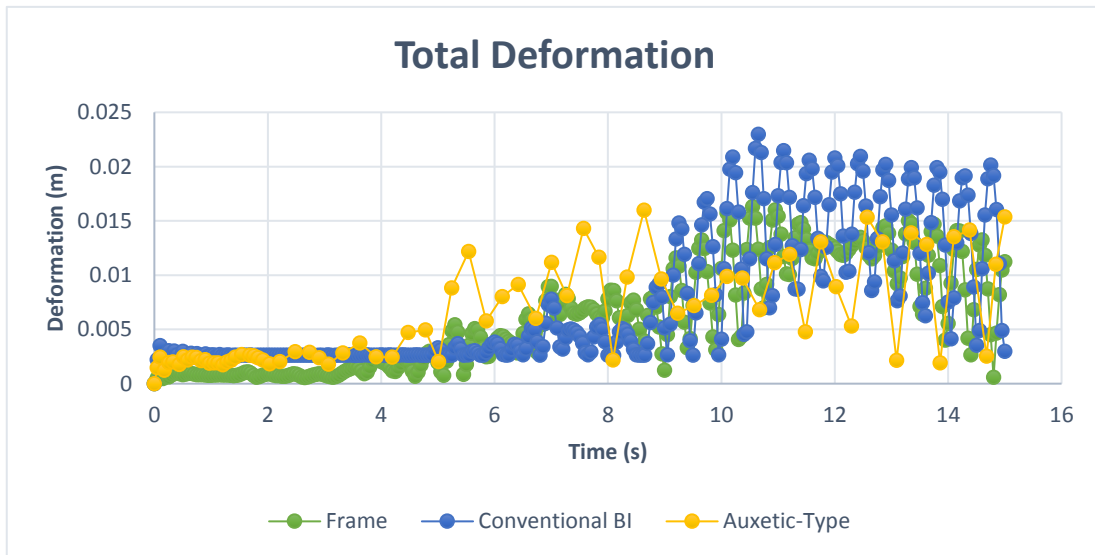


Figure 4 - 8: Total Deformation under the Northridge Earthquake

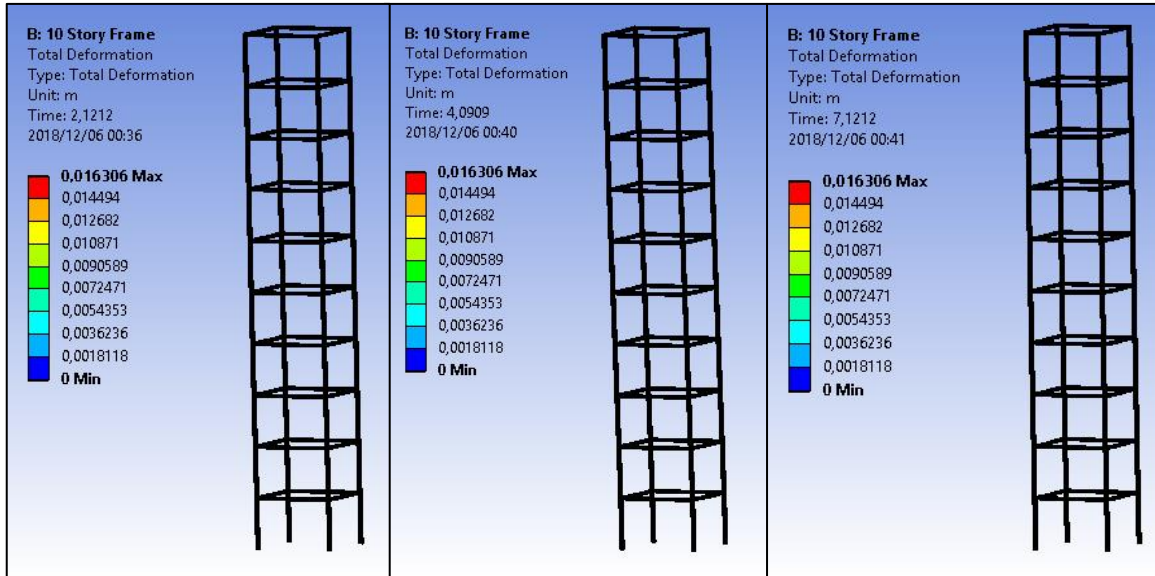


Figure 4 - 9: Deformation of the Fixed Base System at Approximately  $t = 2, 4$  and  $7s$

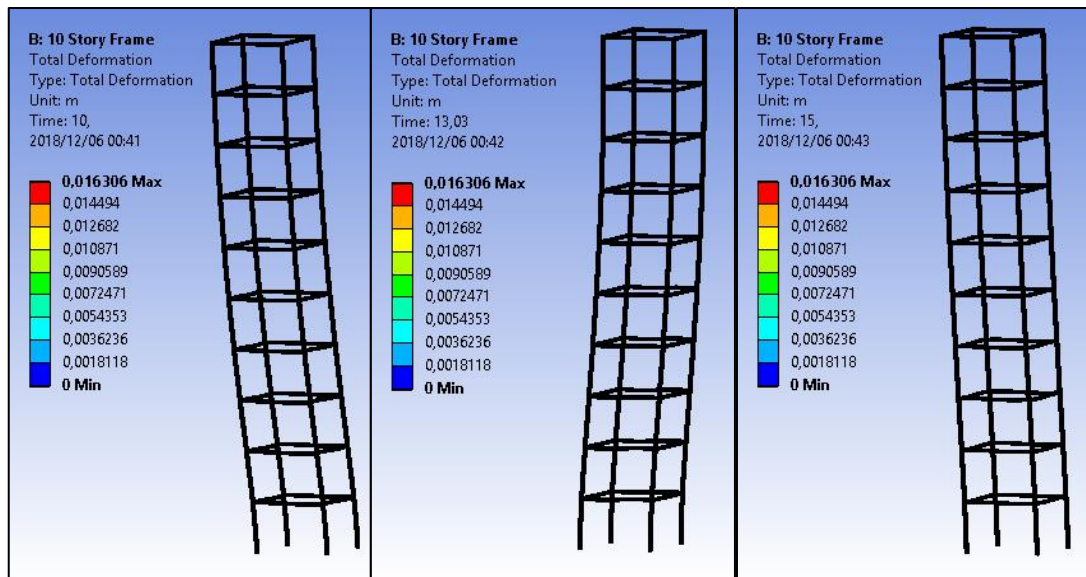


Figure 4 - 10: Deformation of the Fixed Base System at Approximately  $t = 10, 13$  and  $15s$

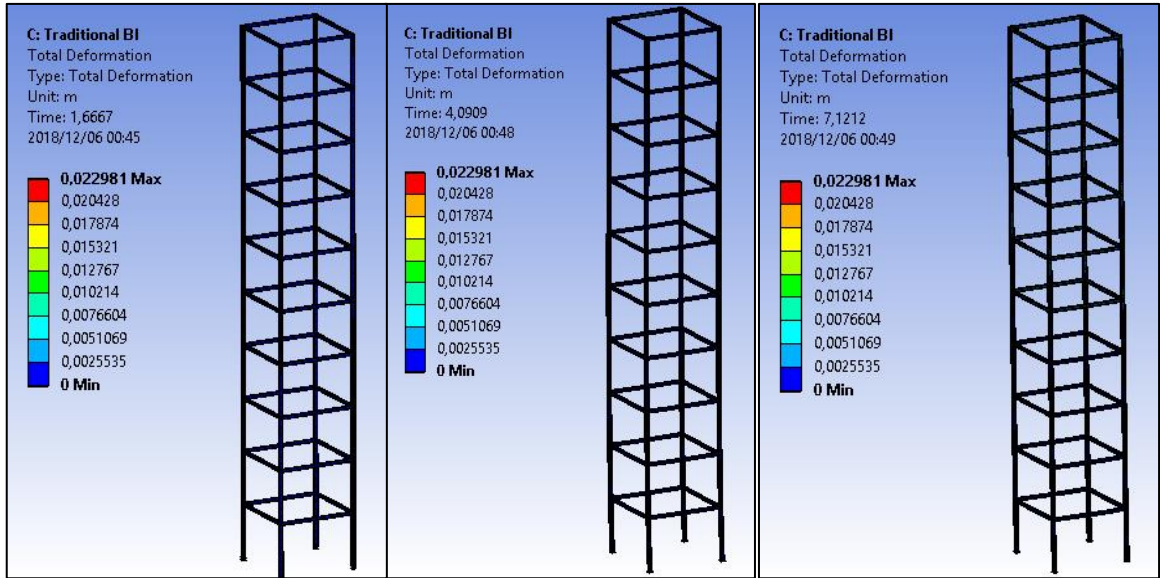


Figure 4 - 11: Deformation of the LRB System at Approximately  $t = 2, 4$  and  $7s$

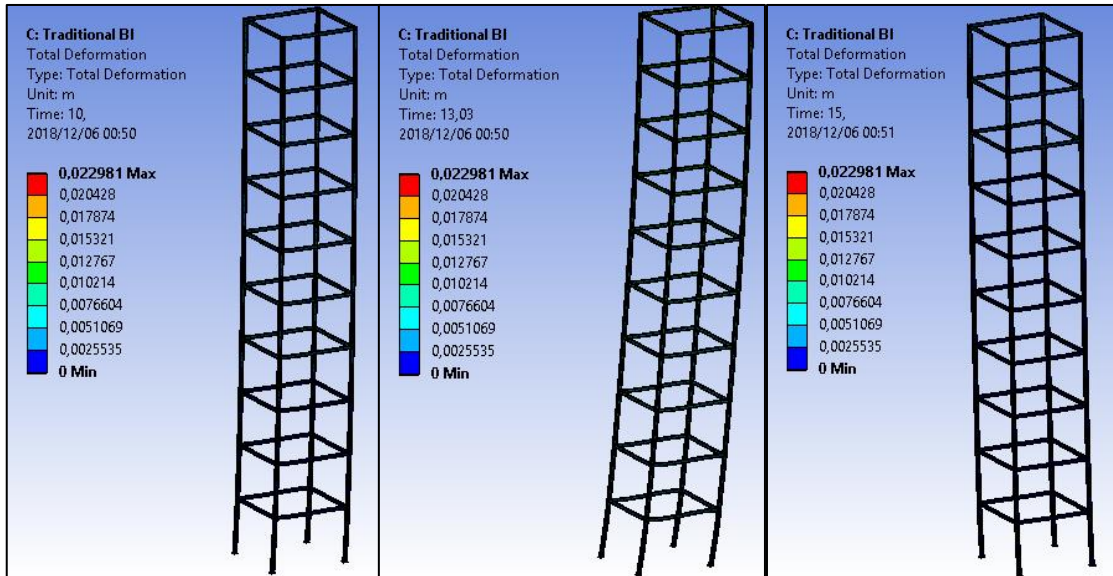


Figure 4 - 12: Deformation of the LRB System at Approximately  $t = 10, 13$  and  $15s$

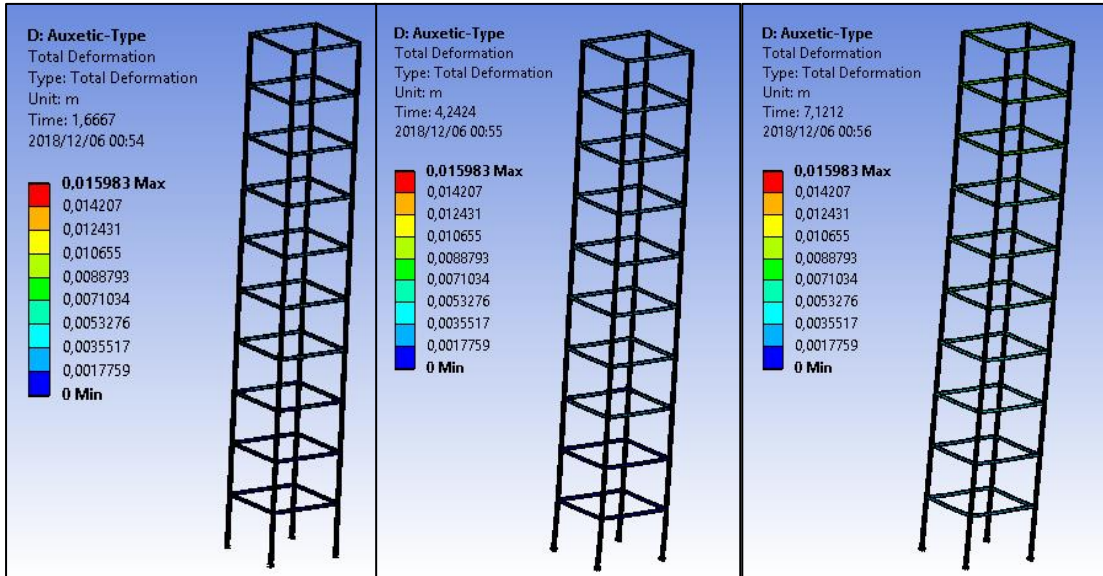


Figure 4 - 13: Deformation of the Auxetic-Type System at Approximately  $t = 2, 4$  and  $7s$

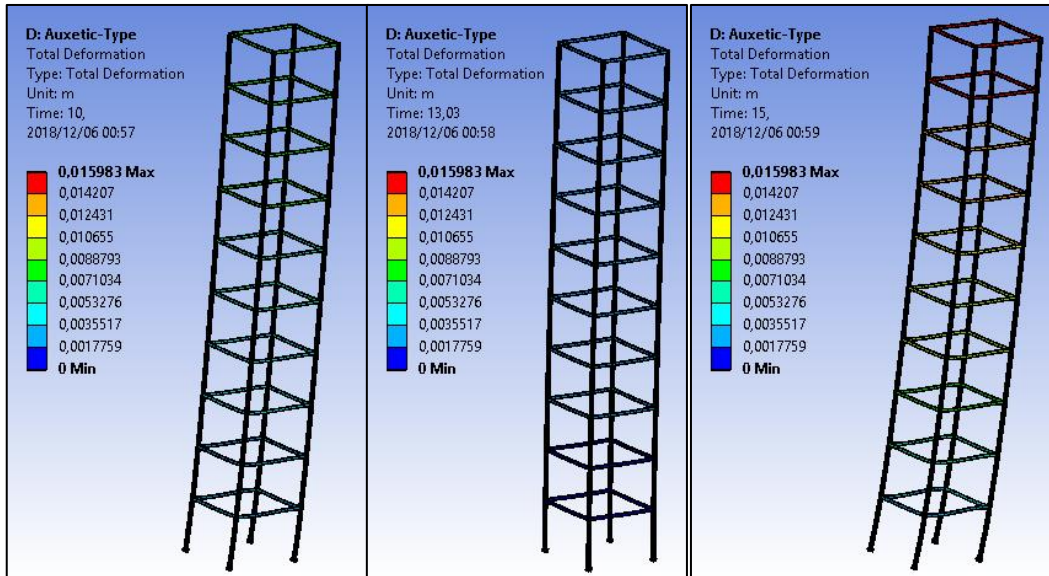


Figure 4 - 14: Deformation of the Auxetic-Type System at Approximately  $t = 10, 13$  and  $15s$

#### 4.4.2 Total Relative Displacement

The total relative displacement refers to the average displacement over time along each axis i.e.  $u_x$ ,  $u_y$  and  $u_z$ , between two consecutive floors. Reducing the overall relative displacements of stories is one of the primary objectives of base isolation. By doing so, the possibilities of both structural and non-structural damage are significantly reduced. As shown in figures 4-15 to 4-17, the auxetic-type system exhibits a favourable performance at all three levels of analysis. In the lower levels, the system occasionally displaying an improved performance. At the middle of the superstructure, the system has performed particularly well with overall lower relative displacements than the LRB system towards the latter part of the seismic loading. In the upper floors, all three systems have behaved in a comparatively similar manner. From  $t = 5 - 9$ s, the auxetic system has responded with relative displacements that exceed that of the other two systems. Similar behaviour has occurred during this interval in the lower floors. The additional displacement that has occurred at these levels may be attributed to the intense vibrations in the x direction that occur at this time interval. Except this case, the proposed auxetic base isolation seems to perform well, depicting a reduction in the relative displacement between the floors, as compared to the fixed frame and LRB base isolation.

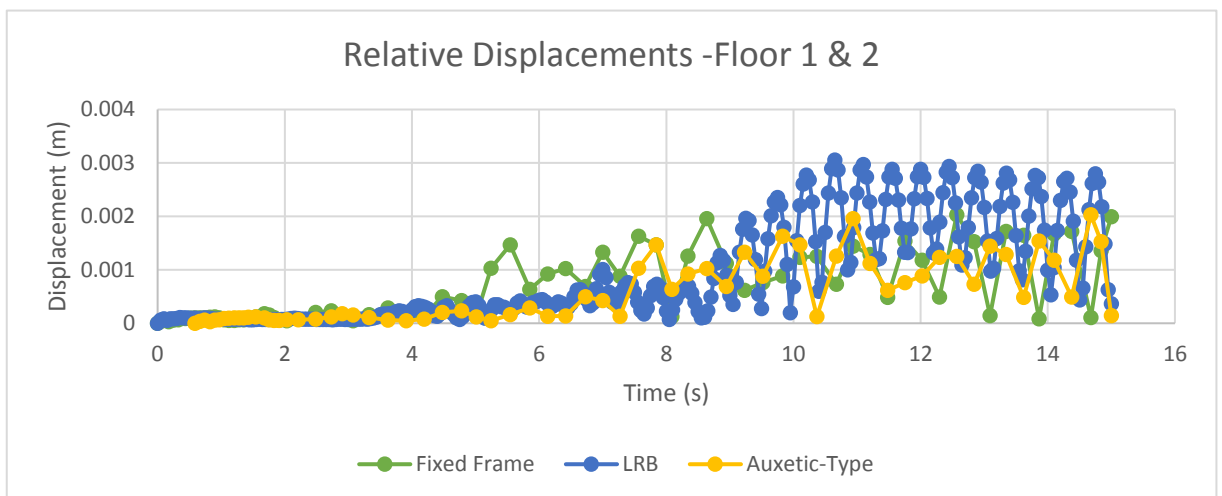


Figure 4 - 15: Relative Displacement of Floors 1 and 2

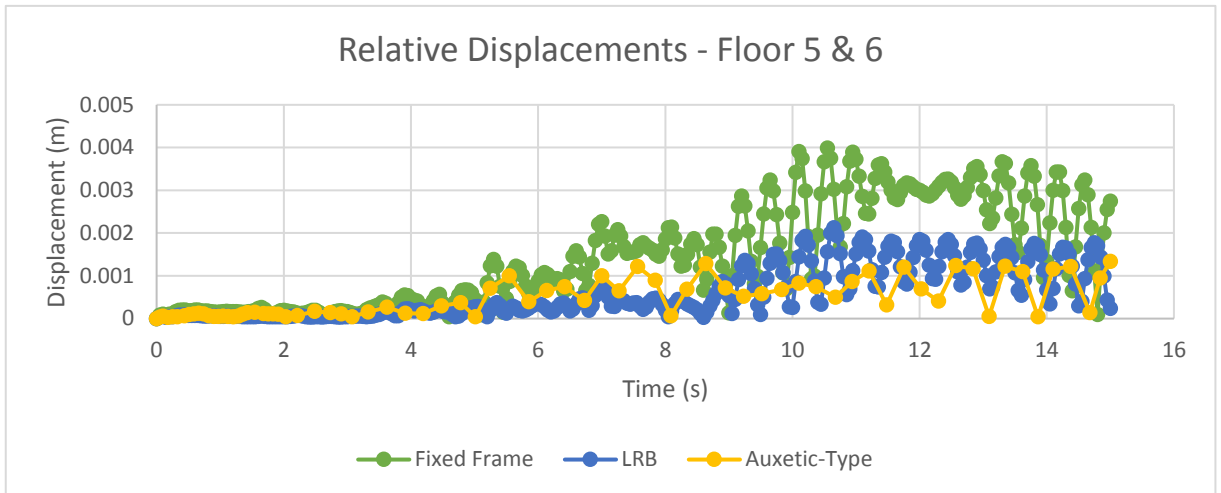


Figure 4 - 16: Relative Displacement of Floors 5 and 6

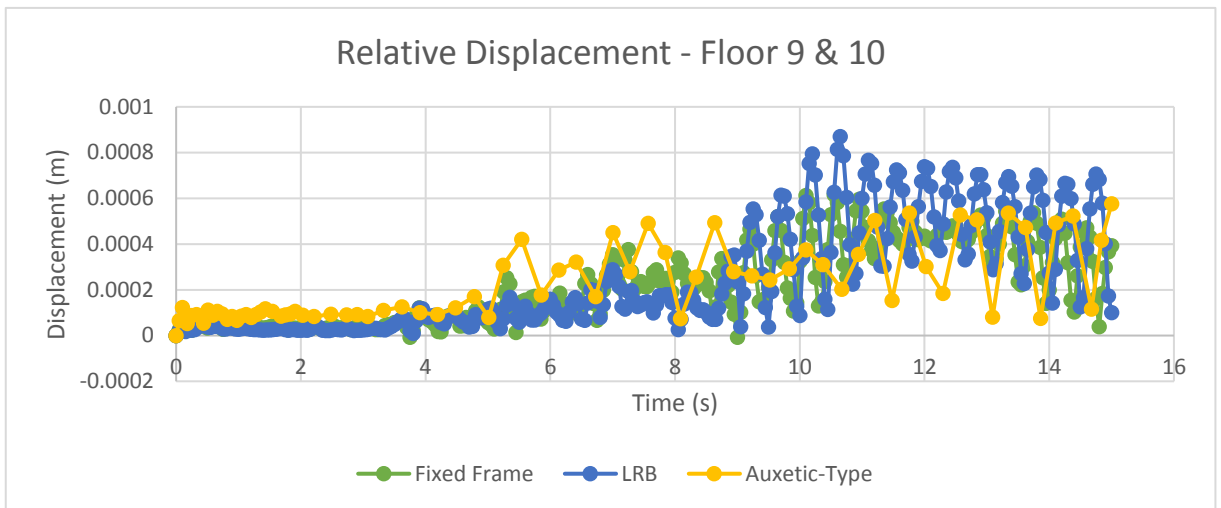


Figure 4 - 17: Relative Displacement of Floors 9 and 10

When analysing the inter-story drifts and maximum relative displacements of the entire superstructure in figures 4-18 and 4-19, it is evident that a very large relative displacement occurs at the bottom of the two isolated systems. As per past literature, this displacement is expected. The bases of the isolation systems are fixed to the surface. Due to the element of lateral flexibility introduced into the system, an initial large displacement of the base isolators occurs as a response to the imposed ground motion. This relatively large displacement serves as a means of increasing the period of the system in order to reduce the harmful effects of the earthquake. An increase in the period of the base isolator is also verified by the eigenvalue analysis that was performed. This behaviour indicates that the auxetic-type system does respond in a manner that is necessary for a base isolation system to perform effectively.

The inter-story drifts within a structure serves as an assessment in terms of a ratio. It relates the average resultant lateral relative floor displacement over time to the height of each floor, resulting in a dimensionless unit of measuring performance. In both the inter-story drifts and maximum relative floor displacement results, the auxetic system consistently improves on the relative displacements noted in the fixed frame system. In terms of maximum relative displacements, the LRB system has not performed effectively compared to the fixed frame, however when considering its inter-story drift performance, there have been some improvements.

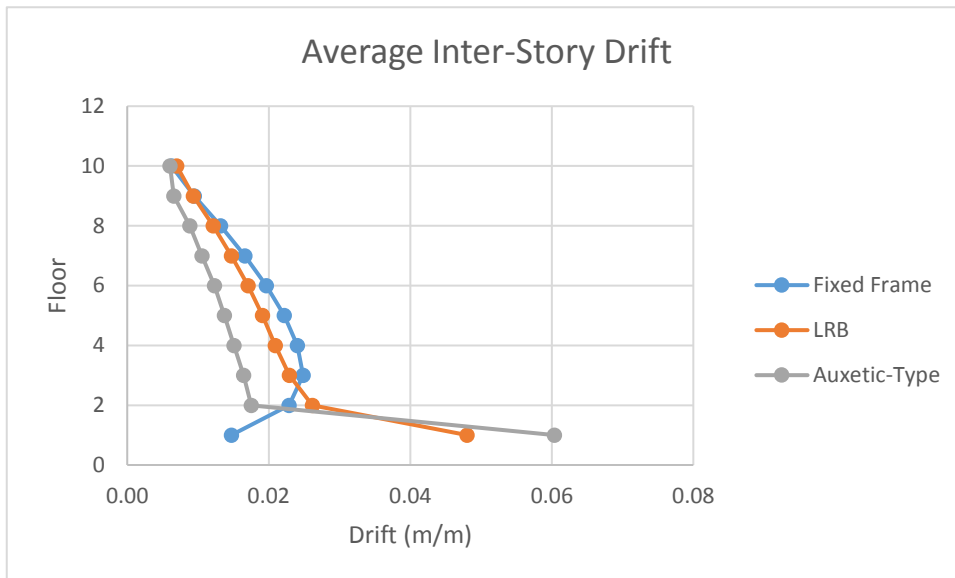


Figure 4 - 18: Average Inter-Story Drift

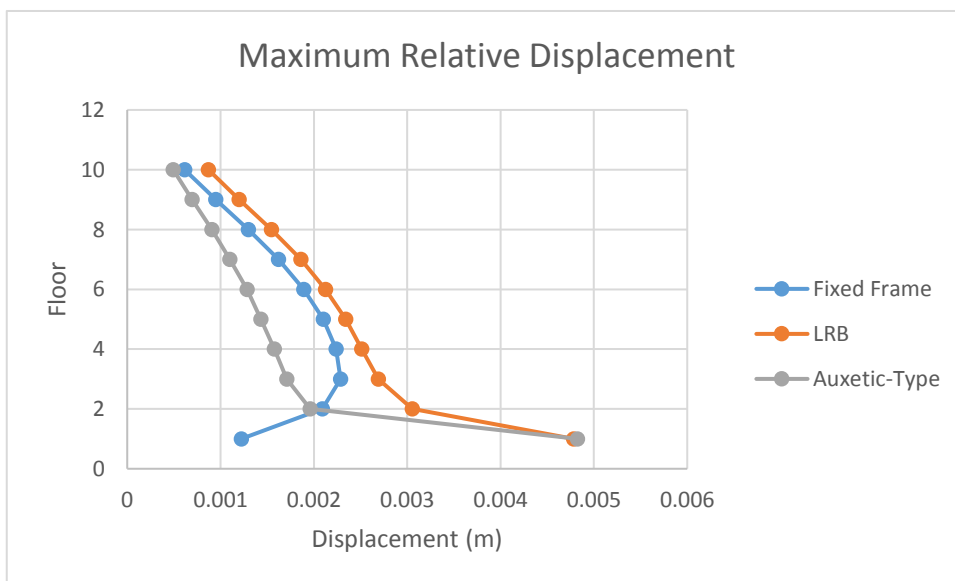


Figure 4 - 19: Maximum Relative Displacement

### 4.4.3 Relative Displacement: X-Axis

The relative displacement along the X-Axis shows that overall the auxetic-type system has performed in a similar manner to the fixed frame model. Despite the severe nature of the seismic vibrations along this axis, there still have been some improvements in performance. The LRB system has performed unexpectedly. Throughout the three levels considered, the system exhibits larger relative displacements along the X-axis compared to the fixed frame model. This is likely due to an excess of lateral flexibility in the LRB isolators in the X-direction Figure 4-20 illustrates the direction of each axis while figures 4-21 to 4-23 illustrate the relative displacement along the X-Axis.

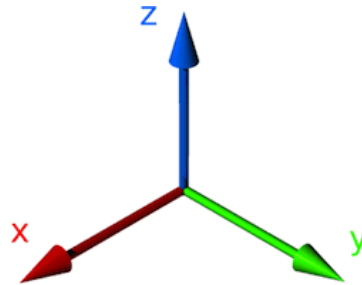


Figure 4 - 20: Orientation of the X-Y-Z Axes

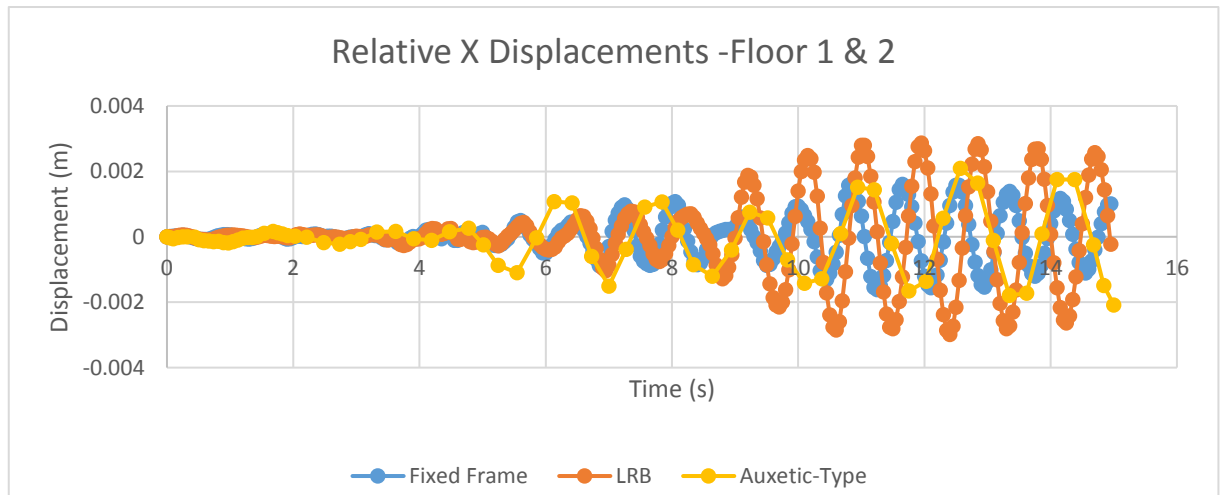


Figure 4 - 21: Relative Displacement of Floors 1 and 2 about the X-Axis

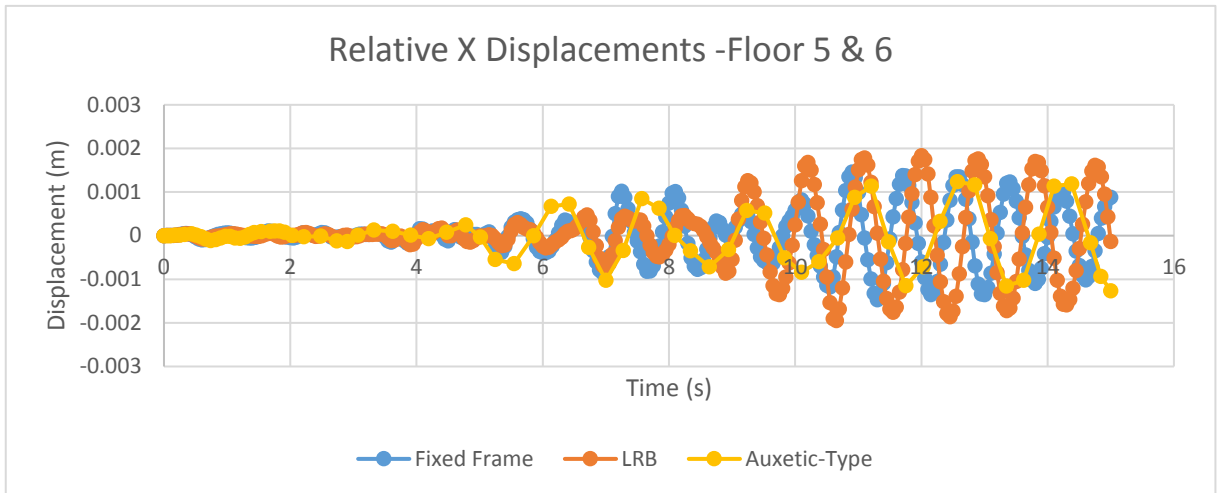


Figure 4 - 22: Relative Displacement of Floors 5 and 6 about the X-Axis

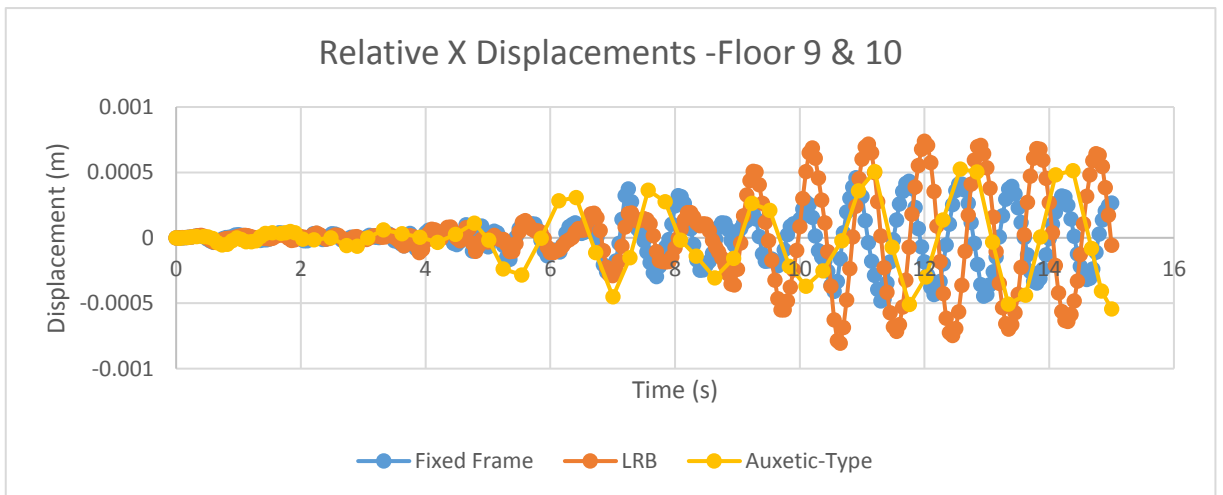


Figure 4 - 23: Relative Displacement of Floors 9 and 10 about the X-Axis

#### 4.4.4 Relative Displacement: Y-Axis

The Y component of the Northridge earthquake is not as intense as its X component. It is shown in figures 4-24 to 4-26 that both the auxetic-type and LRB systems have performed as expected along this axis. From  $t = 4.7 - 8.6\text{s}$ , the auxetic-type system experiences displacements greater than that of the fixed frame. This is attributed to the two largest seismic waves along this axis. Subsequently, the system stabilises and significantly lower relative displacements are recorded. This stabilisation indicates that the auxetic system possesses a reasonable restorative capability and is able to return the system to a more controlled level of displacement following an impulse. During this period, the auxetic system is displaced considerably less than the fixed frame as well as the LRB system.

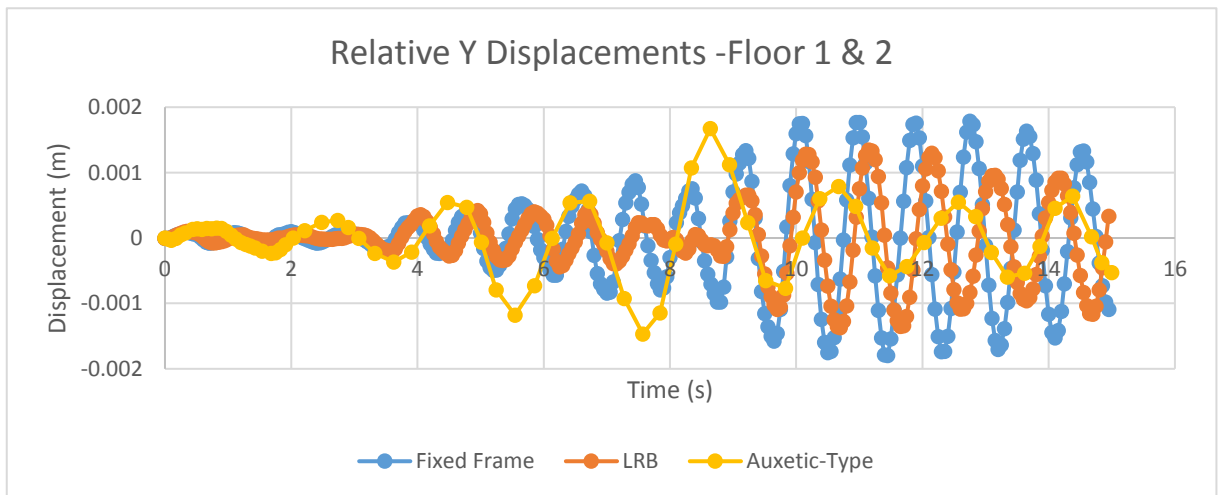


Figure 4 - 24: Relative Displacement of Floors 1 and 2 about the Y-Axis

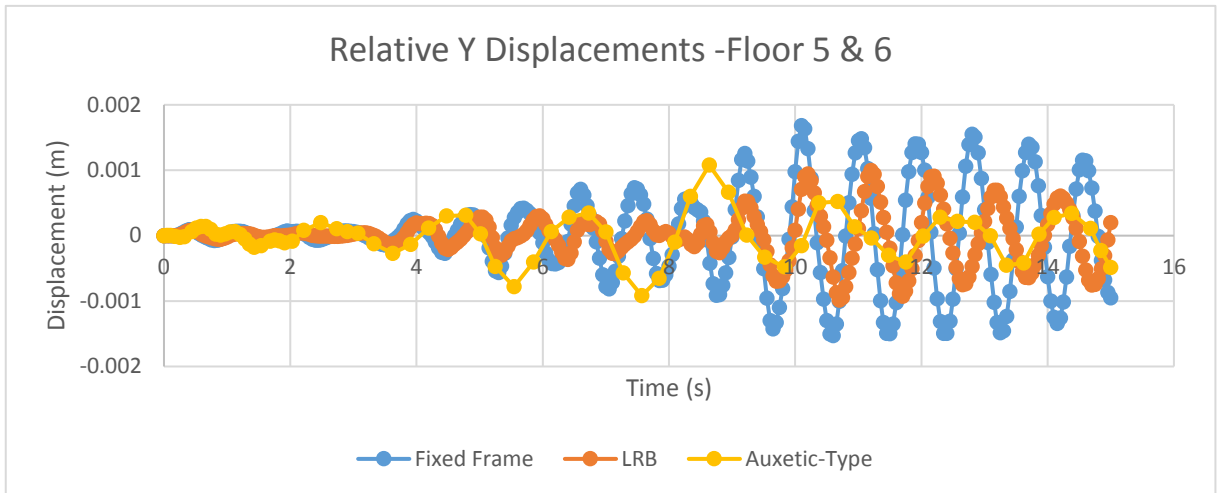


Figure 4 - 25: Relative Displacement of Floors 5 and 6 about the Y-Axis

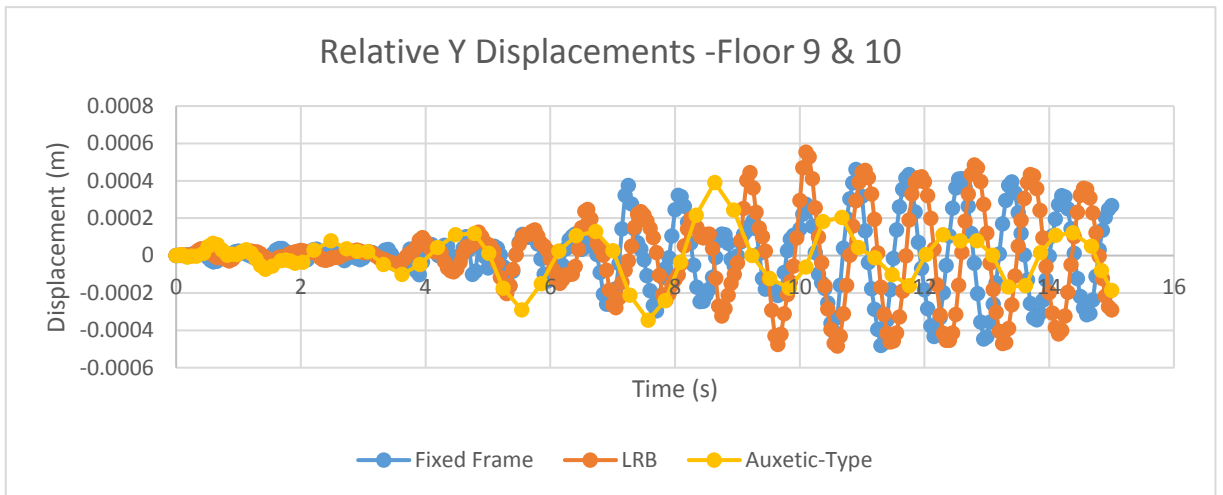


Figure 4 - 26: Relative Displacement of Floors 9 and 10 about the Y-Axis

#### 4.4.5 Relative Displacement: Z-Axis

The Z component of the Northridge earthquake presents a milder seismic loading as opposed to the X and Y components. In some cases, the loading is close to that of the Y-component. It is shown in figures 4-27 to 4-29 that the LRB systems have performed similarly to the fixed frame at all levels. At the lower levels, the auxetic base isolation exhibits slightly larger displacements as opposed to the other two systems. Its performance improves towards the middle of the superstructure, displaying similar displacements to the fixed frame. However, towards the upper floors, the auxetic system performs significantly better than the other systems. Through most of the duration of the earthquake, the system records displacements very close to zero. The range of the displacement is larger than in the middle and lower floors, however the performance is still significantly better despite the range. The slightly higher vertical displacements recorded in the lower floors is likely attributed to the structural nature of the re-entrant honeycomb layers in the base isolation. The auxetic material contracts in all directions when under a compressive load, which could have resulted in the marginally higher vertical displacements.

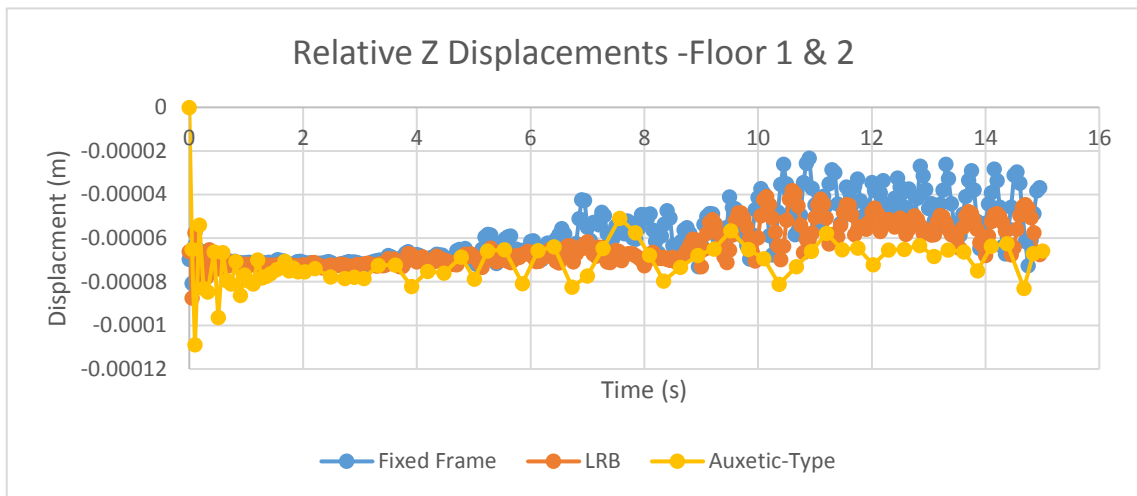


Figure 4 - 27: Relative Displacement of Floors 1 and 2 about the Z-Axis

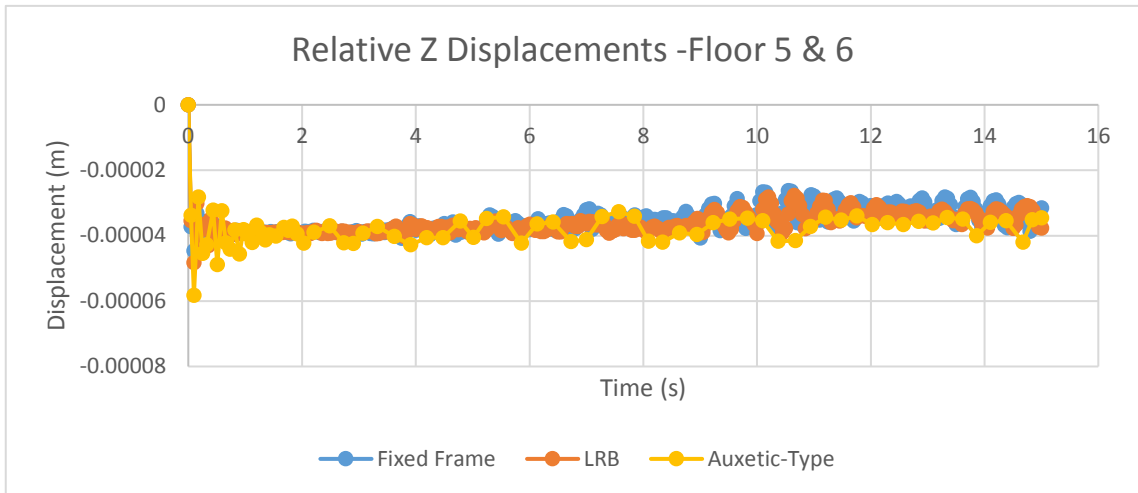


Figure 4 - 28: Relative Displacement of Floors 5 and 6 about the Z-Axis

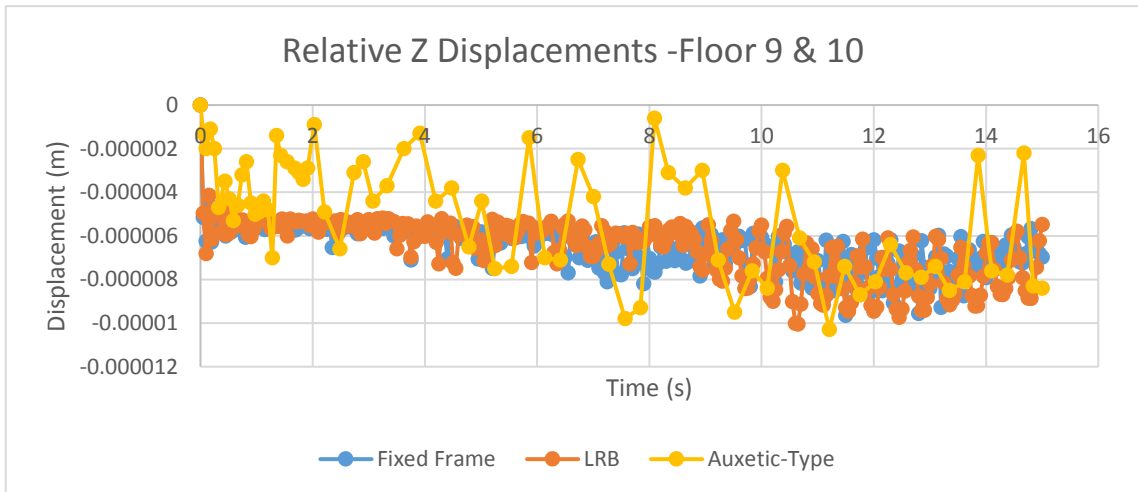


Figure 4 - 29: Relative Displacement of Floors 9 and 10 about the Z-Axis

#### 4.4.6 Acceleration

The reduction of the total acceleration in each floor as a result of the imposed seismic loading is considered to be a notable performance indicator of base isolation systems. The analysis considered the total story acceleration at the first, fifth and tenth floors in order to evaluate the acceleration reduction performance. The general trend illustrated in figures 4-30 to 4-32 reveals that overall, the auxetic-type system experienced significantly lower story accelerations when compared with the LRB and fixed base systems. On the first floor, the auxetic-type system's performance is slightly better than the fixed base system. However, as the story height increases, the acceleration reduction capabilities brought about by the system becomes more evident and for the latter part of the ground motion, it performs notably better than the LRB system. It should be noted that higher than expected total story accelerations were present in the LRB system on the first floor. On floors five and ten, the total acceleration mostly matched or slightly exceeded that of the fixed base system, however during certain portions of the earthquake, the total acceleration experienced have been improved. Figure 4-33 shows the average total floor accelerations throughout the system. The auxetic-type system demonstrates an improved performance throughout the superstructure when compared with the fixed frame. Total accelerations do consistently increase with an increase in height, however this increase occurs at a more controlled rate.

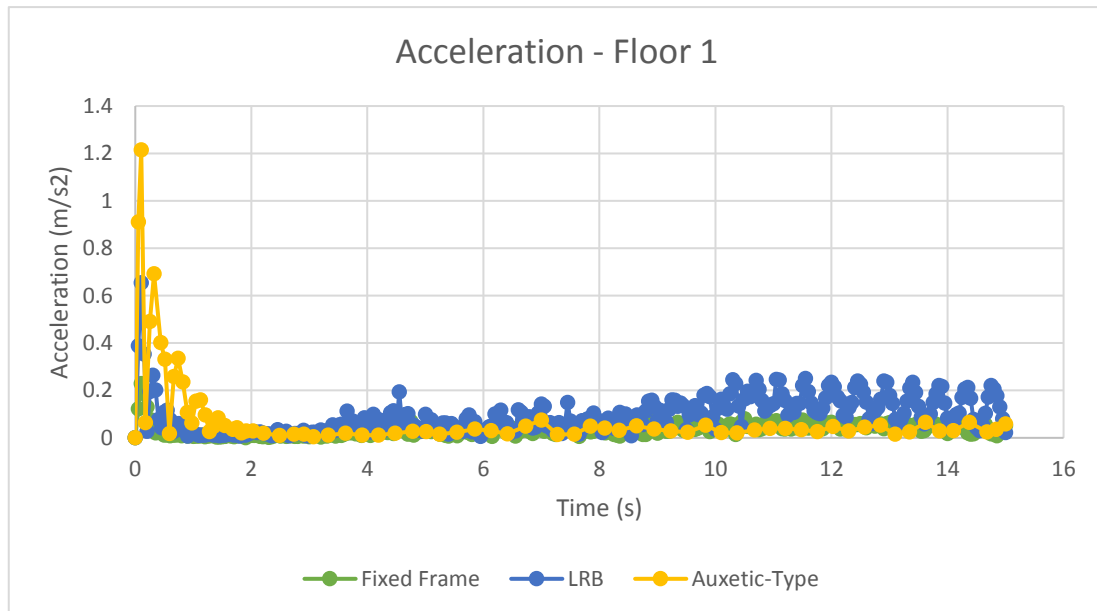


Figure 4 - 30: Acceleration on Floor 1

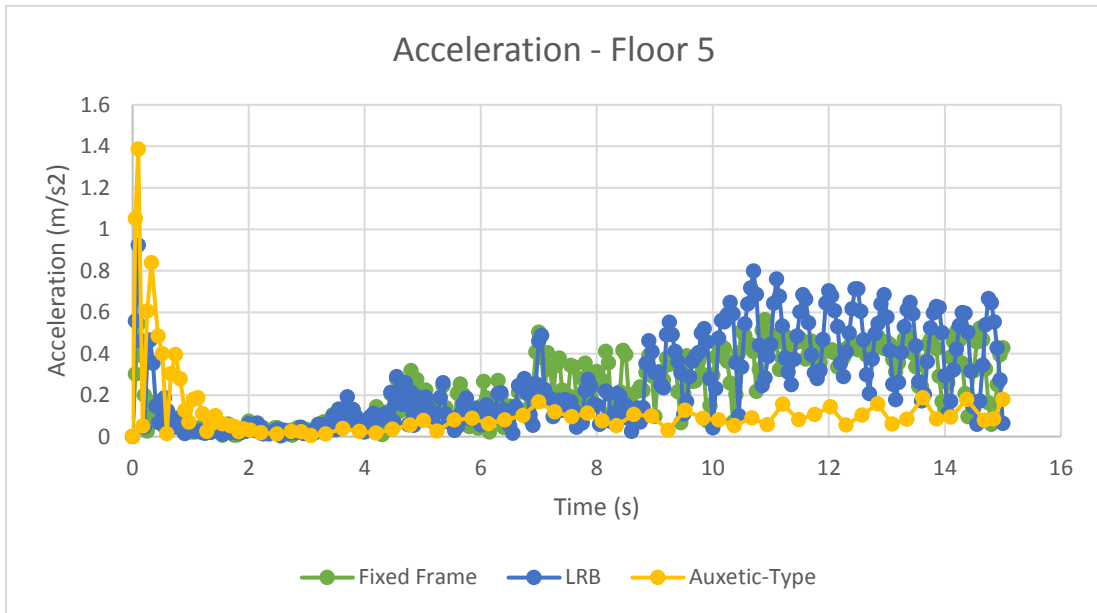


Figure 4 - 31: Acceleration on Floor 5

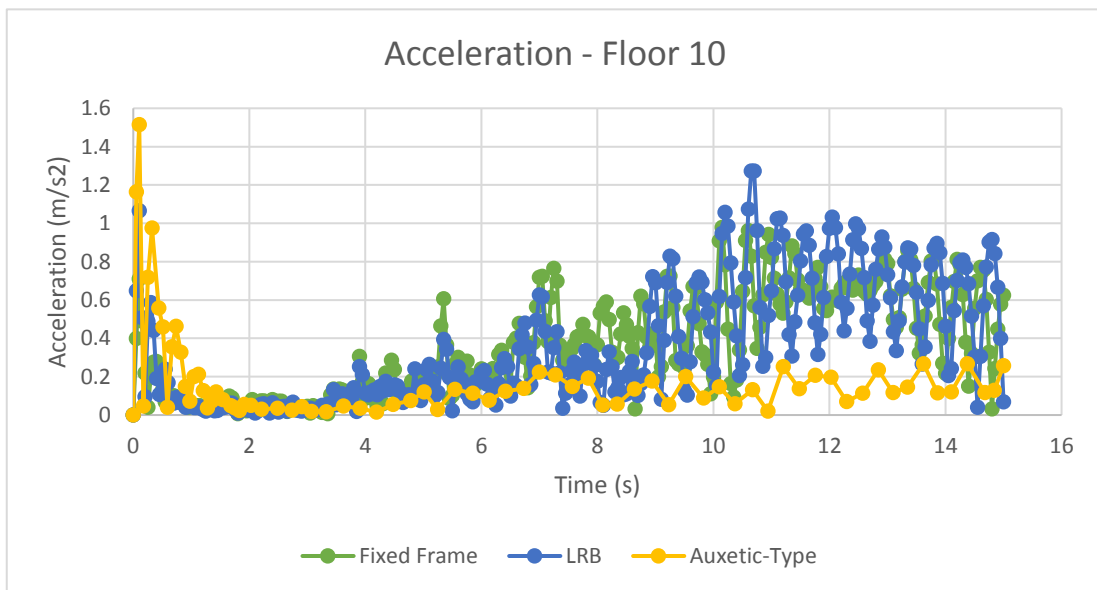


Figure 4 - 32: Acceleration on Floor 10

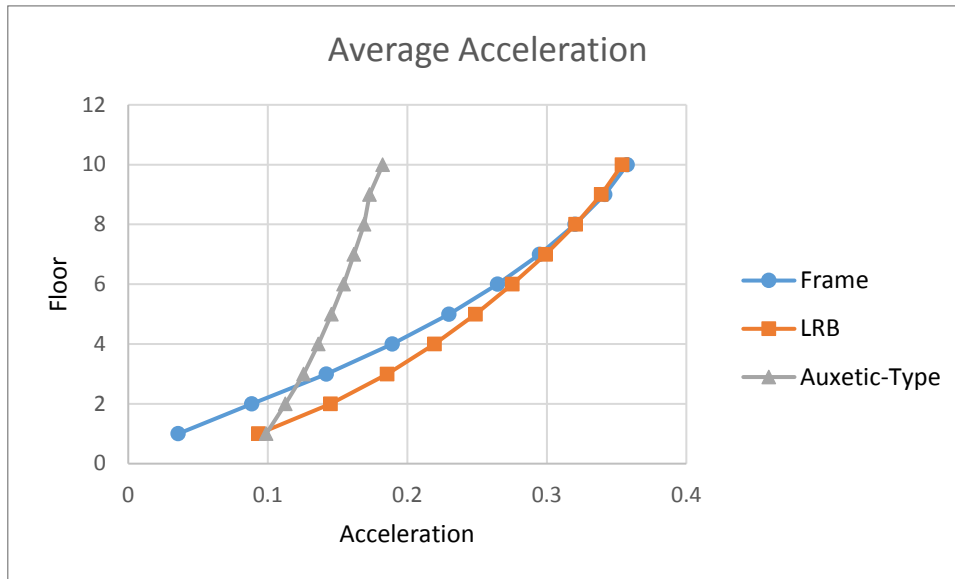


Figure 4 - 33: Average Floor Acceleration with Respect to Time

#### 4.4.7 Reaction Forces

Table 4-2 list the overall reaction forces in each of the three models analysed. Along the horizontal X and Y axes, the forces in the LRB and auxetic-type systems are lower than the fixed base model. While in the vertical Z-axis, the reaction forces are just under 3 KN higher in these systems. The reaction forces were determined using all nodes present at the four fixed supports in each system.

Table 4 - 2: Reaction Forces

Reaction Force (KN)	Frame	LRB	Auxetic-Type
X-Axis (KN)	-3.1617	0.55478	2.387
Y-Axis (KN)	2.7992	-0.80638	0.42292
Z-Axis (KN)	113.47	116.15	116.18
Total (KN)	113.55	116.15	116.21

## 4.5 Irpinia, Italy 1980

The Irpinia earthquake occurred in Italy in 1980 and had a magnitude of 6.9. Like Northridge, Irpinia can be described as being intense early in the ground motion and slowly tapering off after 15 seconds. This earthquake's strongest vibrations occur along the Y-axis, however vibrations along the X and Z axes are significantly close to that of the Y-axis vibrations. The interval of 0 – 15 seconds was noted as being the most intense portion of the earthquake and was therefore used in the analysis. This earthquake data is shown in figure 4-34.

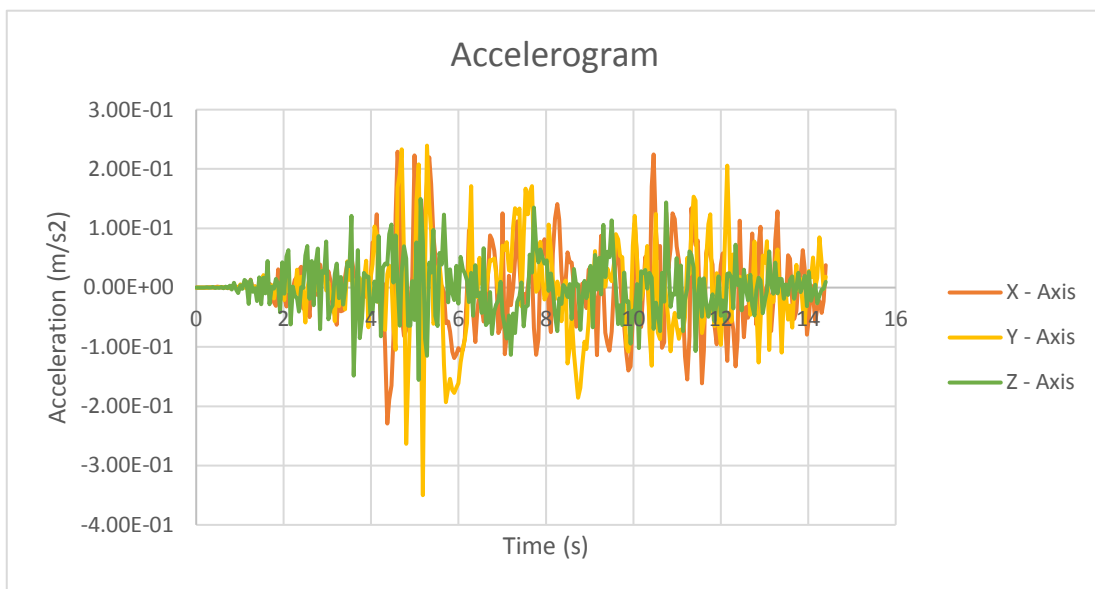


Figure 4 - 34: Irpinia Earthquake Data

The total deformation of the system behaves similarly to the Northridge earthquake and is also in line with deformation trends highlighted in past literature. The auxetic-type system displays a notably higher total deformation during the most severe intervals of the earthquake, namely around  $t = 5s$  and  $t = 10 - 14s$ . The total deformation of the LRB system remains relatively constant throughout this duration. Figure 4-35 depicts the total deformation of the three systems.



Figure 4 - 35: Total Deformation of the Irpinia Earthquake

### 4.5.1 Total Relative Displacement

As shown in figures 4-36 to 4-38, the auxetic-type system exhibits a favourable performance for most of the duration of the earthquake at the lower floors. However, on the upper floors, the performance is only favourable for the first half of the earthquake, notably so between  $t = 0 - 4$ . Following this initial stage of the loading, the relative displacements exceed that of the other two systems. This behaviour is in line with the nature of the seismic loading. The LRB system has consistently shown a reduction in relative displacements throughout the three levels evaluated.

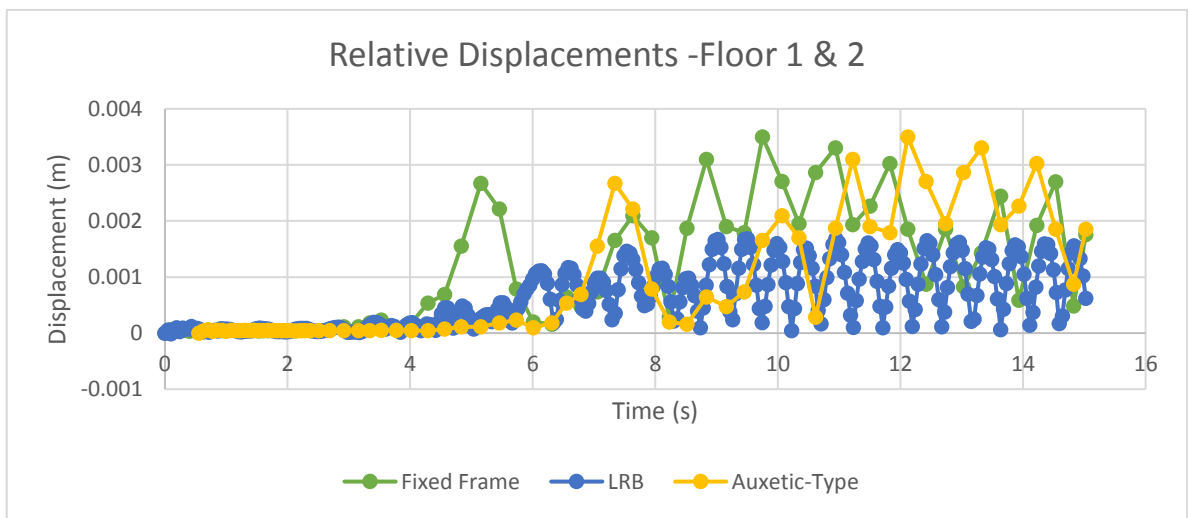


Figure 4 - 36: Relative Displacement of Floors 1 and 2

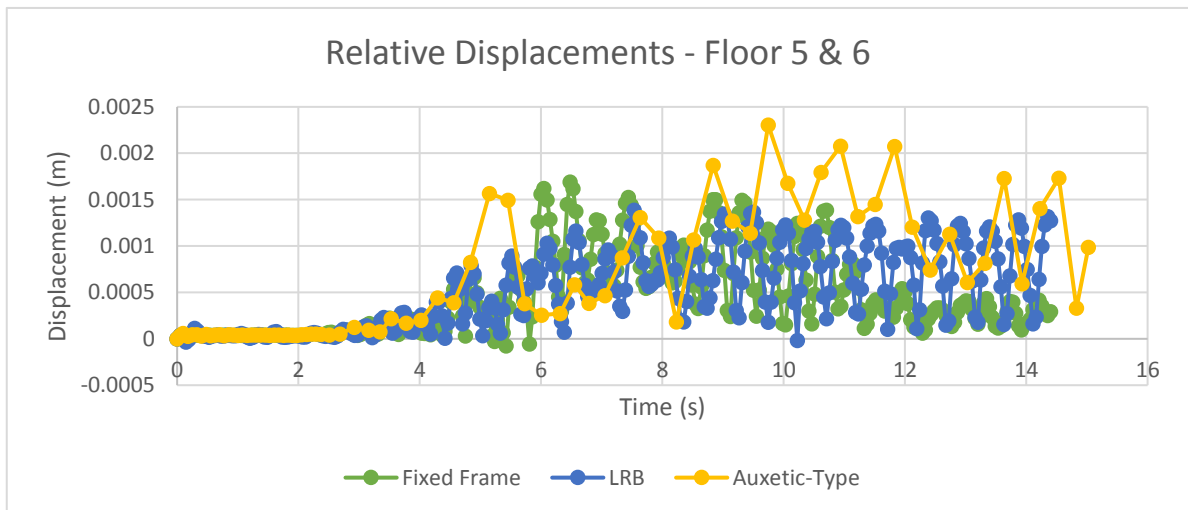


Figure 4 - 37: Relative Displacement of Floors 5 and 6

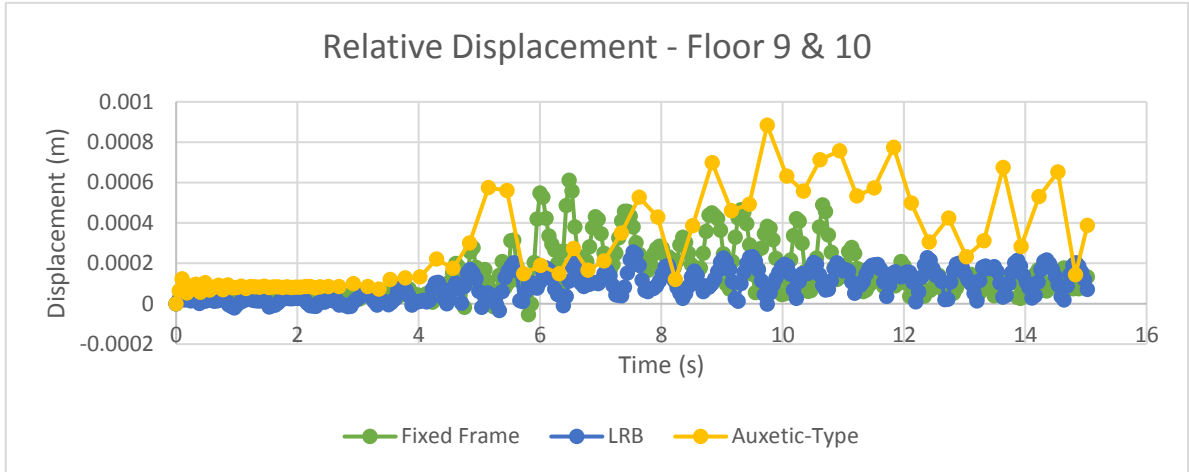


Figure 4 - 38: Relative Displacement of Floors 9 and 10

Figures 4-39 and 4-40 represents the inter-story drifts and maximum relative displacements. The inter-story drift experienced by the auxetic system is identical to the LRB system in the middle of the super structure. At the top and bottom of the superstructure, the auxetic system's drifts are only marginally higher. Additionally, the drifts decrease at a seemingly uniform rate as opposed to the other systems. Unlike its relative displacement performance, the fixed frame experiences the overall most favourable inter-story drifts. The difference between the three systems' performance is only very slightly different. In terms of maximum relative displacements, the LRB system has shown to undergo smaller maximum displacements, while that of the auxetic system is larger than the fixed frame's maximum displacement.

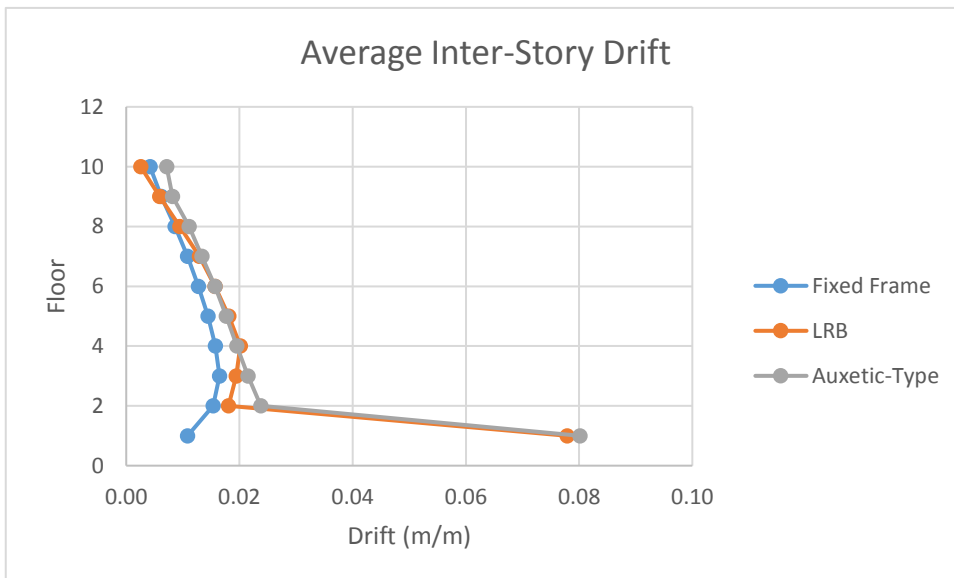


Figure 4 - 39: Average Inter-Story Drift

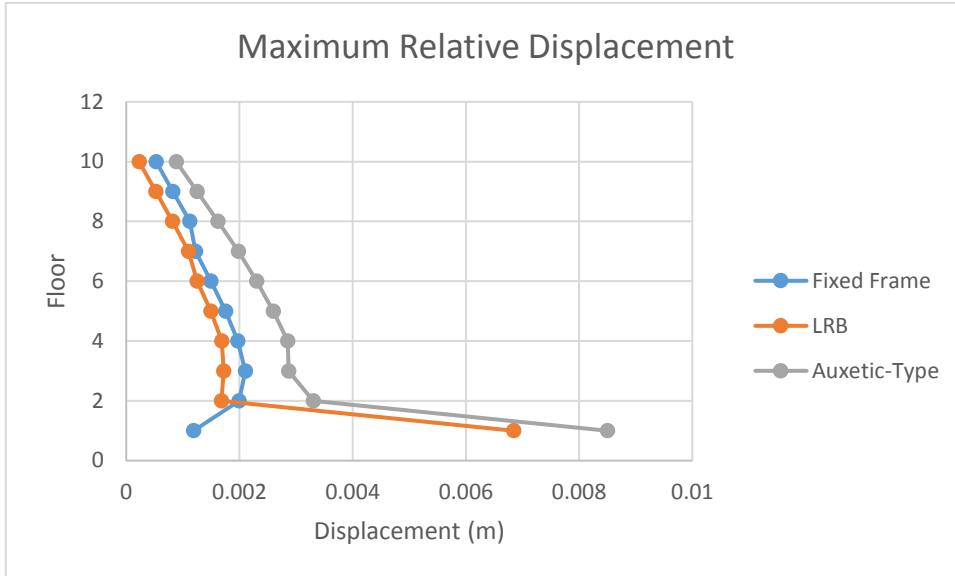


Figure 4 - 40: Maximum Relative Displacement

## 4.5.2 Acceleration

Similarly, to the Northridge earthquake, figures 4-41 to 4-43 indicate that the auxetic-type system experienced significantly lower story accelerations when compared with the LRB and fixed base systems. On the first floor, the auxetic-type system experiences similar accelerations to the fixed base system and marginally exceeds it after  $t = 9.4\text{s}$ . As the story height increases, the acceleration in the auxetic system remains more favourable than the other two systems. Towards the latter part of the earthquake, the accelerations experienced in the auxetic and fixed base systems is similar. The latter part of the earthquake is associated with consistently strong vibrations along all three axes. On the lower floors, the LRB system exhibits a performance that is less favourable than the fixed frame. However, towards the upper floors, the LRB system performs similarly to the fixed base frame and in some instances, the performance has shown an improvement.

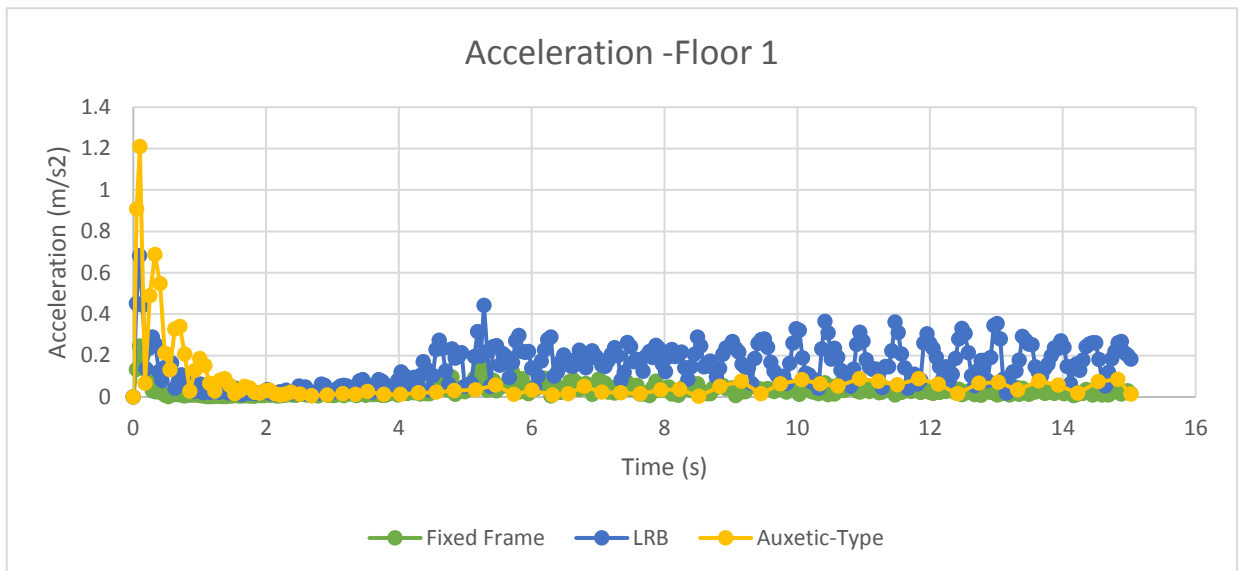


Figure 4 - 41: Acceleration on Floor 1

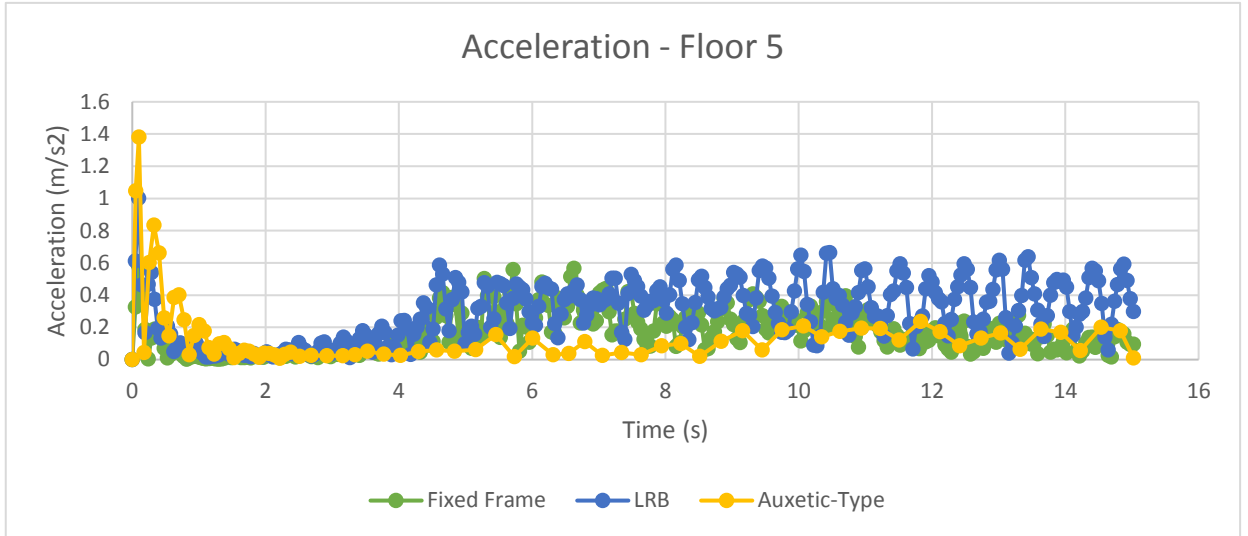


Figure 4 - 42: Acceleration on Floor 5

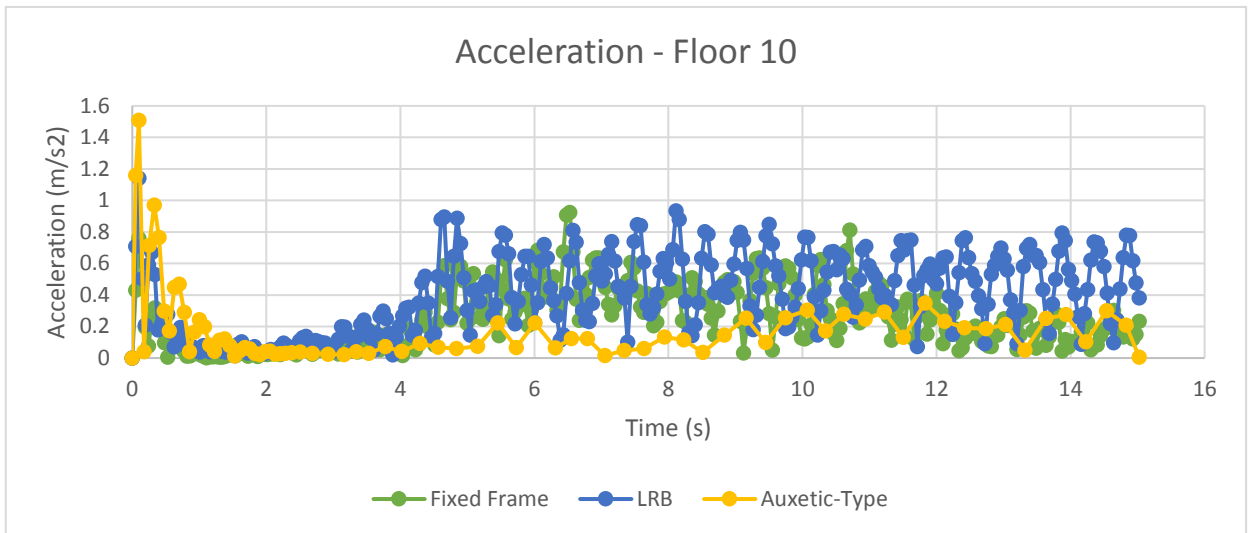


Figure 4 - 43: Acceleration on Floor 10

## 4.6 Düzce, Turkey 1999

The models were evaluated against the magnitude 7.15 earthquake in Düzce, Turkey. The earthquake, which occurred in 1999, exhibited its most severe seismic waves towards the middle of its 43 second duration. Minor initial vibrations occur leading up to this peak. Due to this, the 15 second duration of the earthquake used in the analysis is from  $t = 15 - 30$ s. This is shown in figure 4-44. Vibrations along the Y-Axis are most dominant in this earthquake, however vibrations in the X-Axis remain close to that of the Y-Axis through the duration of the data used in the analysis.

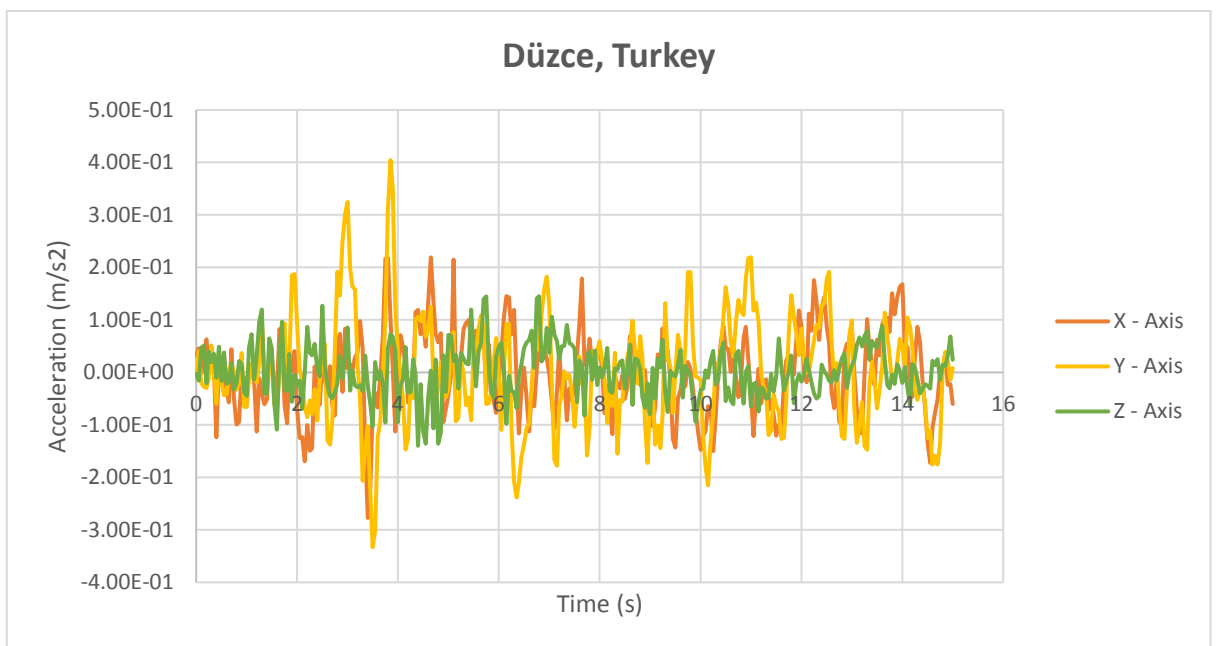


Figure 4 - 44: Düzce Earthquake Data

The total deformation of the auxetic system under this earthquake exhibits a slightly different behaviour than in the Northridge and Irpinia earthquakes. While the LRB system performs as per trends identified in the other two analyses conducted, the auxetic system experiences a lower total deformation initially. From  $t = 9.7$ s, the system's total deformation consistently increases. A spike in its deformation coincides with the largest vibration in the analysis, which lead to a similar total deformation between all three systems at this point. Figure 4-45 depicts the total deformation of the three systems.

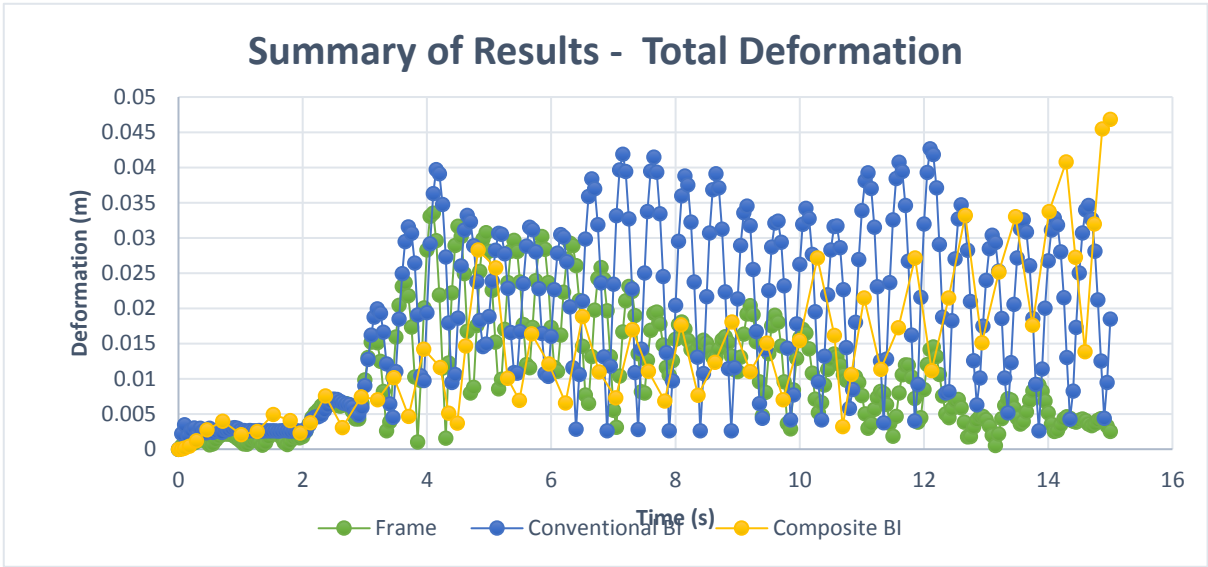


Figure 4 - 45: Total Deformation under the Düzce Earthquake

### 4.6.1 Total Relative Displacement

It can be seen from figures 4-46 to 4-48 that the auxetic base isolation consistently shows an improved performance. The general trend shows the auxetic system performing well until  $t = 10$ s where the relative displacements on throughout the superstructure steadily increases. This is a similar trend that occurs in the total deformation. The LRB system displays relative displacements that are higher than the fixed frame. This man indicate that the system offers an amount of lateral flexibility that is not ideal for an earthquake of this nature. The performance of the LRBs system remains constant throughout the analysis.

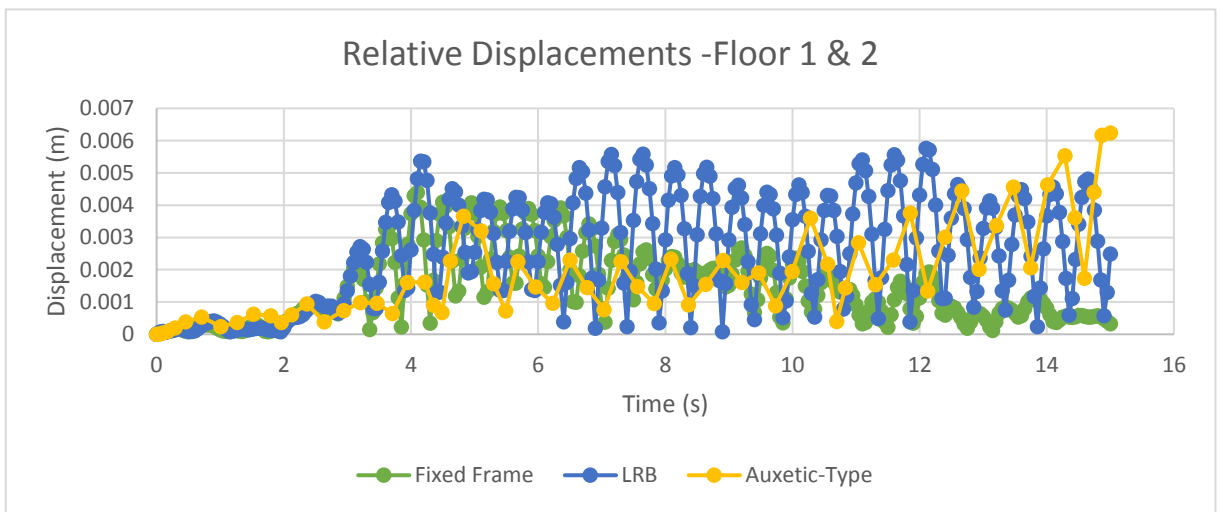


Figure 4 - 46: Relative Displacement of Floors 1 and 2

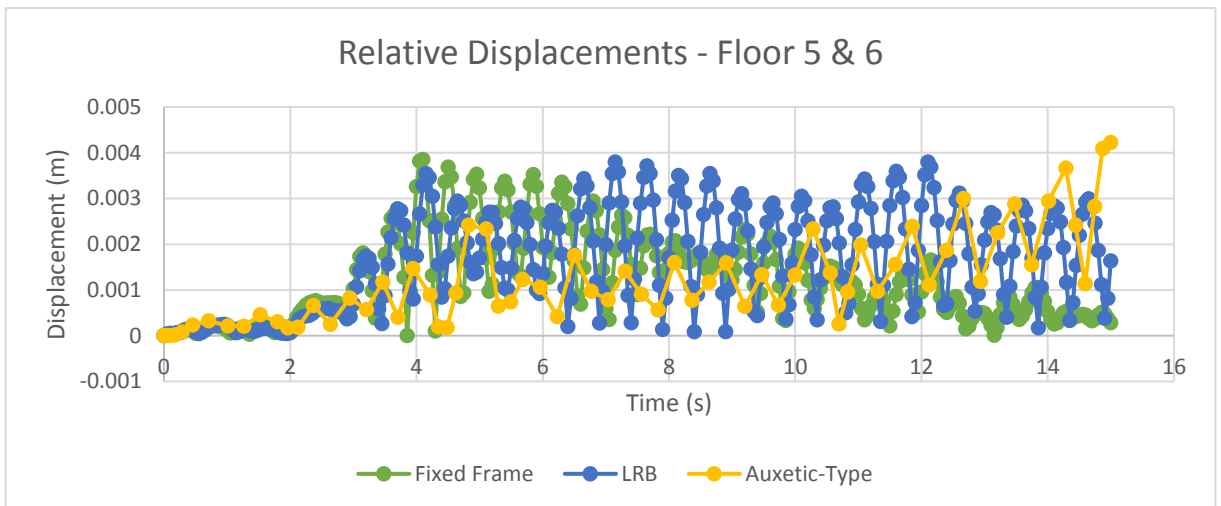


Figure 4 - 47: Relative Displacement of Floors 5 and 6

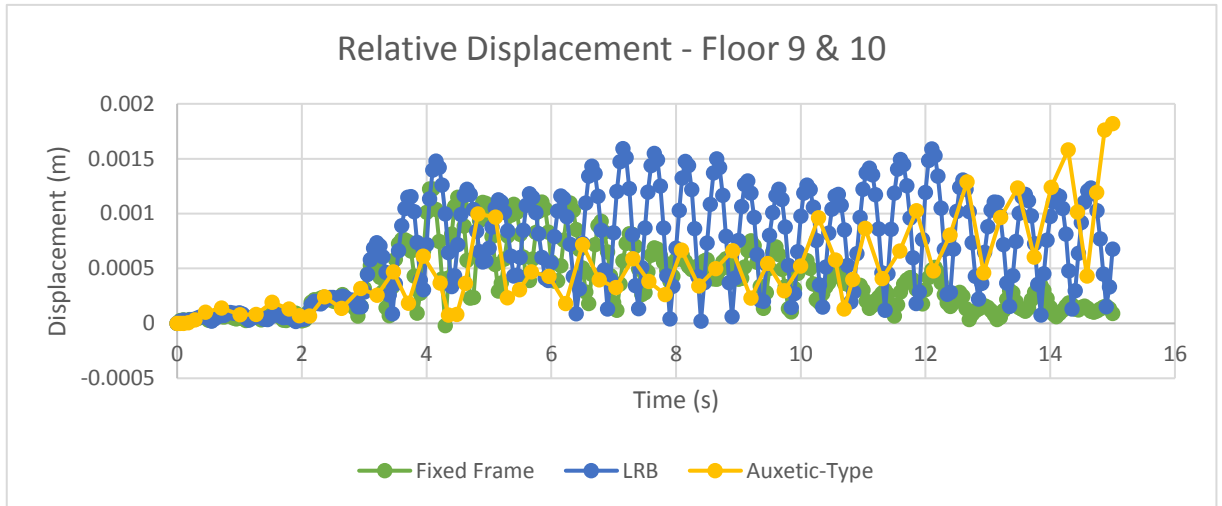


Figure 4 - 48: Relative Displacement of Floors 9 and 10

The inter-story drifts occurring in the auxetic and fixed base systems are similar besides slightly higher drifts in the ninth and tenth floors occurring in the auxetic system. However slight improvements in performance occur in the middle stories from the fourth to sixth floors. The overall performance of the auxetic-type system is a result of the increase in relative displacement towards the latter part of the earthquake loading. Similarly, to its total relative displacement performance, the LRB system experiences larger inter-story drifts as opposed to the other two systems. When analysing the maximum relative story displacements, it is seen that the auxetic system exhibits the largest displacements while the LRB system performs similarly to the fixed base system. While differences in the performance of the systems do exist, the differences in this analysis is minimal. The inter-story drift and maximum relative displacements of the systems are shown in figures 4-49 and 4-50.

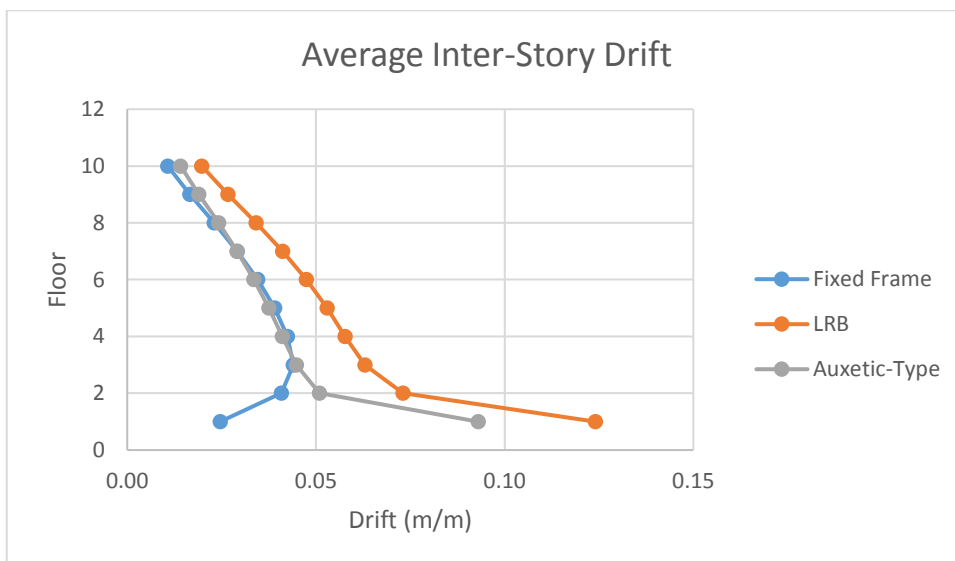


Figure 4 - 49: Average Inter-Story Drift

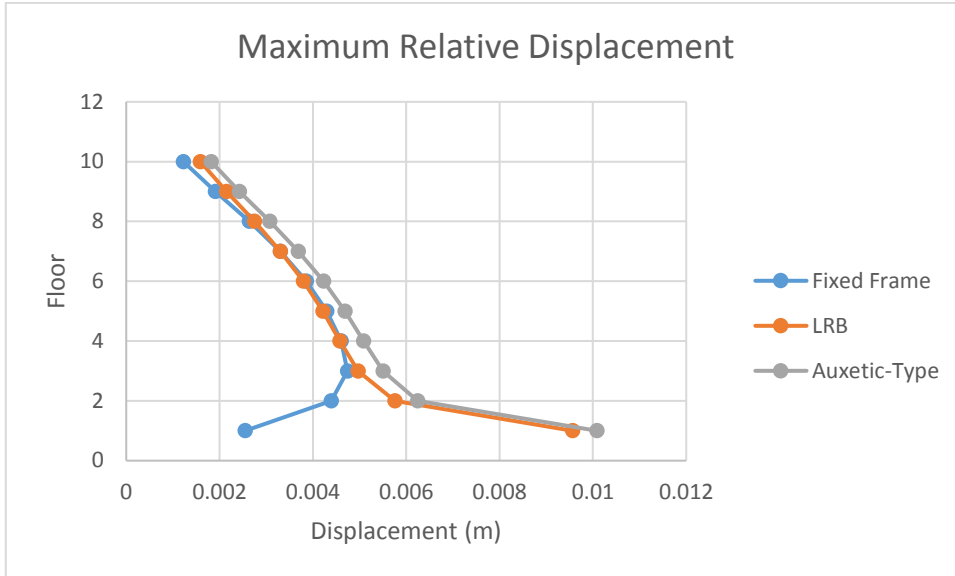


Figure 4 - 50: Maximum Relative Displacement

#### 4.6.2 Relative Displacement: X-Axis

Along the X-Axis, the LRB system has performed well relative to the fixed base system. Its behaviour is similar to the fixed system for the initial part of the loading, after which the performance shows an improvement, lowering the relative displacements throughout the superstructure. The auxetic base isolation exhibits a similar performance to the other two systems during the initial part of the analysis, in some cases showing an improvement in relative displacement. However, during the last five seconds of the loading, the relative displacement gradually increases in the top and bottom floors. This gradual increase occurs around a second later in the middle stories. The increase in relative displacement in the top floor of the superstructure is however significantly less than that of the middle and bottom floors. This is a response to the sudden increase in seismic vibrations along the X-Axis. Figures 4-51 to 4-53 depict the relative displacements along the X-Axis.

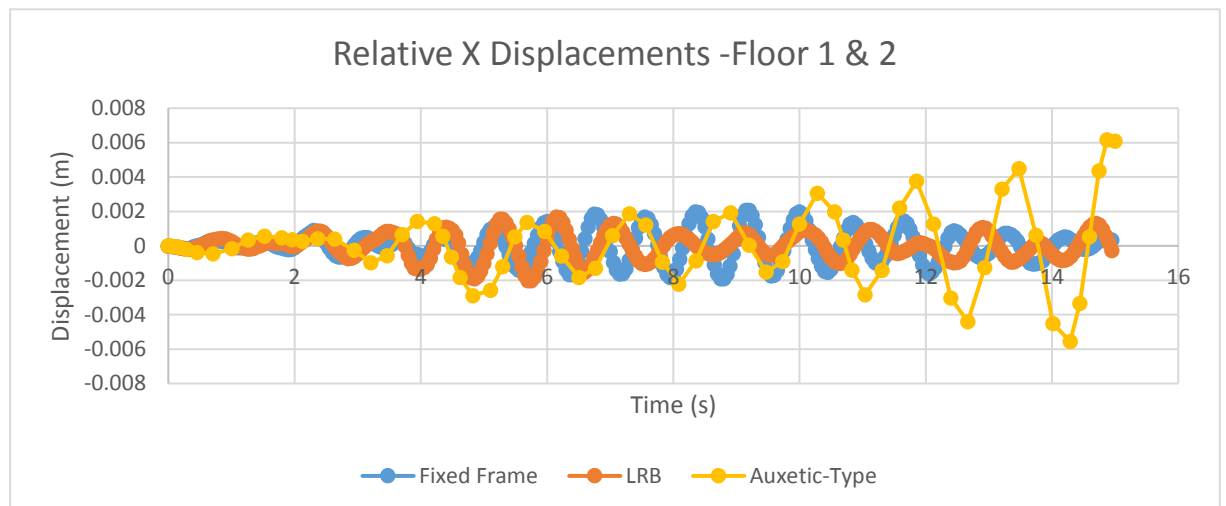


Figure 4 - 51: Relative Displacement of Floors 1 and 2 about the X-Axis

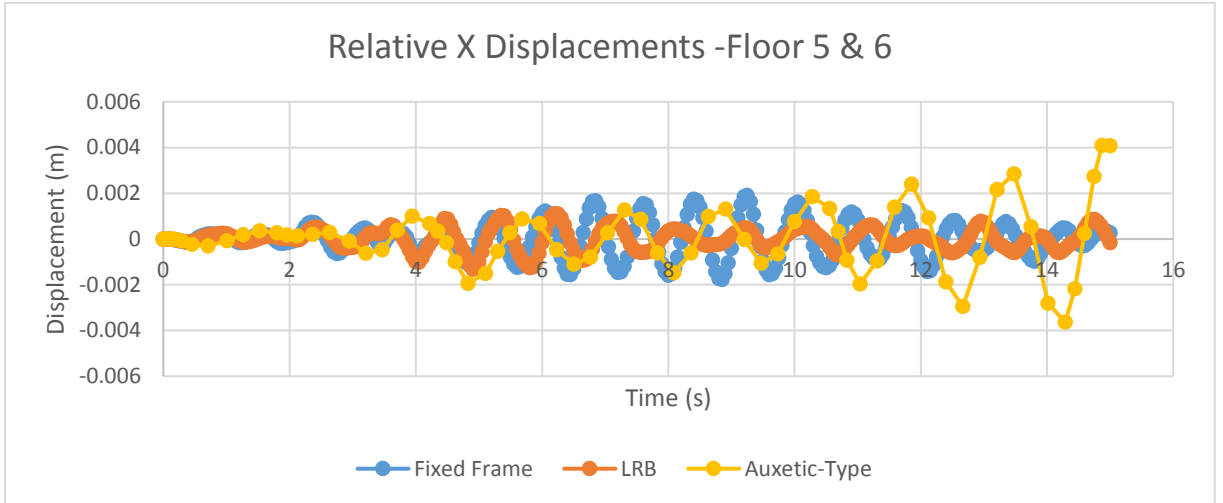


Figure 4 - 52: Relative Displacement of Floors 5 and 6 about the X-Axis

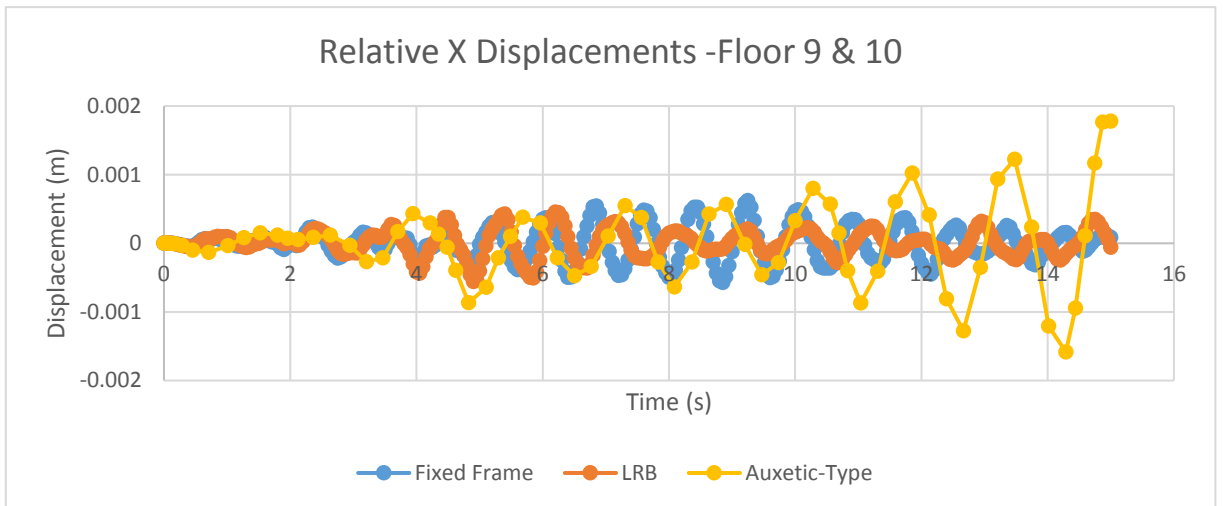


Figure 4 - 53: Relative Displacement of Floors 9 and 10 about the X-Axis

### 4.6.3 Relative Displacement: Y-Axis

As shown in figures 4-54 to 4-56, long the Y-Axis, the conventional base isolator's relative displacement significantly exceeds that of the fixed base during the severe portion of the earthquake. On the upper floors, however, it performs well during the latter part of the loading. This again is an indicator that the system may provide more lateral flexibility that is necessary for an earthquake of this nature. The auxetic-type system has displayed favourable relative displacement results along the Y-Axis, throughout almost the entire duration of the loading. At the lower portion and middle stories of structure the displacements are notably lower than the fixed base, however at higher floors the displacements are similar to the fixed base. Despite the seismic waves of the earthquake being most severe along the Y-Axis, the auxetic system has still performed favourably and has shown an improvement in performance as compared to the fixed and LRB systems.

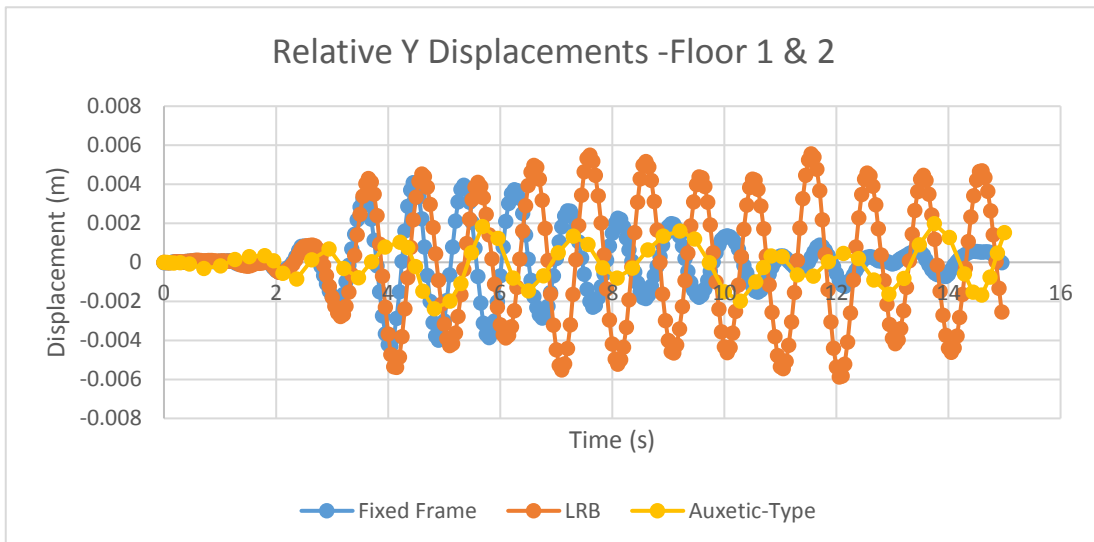


Figure 4 - 54: Relative Displacement of Floors 1 and 2 about the Y-Axis

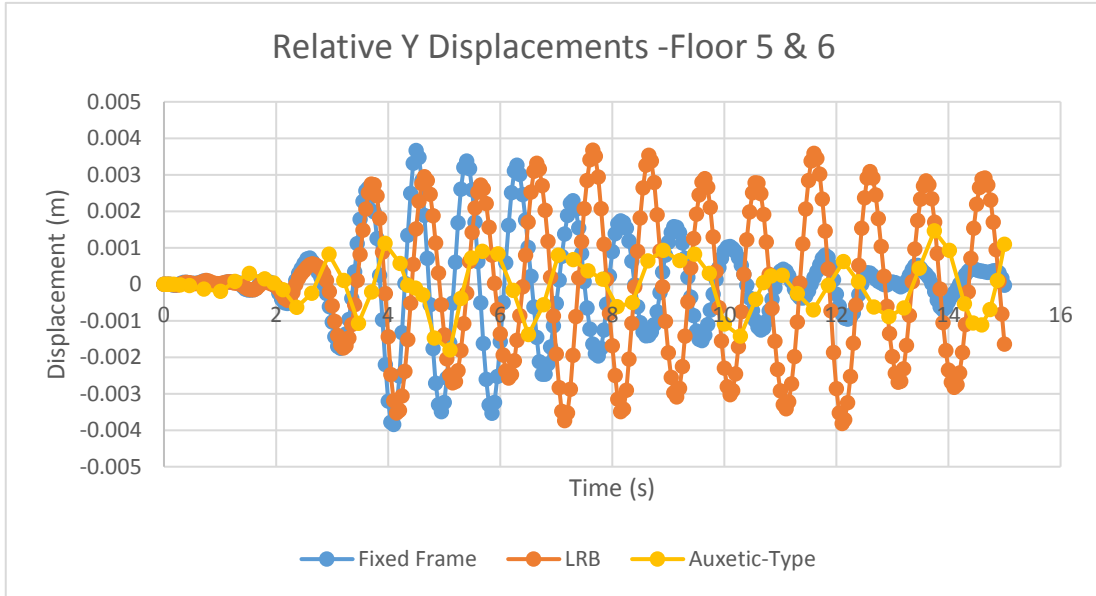


Figure 4 - 55: Relative Displacement of Floors 5 and 6 about the Y-Axis

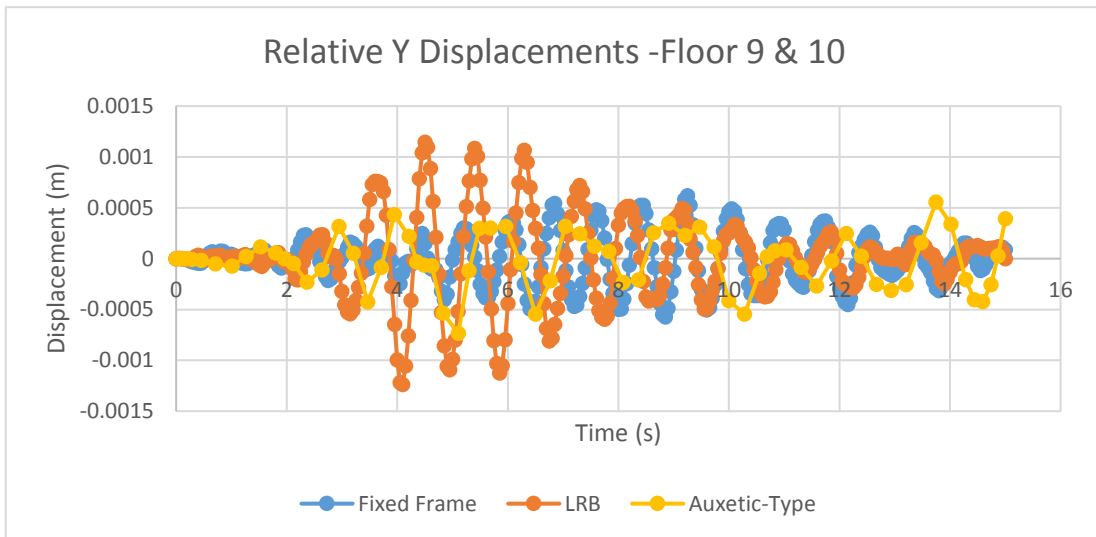


Figure 4 - 56: Relative Displacement of Floors 9 and 10 about the Y-Axis

#### 4.6.4 Relative Displacement: Z-Axis

The Z component of the Düzce earthquake presents a milder seismic loading as opposed to the X and Y components. It is shown in figures 4-57 to 4-59 that the LRB systems have performed similarly to the fixed frame at all levels, with the LRB system sometimes exhibiting a better performance and other times showing larger relative displacements than the frame. The auxetic base isolation has shown a significant improvement in performance throughout the superstructure. It has performed consistently, with relative displacements rarely reaching that of the fixed base system. The sharp increases in relative displacement in the top and bottom floors is likely a result of the auxetic behaviour of in the base isolation system.

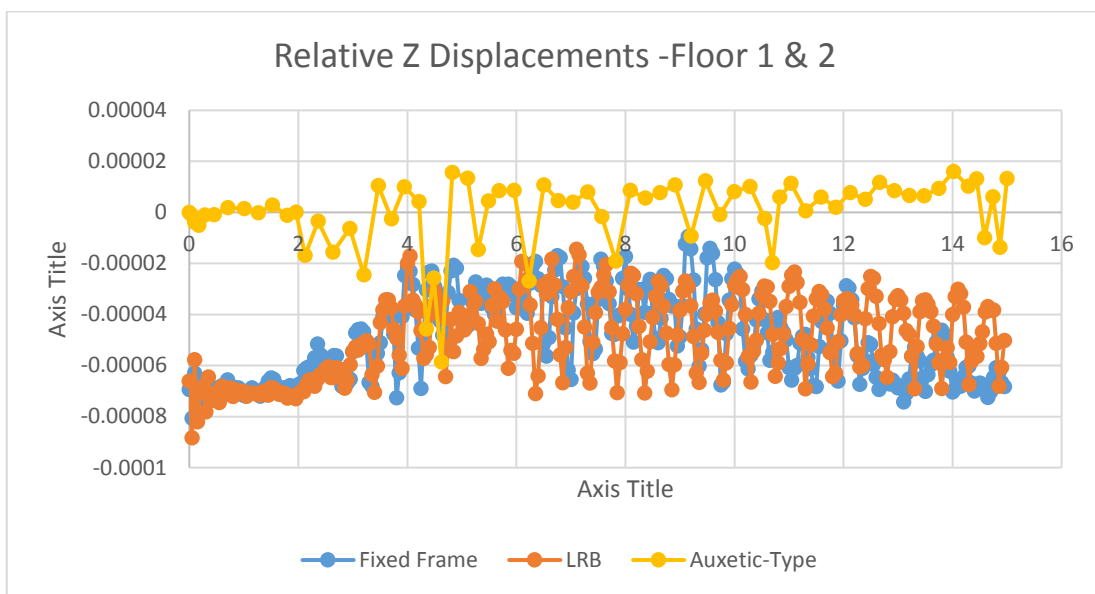


Figure 4 - 57: Relative Displacement of Floors 1 and 2 about the Z-Axis

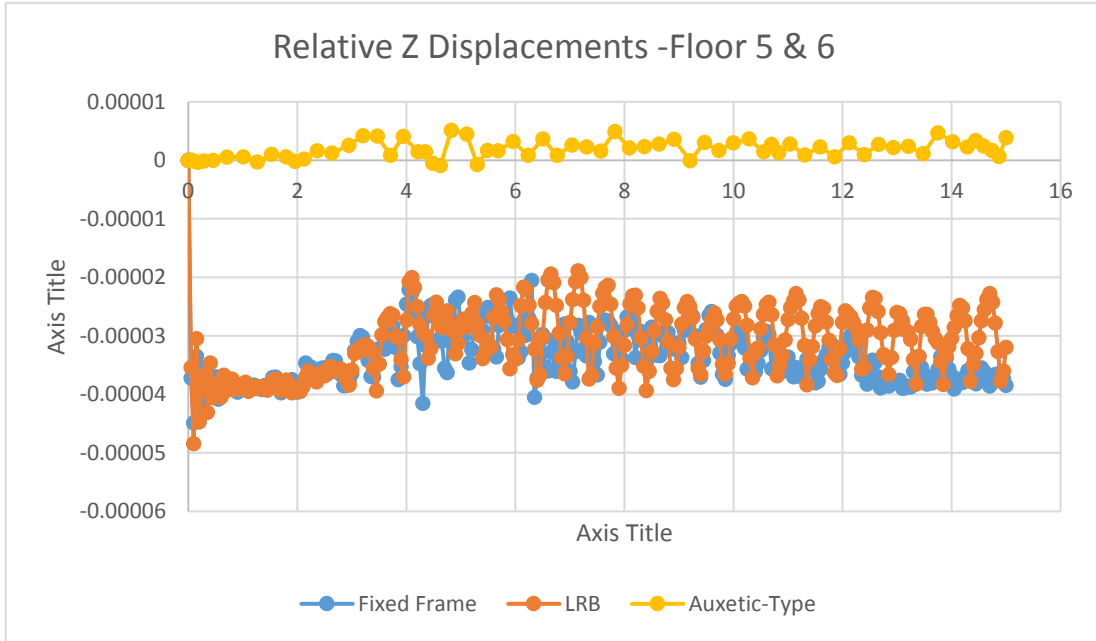


Figure 4 - 58: Relative Displacement of Floors 5 and 6 about the Z-Axis

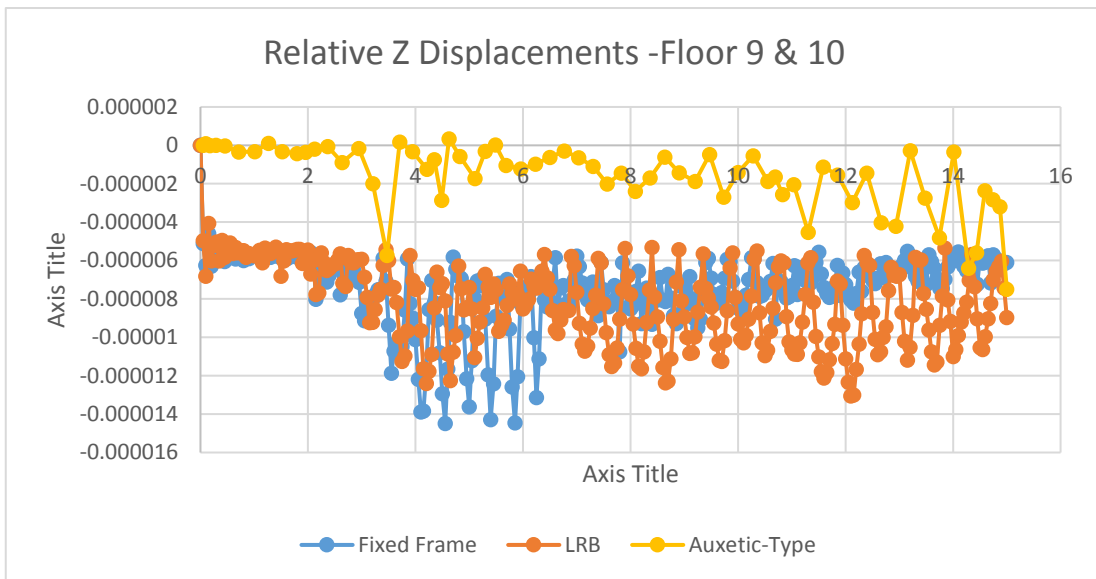


Figure 4 - 59: Relative Displacement of Floors 9 and 10 about the Z-Axis

## 4.7 Discussion and Recommendations

The methodological approach to the study involved defining and numerically testing the three systems using finite element models. The performance of each of these systems was investigated by evaluating the response of the multi-story structural steel superstructure and using the fixed base model as a base line for the assessments. Another idea was to compare the performance of the auxetic-type system to the LRB system. It was decided that the geometric parameters of the two base isolators analysed would be similar. This was done in order to determine the performance of the systems based on the same geometric constraints. The overall performance of the LRB system was unusual. Through analysing its response to all three sets of seismic loading, the response has in some instances been unfavourable when compared to the fixed frame. This may indicate that the design of the isolator was inadequate for earthquakes of this nature. This may be attributed to the geometrics of the system or the material properties used.

An eigenvalue analysis was performed to serve as an initial basic dynamic analysis. This was used to determine the natural frequency, natural period and mode shapes of each system. By doing so, the behaviour of the three systems when subjected to dynamic loads could be determined. The analysis confirmed that the LRB and auxetic systems will theoretically facilitate the reduction of structural damage to a building by elongating its period during a seismic event.

The relative floor displacements of the auxetic system, under the Northridge earthquake, have shown considerable improvements when compared to the fixed base system. This is particularly evident when analysing the inter-story drifts of the systems. The auxetic system is also shown to exhibit a gentler increase in relative displacements with an increase in height. Under the 7.15 magnitude Düzce earthquake, a similar improvement has been noted. However, under the weaker 6.9 magnitude Irpinia earthquake, the overall relative displacement performance did not displace an overall improvement. This difference in results is attributed to the unique nature of each earthquake.

When evaluating the performance along the X, Y and Z axes in all three earthquakes, it is evident that the auxetic system analysed is unable to withstand sharp, impulsive vibrations. Under the strongest seismic waves along the X and Y axes, a sharp increase in relative displacement occurs. This can be seen from  $t = 4.7 - 8.6s$  in figures 4-15 to 4-17 in the Northridge earthquake and figures 4-46 to 4-48 in the Düzce earthquake. Although where additional loading occurred after the impulse, such as in the Northridge earthquake, the system

does stabilise and return to a suitable level of relative displacement. In general, under these sudden shock waves, the auxetic system behaves unfavourably. This indicates that the system possesses adequate restorative capabilities. Overall, total deformation shows an improved behaviour for the auxetic base isolation, for almost the whole earthquake, except a few isolated seconds. Along the X-axis, the auxetic and fixed systems depict similar results. Along the Y-axis, a general significant improvement is recorded when comparing the fixed base and auxetic systems. This is particularly notable in the Düzce earthquake in figures 4-54 to 4-56. Along the Z-Axis in the Northridge earthquake analysis, notable improvements are present in the upper floors of the superstructure. In the Northridge earthquake, the fact that along X-axis, the auxetic base does not notably contribute to an improvement in performance. However, it does along Y and Z axes. This indicates that the total relative deformation with the auxetic base isolation is generally reduced and similarly, with the lead-rubber bearing base isolation. In the Düzce earthquake, the auxetic system significantly improves on the relative displacement performance along the Z-Axis at all levels of the superstructure. In general, along this axis, some sharp increases in vertical relative displacement occurs. This is likely the result of the unique auxetic behaviour of the base isolation. When analysing the Irpinia earthquake, it is evident that the relative displacement performance is not favourable. The auxetic base isolation exhibits relative displacements that exceed the fixed base model and the LRB system. Additional research is necessary to fully determine the relative displacement behaviour of auxetic-type base isolation systems under earthquakes with different characteristics.

The non-linear time history analysis that was performed allows for non-linear responses, such as large deformations, plastic damage to be determined. The changes that occur in the geometry as the structure deforms is considered in formulating the constitutive equilibrium equations. Overall, the auxetic system has performed well over the duration of the loading. Evaluating non-linear aspects in a system is an important factor in seismic analysis. However, the models considered in this analysis do not experience any plastic damage. This is most likely a result of the strong material properties of the structural steel used in the analysis. If a similar study were to be performed on a reinforced concrete model, damage should occur.

Throughout the analysis of all three earthquakes, the auxetic-type system consistently performed well in reducing the story accelerations experienced. Throughout most the duration of the three analyses, the auxetic system's performance displayed a notable improvement when compared to the LRB systems. This result verifies the theory as well as past literature stating that auxetic materials are capable of significantly reducing imposed vibrations.

Yang, et al. (2013) notes that two-dimensional auxetic structures are not consistently able to attain the minimum required mechanical properties needed for structural application. Conversely, three dimensional auxetic structures have displayed numerous advantages in achieving these requirements. The practical use of three-dimensional cellular structures is however limited by the manufacturing processes involved. This has hindered the development and practical verification of design theories. Further research should explore incorporating three-dimensional auxetics, which lend to a practical manufacturing process, in similar base isolation systems. These three-dimensional structures may result in improved damping capabilities under strong impulses along each axis. The research undertaken did not note any damage to the models analysed. Future research should investigate failure criteria of the auxetic base isolation system to determine how it behaves under possible damage.

In further research, topology optimisation, such as that which was incorporated into studies undertaken by Zhang & Yang (2016), should be included in the study. It will serve as a means of enhancing the internal structure of the material in order to achieve the most favourable results. Additionally, alternate auxetic structures should be explored to determine which structure is most applicable to seismic damping in structures.

## CHAPTER 5: CONCLUSION

In this study, non-linear time history analysis is performed using the finite element method. Three base isolation types are simulated, namely a non-isolated fixed base system, a conventional lead-rubber bearing system and an auxetic-type system. The models analysed consist of the base isolation system and a ten-story structural steel frame. The base isolation of structures has historically been shown to significantly reduce the acceleration induced on structures and significantly reduce the damage to structural and non-structural components. This is achieved by essentially decoupling the structure from its substructure thereby reducing the physical demand placed on a building and relieving a building's structural components from the role of dissipating seismic energy. Due to the nature of their internal structure, auxetic materials have the inherent mechanical property of vibration isolation. This study proposed incorporating re-entrant honeycomb auxetic layers into base isolation systems in order to evaluate its performance under seismic loading. By doing so, the objectives of the study are achieved by drawing comparisons between the seismic performance of the fixed base, lead-rubber bearing and the auxetic-type base isolation systems. Subsequently, the performance of the auxetic-type system relative to the fixed base and lead-rubber bearing system may be evaluated. The capabilities of auxetic materials in a structural and seismic engineering context is explored.

A basic dynamic analysis in the form of an eigenvalue analysis was performed to determine the natural frequency, natural period and mode shapes of each system. This initial analysis serves as a means of determining the behaviour of the systems when subjected to dynamic loading. The natural periods of the three systems were compared and it was noted that the natural periods of the LRB and auxetic-type systems were significantly longer than that of the ridged fixed-base structure. The elongated period exhibited by the LRB and auxetic systems analysis confirmed that the systems will theoretically facilitate the reduction of structural damage and potentially possible to reduce the base acceleration experienced by the structure.

Compared to a fixed base system, the results from this study have shown that the auxetic-type system successfully reduces the propagation of seismic vibrations, thereby reducing the relative displacements in the system. This has notably been illustrated in the analysis of the inter-story drifts of the systems. The auxetic-type system has performed more favourably than the fixed base and LRB system, with a more gradual decrease in inter-story drift noted in upper stories. Additionally, the two base isolated systems exhibit a very large initial inter-story drift. This occurrence, which is consistent with past literature, confirms the initial results obtained

from the eigenvalue analysis. The added element of lateral flexibility introduced into the system, which initiates the large initial inter-story drift, serves as a means of increasing the period of the system in order to reduce the harmful effects of the earthquake.

Analysing the **relative displacement** along the X-Y-Z axes, it is evident that the auxetic system was unable to dissipate the impulse-like seismic waves that were particularly larger than the average seismic wave in the analysis. This was indicated by sharp increases in relative displacements which corresponded to the strongest seismic waves. This is locally observed, in a short range of time of the dynamic load history. Subsequently, the system returns to a suitable level of relative displacement. **This indicates that the auxetic-type system does possess adequate restorative capabilities.** Overall, the total relative displacement along the X-Y-Z axes indicates that there is an improvement in the behaviour of the auxetic base isolation system. This improvement is noted for almost the entire duration of the earthquakes, apart from a few isolated seconds. Along the X-axis, the auxetic and fixed systems depict similar results. Along the Y-axis, a general significant improvement is recorded when comparing the fixed base and auxetic systems. In general, some sharp increases in vertical relative displacement occurs along the Z-Axis. This is likely due to the unique nature of the auxetic's internal structure and its behaviour. The **floor accelerations** of the auxetic-type system recorded in all three simulations are considerably lower than the fixed base frame system. This performance remained consistent, even under more severe earthquakes. **On** the first floor, the auxetic-type system's performance is slightly better than the fixed base system. As the story height increases, the acceleration reduction capabilities of the system become more evident. Total accelerations do consistently increase with an increase in height, however this increase occurs at a more controlled rate. **In** most instances, the auxetic system displayed an acceleration performance which was more favourable than the LRB system that had been analysed. **This** further confirms the vibration damping properties of the auxetic material and suggests that by incorporating these materials into base isolation systems, the overall performance of the system may be improved.

Undertaking a non-linear time history analysis with many data inputs is computationally demanding. Computational issues were encountered, due to the lack of sufficient computer hardware, when analysing the auxetic-type system. This prompted the use of just the most severe portion of the earthquake in the analysis. This study **did not note any damage** to the models analysed. Future research should also investigate failure criteria of the auxetic base isolation system to investigate the system's behaviour under possible damage. Future studies which apply topology optimisation and parametric analysis to two and three-dimensional

auxetic structures in order to achieve desired mechanical properties should be carried out. Practical experiments based on the finite element models should be carried out on scale models as a means of verifying and comparing physical and computational performance. These models may be 3D printed and tested on a seismic table.

Additionally, a feasibility study involving a cost-benefit analysis should be included to determine if the system is financially viable.

Overall, the outcomes of this study indicate that auxetic materials have the potential to improve the vibration damping performance of currently used base isolation systems.

## REFERENCES

1. ANSYS Inc., 2015. *ANSYS Help - Version 17.0*, Canonsburg, Pennsylvania: ANSYS Inc..
2. Bhuiyan, A. R. & Okui, Y., 2012. Mechanical Characterization of Laminated. In: H. Sezen, ed. *Earthquake Engineering*. Rijeka, Croatia: InTech, pp. 303-336.
3. Cancellara, D. & De Angelis, F., 2016. Assessment and dynamic nonlinear analysis of different base isolation systems for a multi-story RC building irregular in plan. *Computers and Structures*, Volume 180, pp. 74-88.
4. Chakraborty, S., Roy, K. & Ray-Chaud, S., 2016. Design of re-centering spring for flat sliding base isolation system: Theory and a numerical study. *Engineering Structures*, Volume 123, pp. 66-77.
5. Chopra, A. K., 2015. *Dynamics of Structures: Theory and Applications to Earthquake Engineering*. 4th ed. Upper Saddle River, NJ: Prentice Hall.
6. Choun, Y.-S., Park, J. & Choi, I.-K., 2014. Effects of Mechanical Property Variability in Lead Rubber Bearings on the Response of Seismic Isolation System for Different Ground Motions. *Nuclear Engineering and Technology*, 46(5), pp. 605-618.
7. Dagdelen, J., Montoya, J., de Jong, M. & Persson, K., 2017. Computational Prediction of new Auxetic Materials. *Nature Communications*, 8(1).
8. Doshin Rubber Products, 2018. *Doshin Rubber Engineering - Base Isolation Lead Rubber Bearings*. [Online] Available at: <https://doshinrubber.com/lead-rubber-bearing/> [Accessed 5 November 2018].
9. Fallah, N. & Zamiri, G., 2012. Multi-objective optimal design of sliding base isolation using genetic algorithm. *Scientia Iranica*, 20(1), pp. 87-96.
10. Hu, L. L., Zhou, M. & Deng, H., 2018. Dynamic indentation of auxetic and non-auxetic honeycombs under large deformation. *Composite Structures*, Volume 207, pp. 323-330.
11. Ismail, M., 2018. Seismic isolation of structures. Part I: Concept, review and a recent development. *Hormigón y Acero*, 69(285), pp. 147-161.

12. Jiang, L. & Hu, H., 2017. Finite Element Modeling of Multilayer Orthogonal Auxetic Composites under Low-Velocity Impact. *Materials*, 10(8), p. 908.
13. Kelly, T. E., 2001. *Base Isolation of Structures. Design Guidelines*, Wellington, New Zealand: Holmes Consulting Group Ltd.
14. Kircher, C. . A., 2012. Seismically Isolated Structures. In: FEMA, ed. *2009 NEHRP Recommended Seismic Provisions: Design Examples*. Washington D.C.: US Department of Homeland Security, pp. 12-4 - 12-61.
15. Lakes, R., 1993. Advances in Negative Poisson's Ratio Materials. *Advanced Materials*, 5(4), pp. 293-296.
16. Liu, Q., 2006. *Literature Review: Materials with Negative Poisson's Ratios and Potential Applications to Aerospace and Defence*, Victoria: DSTO Defence Science and Technology Organisation.
17. Mayes, R. L. & Naeim, F., 2001. Design of Structures with Seismic Isolation. In: *The Seismic Design Handbook*. Boston: Springer, pp. 723-756.
18. Ma, Y. et al., 2013. A nonlinear auxetic structural vibration damper with metal rubber particles. *Smart Materials and Structures*, 22(8).
19. Mir, M., Ali, M. N., Sami, J. & Ansari, U., 2014. Review of Mechanics and Applications of Auxetic Structures. *Advances in Materials Science and Engineering*, Volume 2014, pp. 1-17.
20. Nelson, N. A., 1999. *Seismic Base Isolation: A Five-Story Building Example*, Cambridge, Massachusetts: Massachusetts Institute of Technology.
21. Rizzian, L., Léger, N. & Marchi, M., 2017. Multiobjective Sizing Optimization of Seismic-Isolated Reinforced Concrete Structures. *Procedia Engineering*, Volume 199, pp. 372-377.
22. Scarpa, F., Giacomini, J., Zhang, Y. & Pastor, P., 2005. Mechanical Performance of Auxetic Polyurethane Foam for Antivibration Glove Applications. *Cellular Polymers*, 24(5), pp. 253-268.
23. Shaban, N. & Caner, A., 2018. Shake table tests of different seismic isolation systems on a large scale structure subjected to low to moderate earthquakes. *Journal of Traffic and Transportation Engineering (English Edition)*.

24. Skinner, R. I., Robinson, W. H. & McVerry, G. H., 1993. *An Introduction to Seismic Isolation*. New York: John Wiley and Sons.
25. South African Institute of Steel Construction, 2013. *South African Steel Construction Handbook*. 8th ed. Johannesburg: South African Institute of Steel Construction.
26. Stavroulakis, G. E., 2005. Auxetic behaviour: appearance and engineering applications. *Physica Status Solidi (b)*, 242(3), p. 710–720.
27. Tafheem, Z., Arafat, T. A., Chowdhury, A. & Iqbal, A., 2015. *Seismic Isolation Systems in Structures- the State of Art Review*. Dhaka, Bangladesh, BIAM Foundation.
28. TechStar Inc., 2018. *TechStar Inc. - Lead Rubber Bearing*. [Online] Available at: <https://www.techstar-inc.com/products/isolators/lrb> [Accessed 5 November 2018].
29. Theocaris, P. S., Stavroulakis, G. E. & Panagiot, P. D., 1997. Negative Poisson's Ratios in Composites with Star-Shaped Inclusions: A Numerical Homogenization Approach. *Archive of Applied Mechanics (Ingenieur Archiv)*, 67(4), pp. 274-286.
30. Ungureanu, B. et al., 2015. *Auxetic-Like Metamaterials as Novel Earthquake Protections*. [Online] Available at: <https://arxiv.org/ftp/arxiv/papers/1510/1510.08785.pdf> [Accessed 2 October 2018].
31. Varnava, V. & Komodromos, P., 2012. Analysis, design and techno-economic assessment of a base isolated steel building. *15th World Conference*, Volume 4, pp. 2586-2595.
32. Yang, L. et al., 2013. *Design of Auxetic Sandwich Panels for Structural Applications*. Austin, Texas, Solid Freeform Fabrication Symposium, pp. 929-938.
33. Yang, L., Harrysson, O., West, H. & Cormier, D., 2015. Mechanical Properties of 3D Re-Entrant Honeycomb Auxetic Structures. *International Journal of Solids and Structures*, Volume 69-70, p. 475–490.
34. Zhang, X.-W. & Yang, D.-Q., 2016. Numerical and Experimental Studies of a Light-Weight Auxetic Cellular Vibration Isolation Base. *Shock and Vibration*, Volume 2016, pp. 1-16.

# APPENDIX A – IRPINIA, ITALY

## A.1 Three-Dimensional Model Deformation

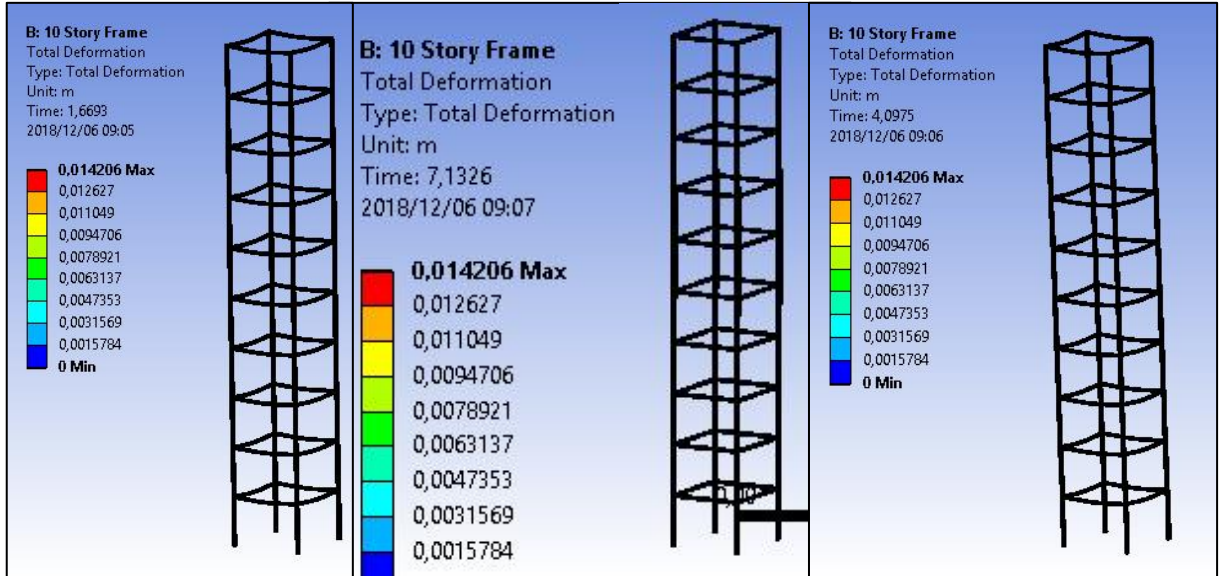


Figure A - 1: Deformation of the Fixed Base System at Approximately  $t = 2, 4$  and  $7s$

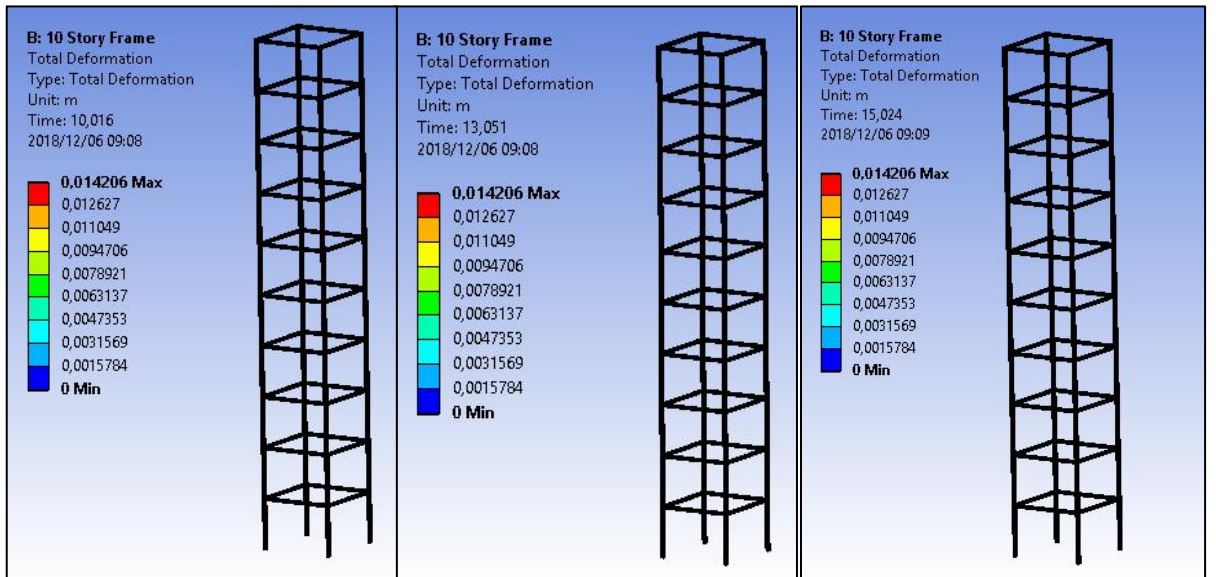


Figure A - 2: Deformation of the Fixed Base System at Approximately  $t = 10, 13$  and  $15s$

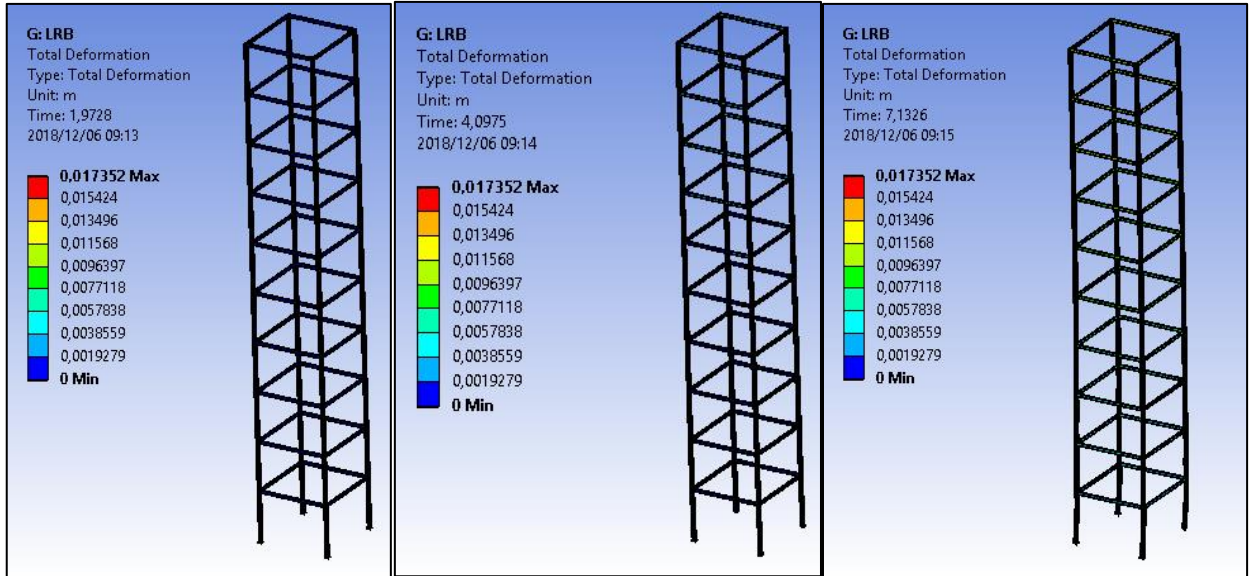


Figure A - 3: Deformation of the LRB System at Approximately  $t = 2, 4$  and  $7s$

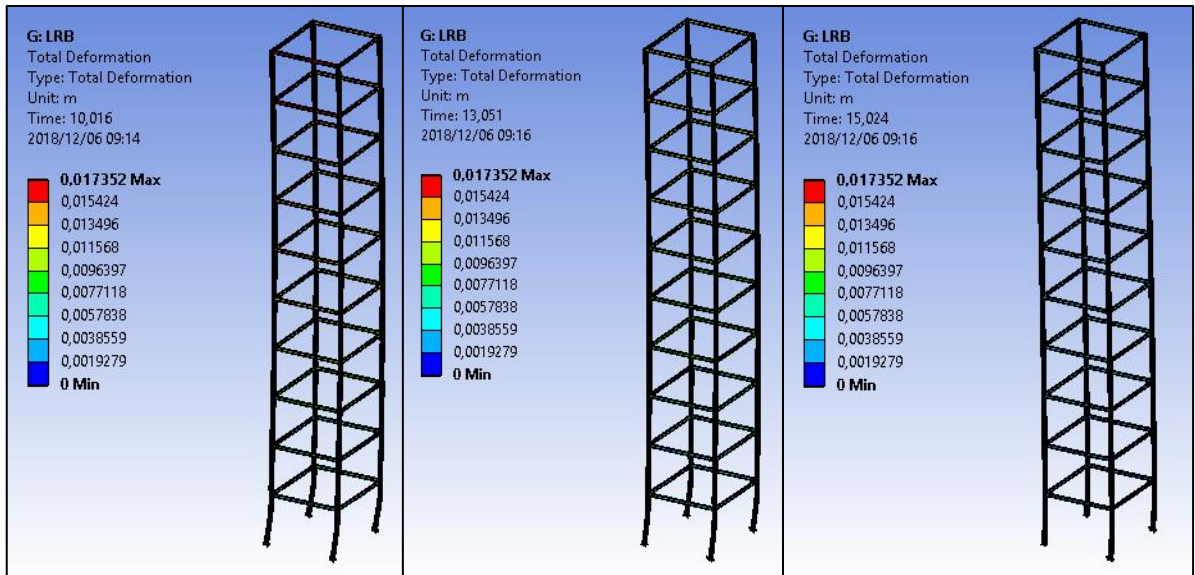


Figure A - 4: Deformation of the LRB System at Approximately  $t = 10, 13$  and  $15s$

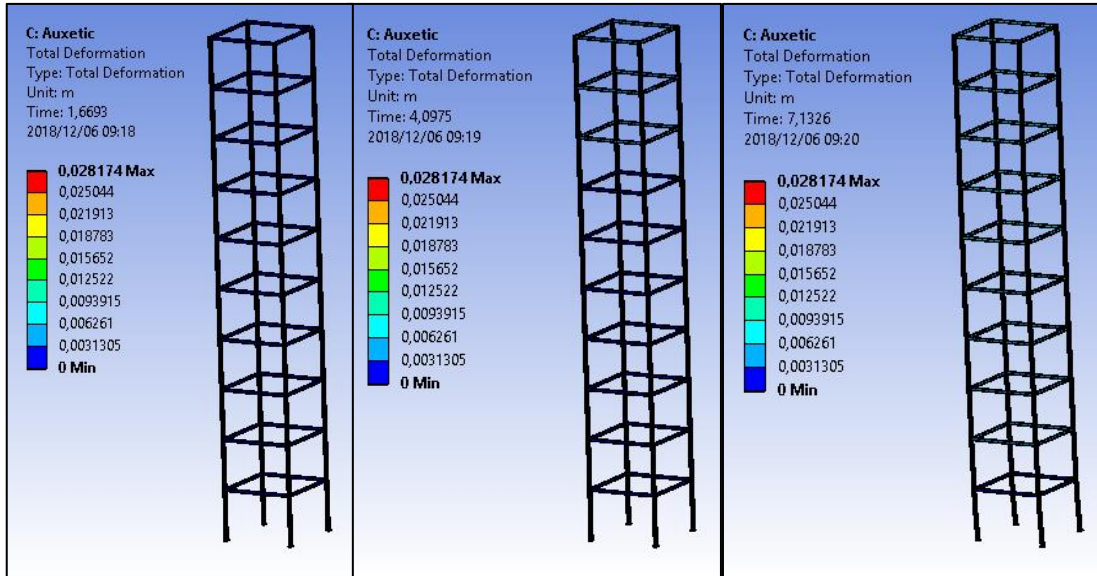


Figure A - 5: Deformation of the Auxetic-Type System at Approximately  $t = 2, 4$  and  $7s$

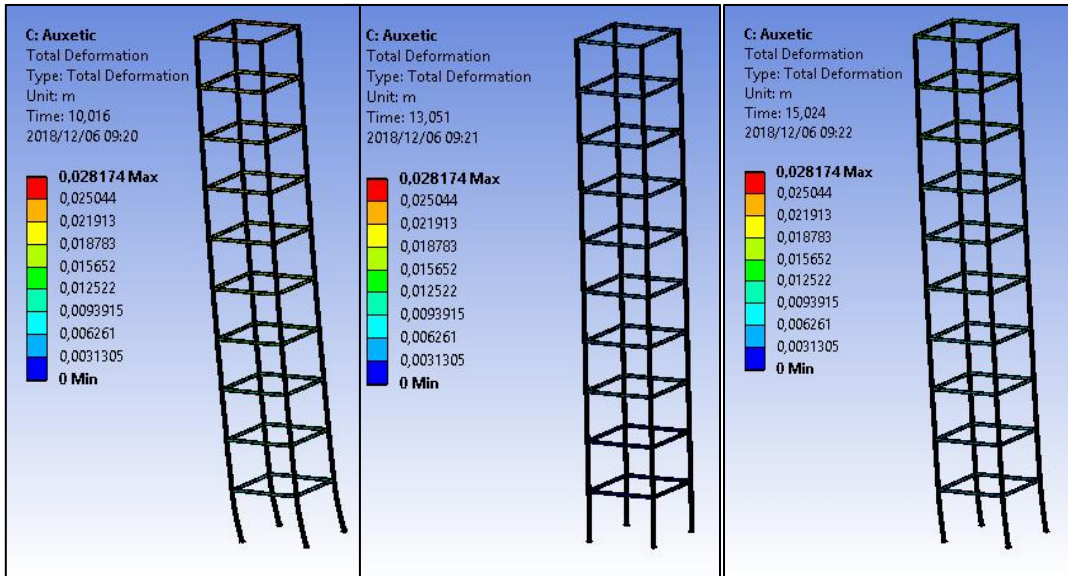


Figure A - 6: Deformation of the Auxetic-Type System at Approximately  $t = 10, 13$  and  $15s$

## A.2 Relative Displacement: X-Axis

The performance of the three systems about the X-Axis correlates with the results obtained for the total and relative displacements. The LRB system exhibits a consistent and favourable performance at all levels. The auxetic base isolation performs well during the first half of the earthquake, but from  $t = 9.1$ s, the relative displacement sharply increases. This coincides with a series of sharp and continuous seismic vibrations along the X-Axis between  $t = 9 - 12$ s. The system begins to normalise after this 2 second duration and is expected to return to its previous behavioural pattern. Figures A-7 to A-9 depict the relative displacement about the X-Axis.

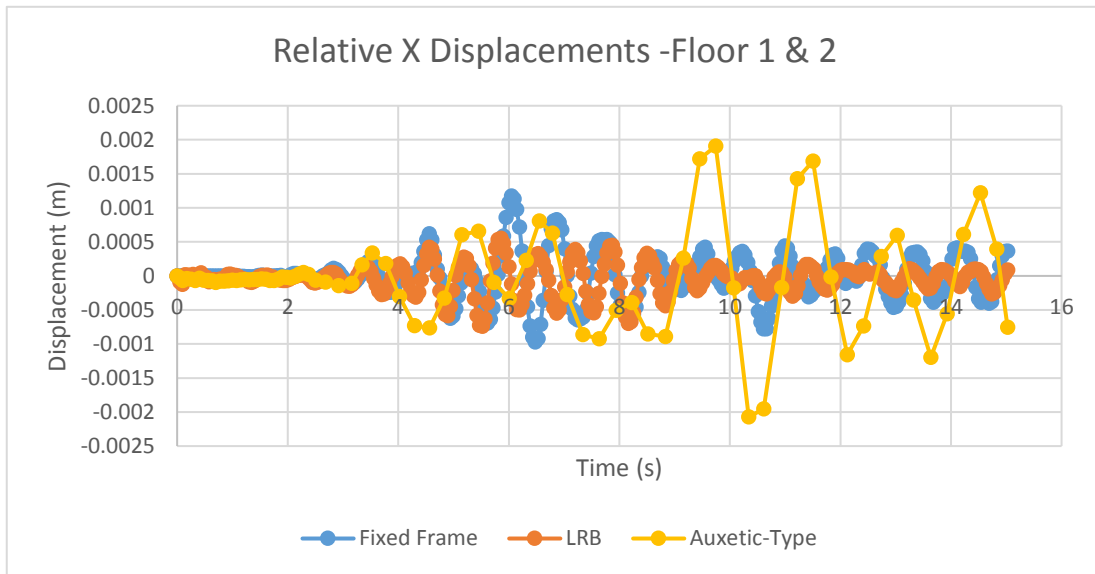


Figure A - 7: Relative Displacement of Floors 1 and 2 about the X-Axis

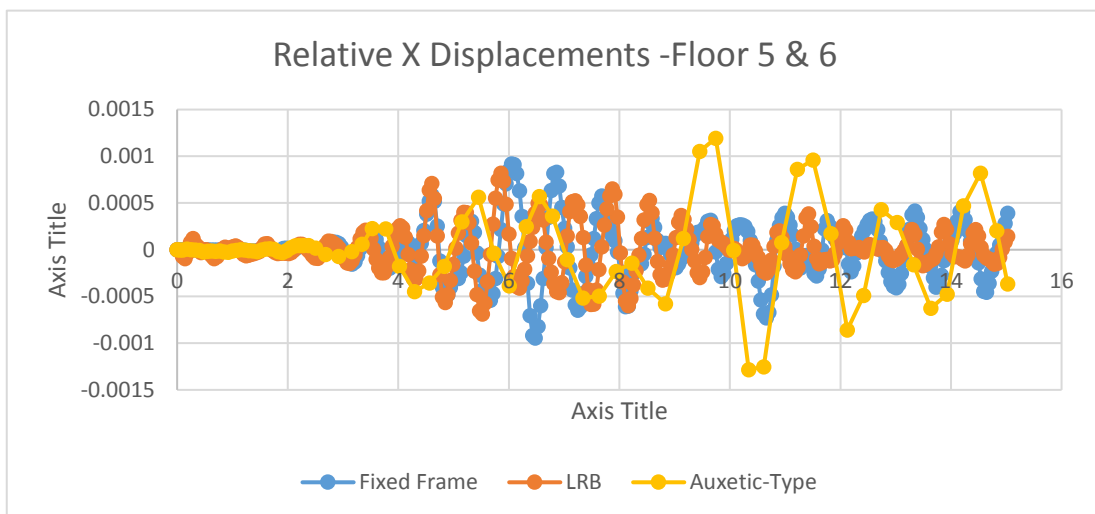


Figure A - 8: Relative Displacement of Floors 5 and 6 about the X-Axis

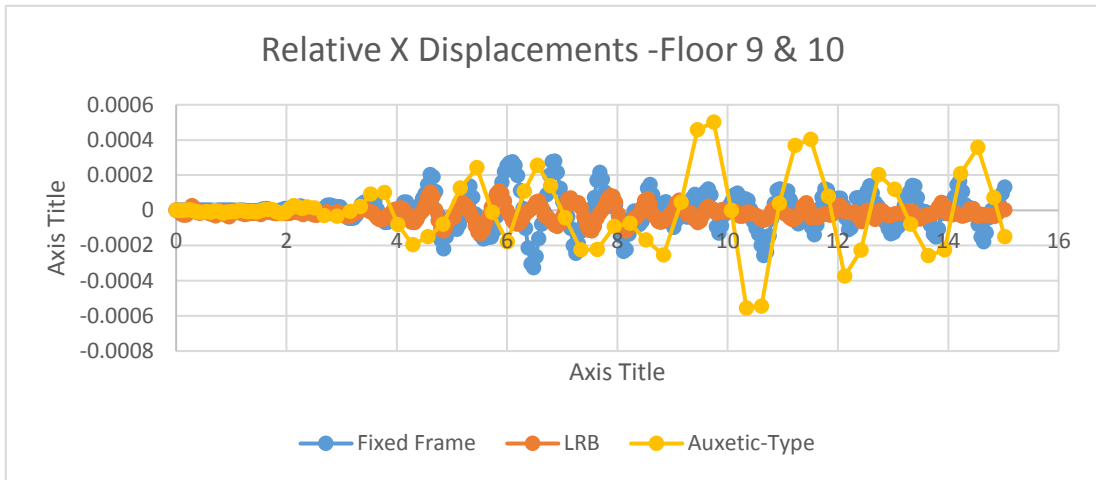


Figure A - 9: Relative Displacement of Floors 9 and 10 about the X-Axis

### A.3 Relative Displacement: Y-Axis

The relative displacement along the Y-Axis is similar to that of the X-Axis. The LRB system performs well throughout the earthquake, however during the latter part of the ground motion, unfavourable amounts of relative displacement occurs. The top floor of the superstructure is an expectation to this, where the LRB system shows an improvement in performance as compared to the fixed base frame system. The overall performance of the auxetic system has not been favourable along this axis owing to the intense nature of the Y-component of the earthquake loading. The system has performed favourably during  $t = 0 - 4.3s$  and  $t = 5.7 - 8.5s$ . An analysis of balance of this duration of the earthquake has revealed that the system's relative displacements is larger than that of the other two systems. The first spike in displacement occurs at the first impulsive wave and likewise, the system's unfavourable deformation coincides with the sharp increase in seismic vibrations along the Y-Axis during this time. Figures A-10 to A-12 depict the relative displacement about the X-Axis.

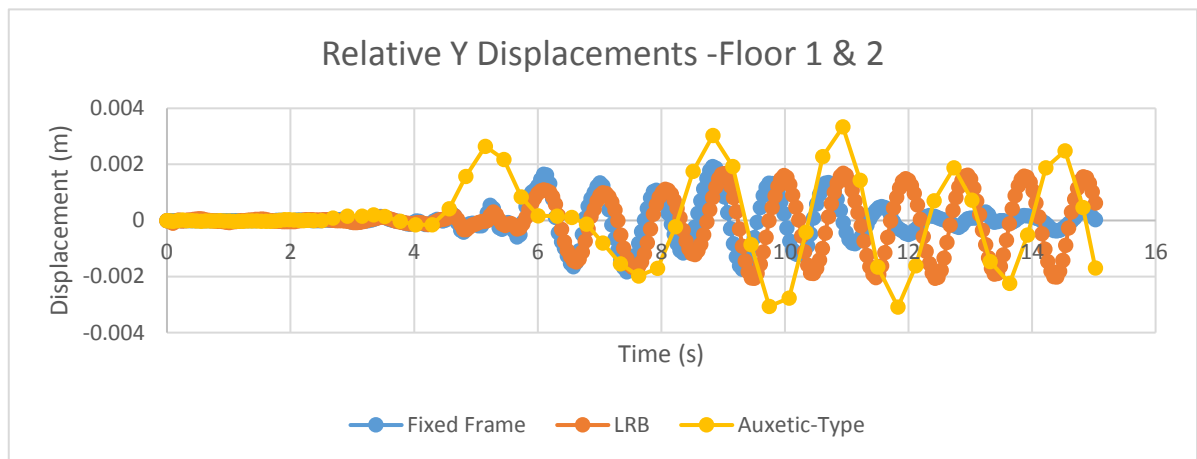


Figure A - 10: Relative Displacement of Floors 1 and 2 about the Y-Axis

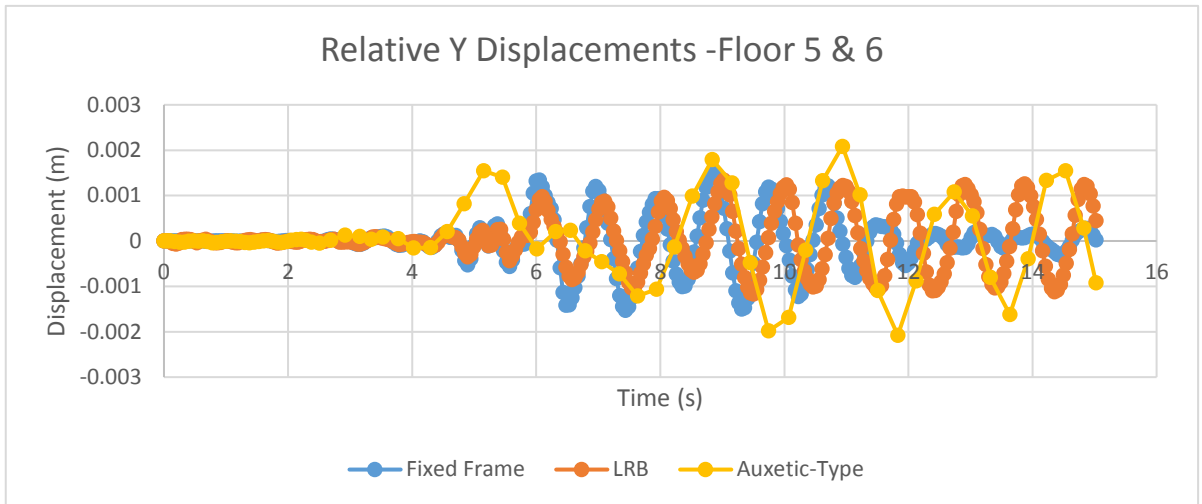


Figure A - 11: Relative Displacement of Floors 5 and 6 about the Y-Axis

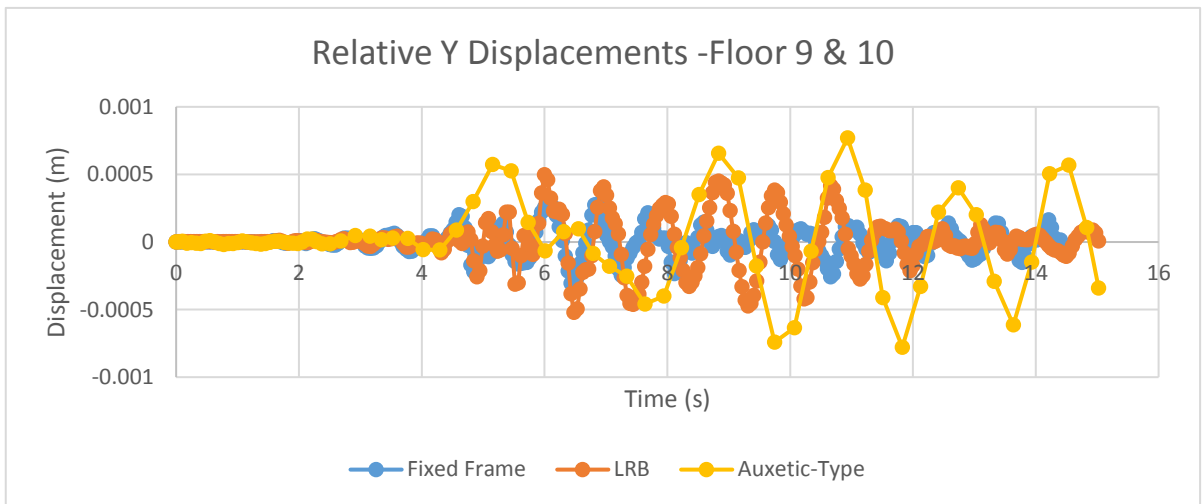


Figure A - 12: Relative Displacement of Floors 9 and 10 about the Y-Axis

# APPENDIX B - DÜZCE, TURKEY

## B.1 Three-Dimensional Model Deformation

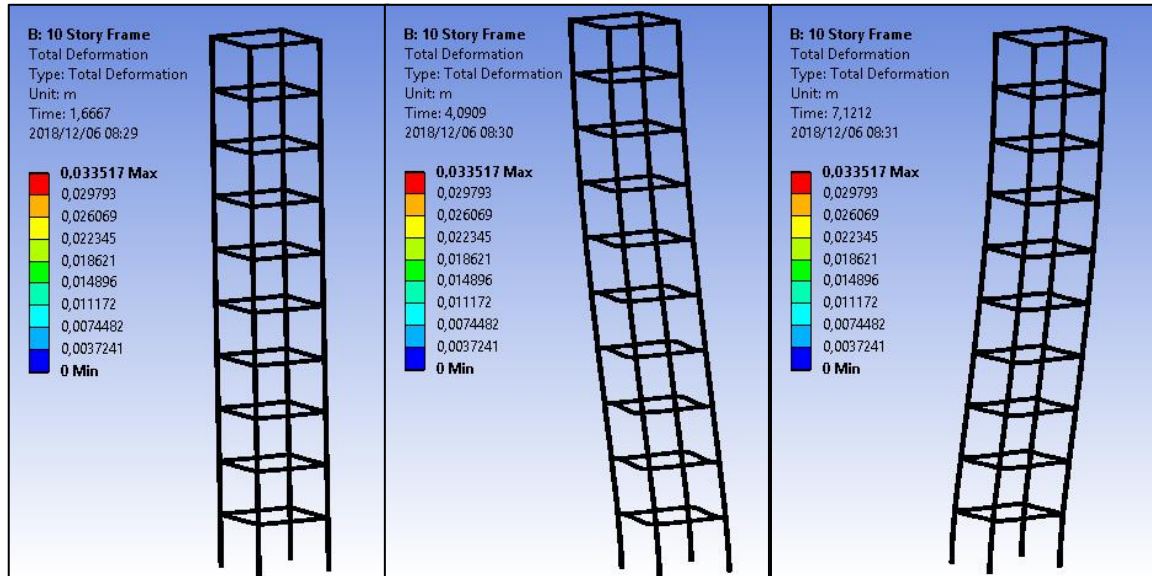


Figure B - 1: Deformation of the Fixed Base System at Approximately  $t = 2, 4$  and  $7s$

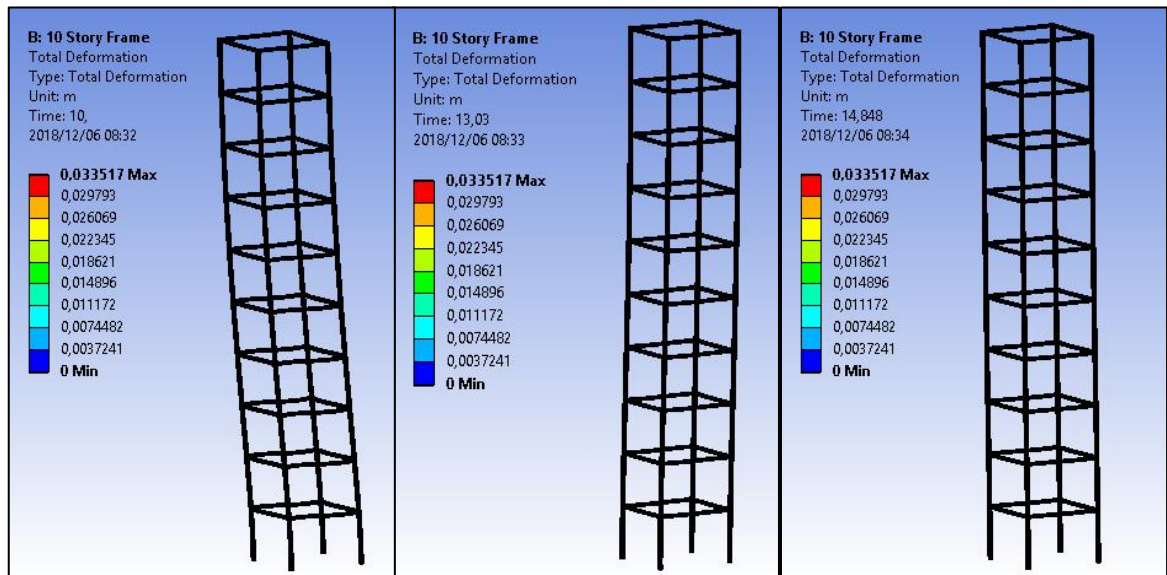


Figure B - 2: Deformation of the Fixed Base System at Approximately  $t = 10, 13$  and  $15s$

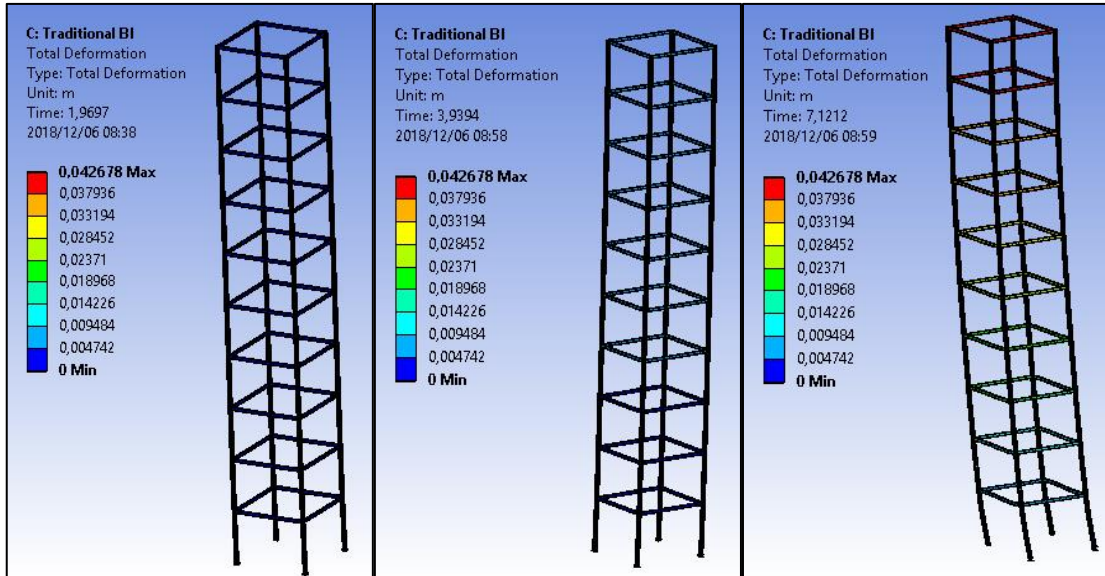


Figure B - 3: Deformation of the LRB System at Approximately  $t = 2, 4$  and  $7s$

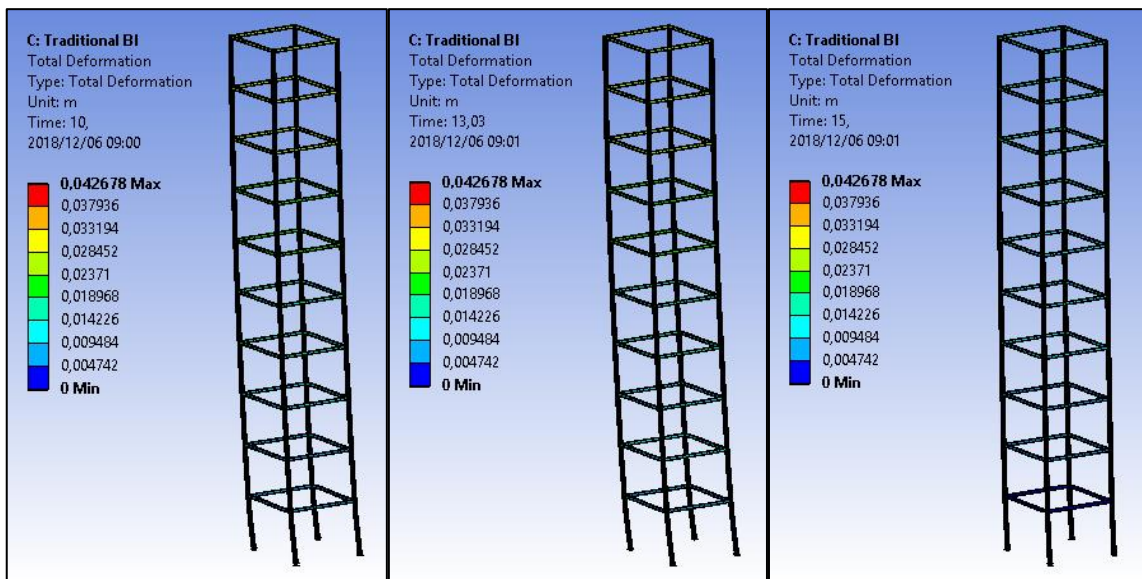


Figure B - 4: Deformation of the LRB System at Approximately  $t = 10, 13$  and  $15s$

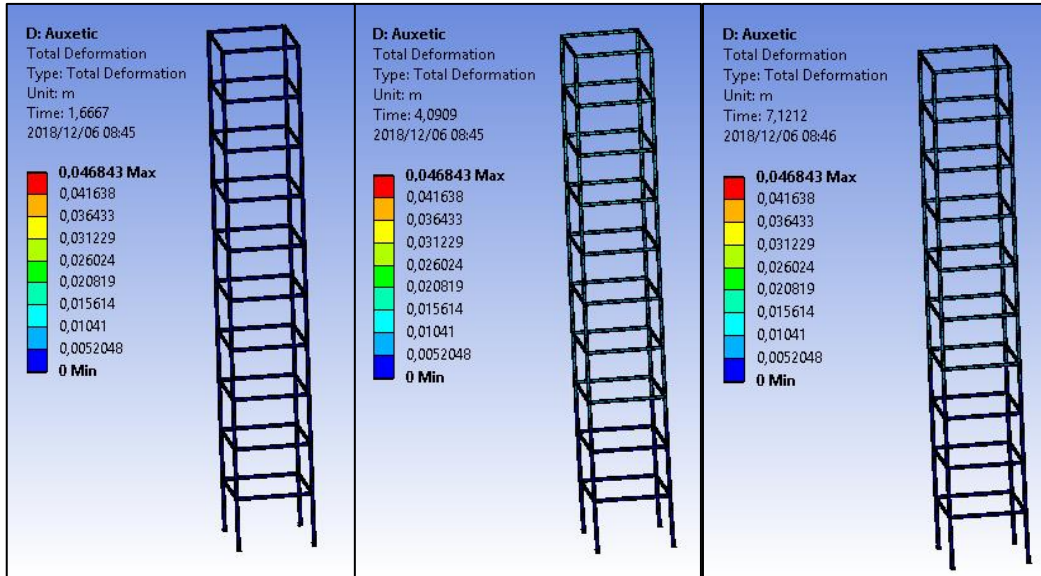


Figure B - 5: Deformation of the Auxetic-Type System at Approximately  $t = 2, 4$  and  $7s$

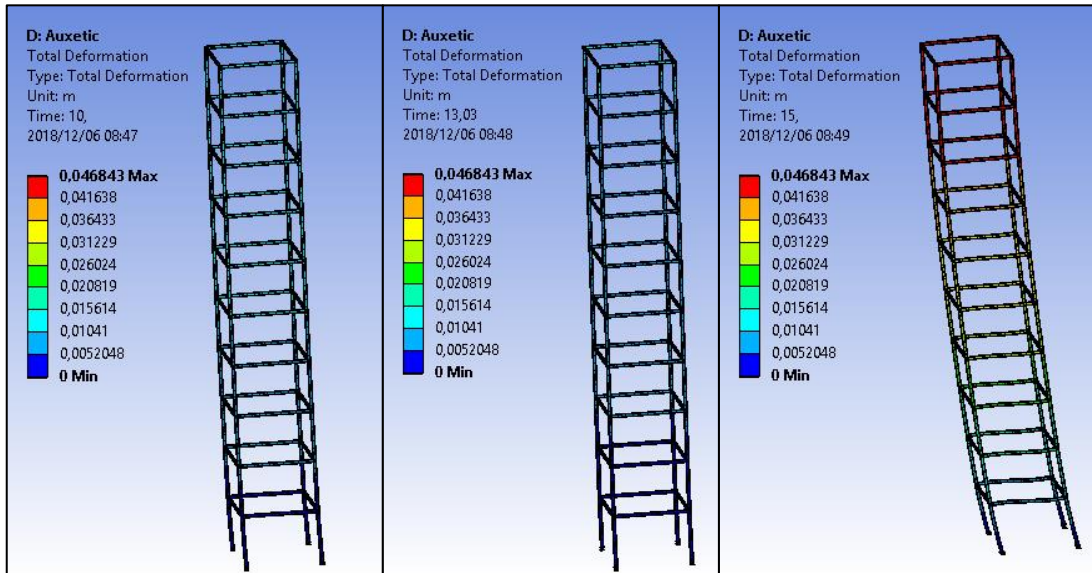


Figure B - 6: Deformation of the Auxetic-Type System at Approximately  $t = 10, 13$  and  $15s$

## B.2 Acceleration

The acceleration performance of the systems under the Düzce earthquake is shown in figures B-7 to B-9. Similarly, to the Northridge and Irpinia earthquakes, the auxetic-type system experienced significantly lower story accelerations when compared with the LRB and fixed base systems. On the first floor, the auxetic-type system experiences similar accelerations to the fixed base system, marginally exceeding it after  $t = 4.3\text{s}$ . As the story height increases, the acceleration in the fixed base and LRB systems increase, however the auxetic system experiences a favourable acceleration through most of the duration of the earthquake. Towards the latter part of the earthquake, at all three levels, the accelerations experienced in the auxetic system gradually increases, exceeding that of the fixed base system. This part of the earthquake is associated with consistently strong vibrations along the X and Y axes which accounts for this increase. The reduction in favourable performance at this duration of the loading is similar to the behaviour of the auxetic system's total and relative displacement.

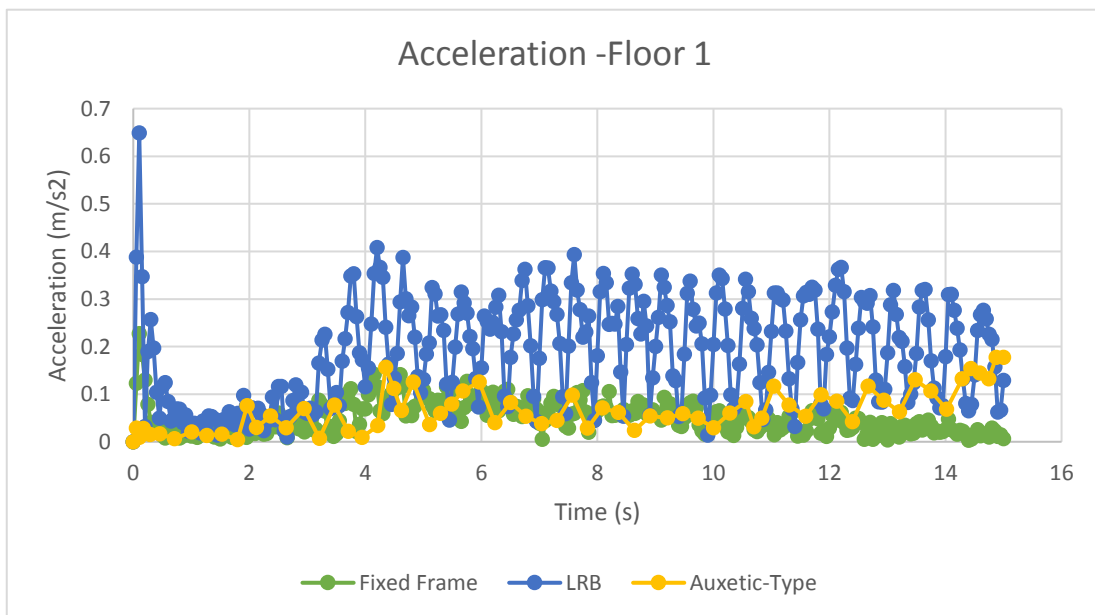


Figure B - 7: Acceleration on Floor 1

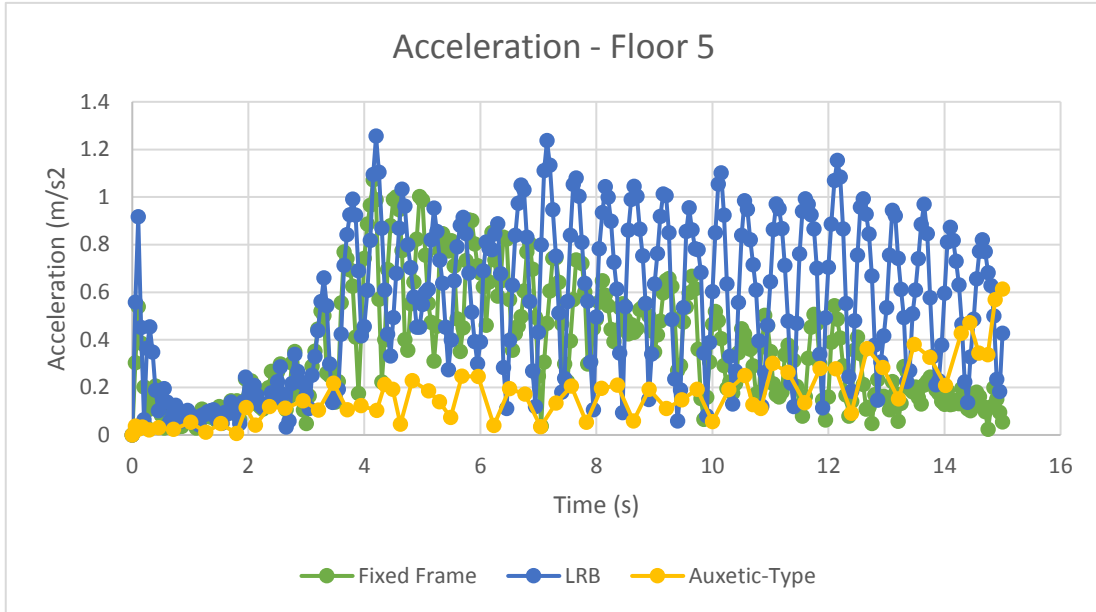


Figure B - 8: Acceleration on Floor 5

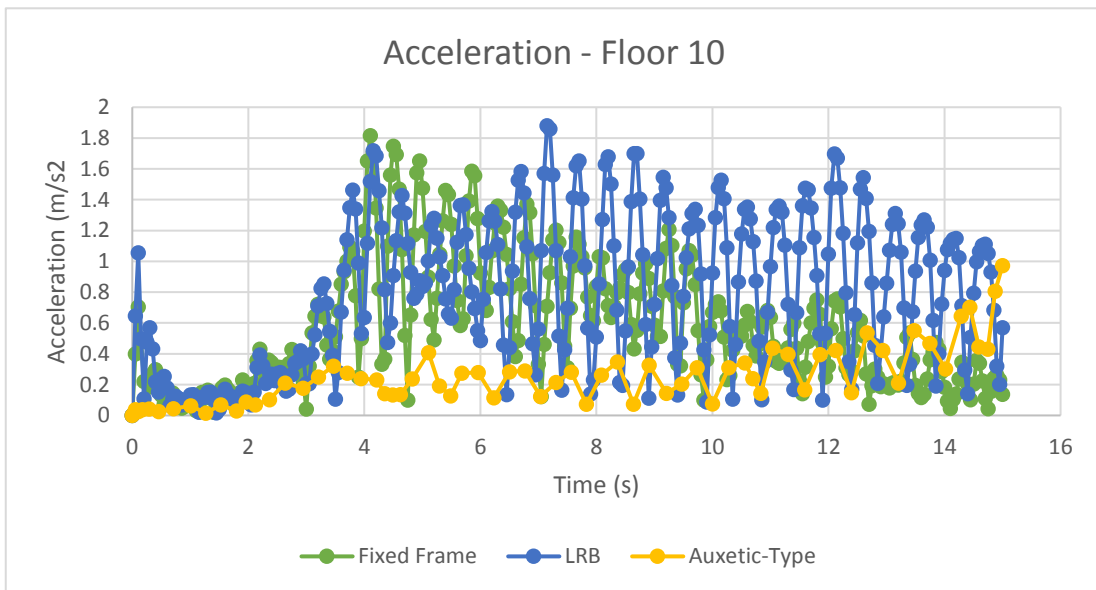


Figure B - 9: Acceleration on Floor 10

### B.3 Reaction Forces

Table B-1 list the overall base shear and reaction forces in each of the three models analysed. Along the horizontal X-axis, the LRB system has shown a reduction in the reaction force, while the auxetic-type system is significantly higher than both systems. However, along the Y-Axis, the opposite occurs. The auxetic-type system experiences a lower Y component of the reaction force than the fixed base and the LRB system has a significantly higher reaction force. Along the vertical Z-axis, the LRB and fixed base system experience similar reaction forces as in the Northridge earthquake. The auxetic system has a significantly low Z component which does not correlate with previous models in the study and the other systems analysed in this set of results. Overall, the fixed base system possesses a total reaction force that is 3 KN lower than the LRB system. This result is similar to that of the total reaction force of the systems found in the Northridge earthquake. The reaction forces were determined using all nodes present at the four fixed supports in each system.

*Table B - 1: Reaction Forces*

<b>Reaction Force (KN)</b>	<b>Frame</b>	<b>LRB</b>	<b>Auxetic-Type</b>
X-Axis	-1.1476	0.59701	-7.2999
Y-Axis	0.040698	5.5671	-1.4851
Z-Axis	113.72	116.55	0.36885
Total	113.73	116.68	7.4585